Mathematical Biology



Operon dynamics with state dependent transcription and/or translation delays

Received: 18 June 2021 / Revised: 18 June 2021 / Accepted: 16 November 2021 © The Author(s), under exclusive licence to Springer-Verlag GmbH Germany, part of Springer Nature 2021

Abstract

Transcription and translation retrieve and operationalize gene encoded information in cells. These processes are not instantaneous and incur significant delays. In this paper we study Goodwin models of both inducible and repressible operons with state-dependent delays. The paper provides justification and derivation of the model, detailed analysis of the appropriate setting of the corresponding dynamical system, and extensive numerical analysis of its dynamics. Comparison with constant delay models shows significant differences in dynamics that include existence of stable periodic orbits in inducible systems and multistability in repressible systems. A combination of parameter space exploration, numerics, analysis of steady state linearization and bifurcation theory indicates the likely presence of Shilnikov-type homoclinic bifurcations in the repressible operon model.

Mathematics Subject Classification $92C37 \cdot 92-10 \cdot 37N25 \cdot 34K43 \cdot 37G15 \cdot 34K16$

Contents

1	Introduction
2	Basic operon equations
	2.1 The Goodwin model
	2.2 The effects of cell growth and state dependent transcription and translation delays
	2.3 Evolution equations incorporating state-dependent transcription and translation rates
	mRNA dynamics
	Intermediate dynamics
	Effector dynamics
	Putting it all together
	2.4 The control of transcription initiation rates

This work was supported by the Natural Sciences and Engineering Research Council (NSERC) of Canada (ARH and MCM) and the Alexander von Humboldt Stiftung of Germany (H-OW). TG was partially supported by NSF Grant DMS-1951510.

Extended author information available on the last page of the article

Published online: 14 December 2021



2 Page 2 of 74 T. Gedeon et al.

	2.5 Transcriptional and translational velocities	11
	2.6 Equilibria	12
	2.7 Linearization by expansion	18
3	Numerical methods	22
	3.1 Steady state computations: linearization correction	23
	3.2 Steady state and periodic orbit computation: delay discretization	24
	3.3 Solving initial value problems (IVPs)	27
4	Dynamics of repressible and inducible operons with state-dependent delays	29
	4.1 Repressible operon with one state-dependent delay	29
	Homoclinic bifurcation	32
	Zero-Hopf bifurcation and 3DL transition	35
	4.2 Inducible operon with one state-dependent delay	40
	Inducible supercritical hopf bifurcation	40
	Inducible subcritical hopf bifurcation	42
	Fold bifurcation of periodic orbits	45
	4.3 Two state-dependent delays	48
5	Discussion and summary	50
A	ppendices	52
A	The semiflow of differentiable solution operators generated by the system (2.15)–(2.17) and (2.18)–	
	(2.19)	52
В	Positivity, dissipativity, global attractor	61
	Linearization	68
	of such and	71

1 Introduction

The regulation of information encoding and transmission in biological systems has intrigued and occupied mathematicians and physicists for decades. One of the earliest published papers along these lines is Timoféeff-Ressovsky et al. (1935) which played a major role in the motivation of Erwin Schrödinger to give the 1943 Dublin lectures that are immortalized in Schrödinger (1944). The regulation of information retrieval started to become understood very quickly after the seminal work of Jacob and Monod (Jacob et al. 1960; Jacob and Monod 1961) elucidating the nature of the regulation of lactose production in bacteria. The molecular apparatus carrying out this procedure in bacteria, involving transcription of DNA to produce mRNA and the translation of the mRNA to ultimately produce an effector protein, was named an 'operon' by them. In Fig. 1 we have illustrated the operon concept using the lactose (*lac*) operon as an example (Jacob et al. 1960; Jacob and Monod 1961).

Rather astonishingly, mathematical models of the process of transcription and translation rapidly appeared (Goodwin et al. 1963; Goodwin 1965). These first attempts were swiftly followed by an analysis of a simple repressible operon (Griffith 1968a) and an inducible operon (Griffith 1968b). These and other results were summarized in the Tyson and Othmer (1978) review which is still relevant today.

Though Goodwin clearly noted the existence of significant delays in both transcription and translation in Goodwin et al. (1963), and thought that the delays might have significant dynamic influences, he did not examine their potential effects. Apparently the first to incorporate constant transcriptional and translational delays into the Goodwin model was Banks (1977) and then MacDonald (1977) followed in rapid succession

¹ Personal conversation with MCM, November, 1994.



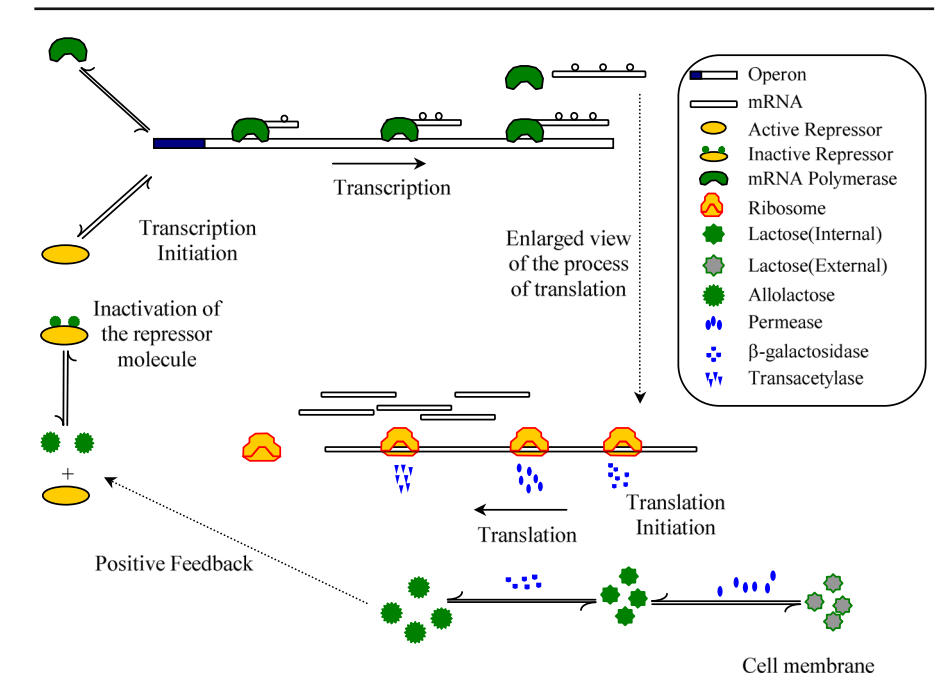


Fig. 1 A cartoon representation of the operation of the *lac* operon enabling bacteria to utilize lactose as an energy source in the absence of glucose, as elucidated by Jacob et al. (1960), Jacob and Monod (1961). The process starts (upper left) when the operator region (dark-blue) is free of active repressor molecules so mRNA polymerase can attach to the DNA and start moving along the structural genes to produce mRNA. Once the mRNA is fully formed, ribosomes start the translation process which, for the *lac* operon, produces, in sequence, β -galactosidase, permease, and transacetylase. The permease facilitates the transport of extracellular lactose to the intracellular space (bottom right), while the permease is essential for the conversion of the internalized lactose into allolactose. Allolactose, in turn, is able to bind to active repressor molecules thereby inactivating them and giving rise to the positive feedback nature of the *lac* operon. Modified from Yildirim and Mackey (2003)

by Banks and Mahaffy (1978a,b), an der Heiden (1979, 1983) and Mahaffy and Pao (1984). These were followed by a number of subsequent investigations.

Since the processes of transcription and translation are rather complicated, the assumption of constant delay may limit our ability to appreciate the richness of dynamics that the process of protein production can impose on the cell. The goal of this paper is to derive a Goodwin-like delay-differential equation (DDE) model with *state dependent delays* that we feel may more closely correspond to biological reality, explore the potential dynamics both in repressible and inducible cases and contrast these dynamics with that of a system with constant delays.

This paper is rather long and detailed, and a summary of the contents may be of help to the reader. Section 2 outlines the basic operon equations starting with a summary of the Goodwin model in Sect. 2.1 and a summary of the equations we derive in this paper in Sect. 2.2. Section 2.3 details the full derivation of the model equations we study here while Sect. 2.4 summarizes the functional forms for the transcription initiation rates that we use for inducible and repressible operons.



2 Page 4 of 74 T. Gedeon et al.

Section 2.5 contains our arguments for the nature and form of the transcriptional and translational velocities in the two types of operons that lead naturally to the state dependent delays that are central to our study. Section 2.6 deals with the quantitative and qualitative nature of the possible equilibrium states of our model equations developed in Sect. 2.3, and the following Sect. 2.7 gives a linearization procedure in the neighborhood of these steady states that is not fully justified mathematically but easily understood by most readers. (The analytically exact linearization is to be found in "Appendix C" and leads to precisely the same result). These linearizations are needed for stability determinations based on the eigenvalues evaluated at the equilibria.

Section 3 contains the details of the numerical methods we have used in our numerical studies of this model, while the following Sect. 4 contains the extensive details of our numerical studies for both the repressible (Sect. 4.1) and inducible (Sect. 4.2) operon models. In both cases we have found that significant new types of dynamics are introduced by the state dependency of the delays. In the inducible operon model we found a stable periodic orbit as well as tristability between a periodic orbit and two steady states. In the repressible operon model we found bistability between two steady states as well as between a periodic orbit and a steady state. All of these results are obtained with one state dependent delay and are not present in the corresponding DDE model with a constant delay. In addition, in the repressible operon model we found evidence of a homoclinic bifurcation of Shilnikov type (Shilnikov 1965; Kuznetsov 2004), indicating the potential for complex dynamics. Finally, in both types of operons there are stable periodic orbits, where a short burst of transcription and translation is interspersed with longer periods of quiescence. These orbits represent a pulse-generating mechanism on a sub-cellular level and may be connected to the phenomena of transcriptional bursting (Tunnacliffe and Chubb 2020). The main body of the paper concludes with a discussion and summary in Sect. 5 and is followed by three mathematical appendices. "Appendix A" treats the semiflows arising from our basic model with state dependent delays, "Appendix B" considers some aspects of the nature of the model solutions including positivity and the global attractor, while "Appendix C" treats the linearization mentioned above.

2 Basic operon equations

2.1 The Goodwin model

The Goodwin (1965) model for operon dynamics considers a large population of cells, each of which contains one copy of a particular operon, and we use that as a basis for discussion. We let (M, I, E) respectively denote the mRNA, intermediate protein, and effector protein *concentrations*. For a generic operon the dynamics are assumed to be given by (Goodwin et al. 1963; Goodwin 1965; Griffith 1968a, b; Othmer 1976; Selgrade 1979)



$$\frac{dM}{dt}(t) = \mathcal{F}(E(t)) - \gamma_M M(t), \qquad (2.1)$$

$$\frac{dI}{dt}(t) = \beta_I M(t) - \gamma_I I(t), \qquad (2.2)$$

$$\frac{dE}{dt}(t) = \beta_E I(t) - \gamma_E E(t). \tag{2.3}$$

It is assumed here that the flux \mathcal{F} (in units of [concentration · time⁻¹]) of initiation of mRNA production is a function of the effector level E. Furthermore, the model assumes that the flux of protein and metabolite production are proportional (at rates β_I , β_E respectively) to the amount of mRNA and intermediate protein respectively. All three of the components (M, I, E) are subject to degradation at rates $\gamma_M, \gamma_I, \gamma_E$. The parmeters β_I , β_M , γ_M , γ_I and γ_E have dimensions [time⁻¹].

2.2 The effects of cell growth and state dependent transcription and translation delays

We will study an extended Goodwin model taking into account the effects of cell growth and delays which are introduced by state dependent transcription and translation processes. The cell growth affects the volume and hence the concentrations of all the molecules in the cell.

The following sections are devoted to the derivation of the generalization of the Goodwin model:

$$\frac{dM}{dt}(t) = \beta_M e^{-\mu \tau_M} \frac{v_M(E(t))}{v_M(E(t - \tau_M))} f(E(t - \tau_M)) - \bar{\gamma}_M M(t), \qquad (2.4)$$

$$\frac{dM}{dt}(t) = \beta_M e^{-\mu \tau_M} \frac{v_M(E(t))}{v_M(E(t - \tau_M))} f(E(t - \tau_M)) - \bar{\gamma}_M M(t), \qquad (2.4)$$

$$\frac{dI}{dt}(t) = \beta_I e^{-\mu \tau_I} \frac{v_I(M(t))}{v_I(M(t - \tau_I))} M(t - \tau_I) - \bar{\gamma}_I I(t), \qquad (2.5)$$

$$\frac{dE}{dt}(t) = \beta_E I(t) - \bar{\gamma}_E E(t). \tag{2.6}$$

In Eqs. (2.4)–(2.6) there are several changes to be noted relative to the original Goodwin model (2.1)–(2.3). The first is the introduction of the two delay terms E(t - τ_M) and $M(t-\tau_I)$ indicating that E and M are now to be evaluated at a time in the past due to the non-zero times required for transcription and translation. From a dynamic point of view, the presence of these delays can have a dramatic effect.

The second change² is the appearance of the terms $e^{-\mu\tau_M}$ and $e^{-\mu\tau_I}$ which respectively account for an effective dilution of the maximal mRNA production and intermediate protein fluxes because the cell is growing at a rate μ (in units of [time⁻¹]).

The third change from (2.1)–(2.3) to (2.4)–(2.6) is the alteration of the decay rates γ_i to $\bar{\gamma}_i \equiv \gamma_i + \mu$ because the dilution due to cell growth leads to an effective increase in the rate of destruction.

² We note that previous inclusions of cell growth and transcription/translation delays (Yildirim and Mackey 2003; Yildirim et al. 2004) contained an error which we correct here. In the original Yildirim and Mackey (2003) paper, the term $e^{-\mu\tau_M}$ in (2.4) was mistakenly inserted within the argument of f instead of being in front of f.



2 Page 6 of 74 T. Gedeon et al.

A fourth change is the replacement of \mathcal{F} in (2.1) by $\beta_M f$ in (2.4). Here β_M is the *maximal* production rate (in units of [concentration · time⁻¹]) possible and f is the fraction of free operator sites on the operon, a function that will vary between a maximal value of 1 and a minimal value in [0, 1). We remark that β_M thus has different units than the linear rate constants β_I and β_E .

Finally, velocity ratio terms of the form $\frac{v_j(w)}{v_j(w(t-\tau))}$ appear in (2.4) and (2.5) as a consequence of the delays τ_M and τ_I being non-constant and depending on the state variables, as explained in Sect. 2.5.

2.3 Evolution equations incorporating state-dependent transcription and translation rates

Transcription is initiated when RNA polymerase (RNAP) is recruited to the promoter region by one or more transcription factors, partially unwinds the promoter DNA to form the transcription bubble, and subsequently leaves the promoter region, moving along the DNA. If multiple initiations take place in rapid succession, then transcribing RNAPs start to interfere with each other, and as a result the average velocity of individual RNAPs transcription events will decrease. This, in turn, leads to an increased time of transcription.

Translation is initiated by assembly of the ribosome on the initiation region of the mRNA. Ribosomes catalyze subsequent binding of codon specific transfer RNAs (tRNA) to the mRNA and transfer of the attached amino acid to the nascent polypeptide. Subsequent translocation of the ribosome completes the cycle.

The result is a bio-polymerization process whose velocity depends on current demand for both ribosomes and tRNAs, which is affected both by the number of actively translated mRNAs and the growth rate of the cell. Both transcription and translation share key characteristics that lead to a common model of these processes. The most basic model, from which other models are derived, is a stochastic Totally Asymmetric Simple Exclusion Process (TASEP) model for particles hopping on a strand with a finite number of discrete sites, that represent nucleotides (Derrida et al. 1993; Schütz and Domany 1993; Kolomeisky 1998; Shaw et al. 2003; Zia et al. 2011).

It should be noted that in eukaryotes (as opposed to our consideration in this paper of prokaryotic gene regulation) transcription takes place in the nucleus while translation takes place in the cytoplasm and the consequent transport of intermediate from cytoplasm into the nucleus gives rise to a *transport delay* that may, on occasion, be considered as state dependent (Ahmed and Verriest 2017; Wang and Pei 2021).

mRNA dynamics

For the mRNA molecules we start with the mRNA transcripts and consider their density r(t, a) at time t and location a along the DNA, so

$$\int_{a_1}^{a_2} r(t,a) da$$



is the number of mRNA molecules with positions between a_1 and a_2 , $0 \le a_1 < a_2 \le a_M$, where a_M is the end of the transcription region. The velocity of transcription along the DNA is given by a function v_M , and we assume that the actual velocity of the process depends on the value w(t) of a function w, to be determined later. If the transcription process takes place without any loss of mRNA transcripts, then the evolution equation for the density r(t, a) is given by

$$\frac{\partial r}{\partial t}(t,a) + v_M(w(t))\frac{\partial r}{\partial a}(t,a) = 0.$$
 (2.7)

We look for a differential equation

$$\frac{dm}{dt}(t) = p(t) - \gamma_M m(t)$$

for the number m(t) of complete mRNA molecules at time t, with a constant rate $\gamma_M > 0$ of degradation and a *production function p* which describes the contribution of the release of completed mRNA molecules at time t to the rate of change $\frac{dm}{dt}(t)$. In order to determine p(t) consider the number of mRNA molecules undergoing transcription at time t, which is

$$J(t) = \int_0^{a_M} r(t, a) da.$$

Using Eq. (2.7) we have a balance equation for J,

$$\frac{dJ}{dt}(t) = v_M(w(t))r(t, 0) - v_M(w(t))r(t, a_M),$$

where the term $v_M(w(t)r(t,0))$ represents the initiation rate of transcription of mRNA molecules contribution to $\frac{dJ}{dt}(t)$, and $-v_M(w(t))r(t,a_M)$ is the release rate of completed mRNA molecules. Therefore the term $v_M(w(t))r(t,a_M)$ is the desired contribution p(t) to $\frac{dm}{dt}(t)$. Using characteristics we obtain

$$p(t) = v_M(w(t))r(t, a_M) = v_M(w(t))r(t - \tau, 0),$$

with the time $\tau = \tau_M(t)$ needed for production of mRNA molecules which reach the final length a_M at time t,

$$a_M = \int_{t-\tau_M(t)}^t v(w(s))ds = \int_{-\tau_M(t)}^0 v(w(t+s))ds.$$
 (2.8)

We arrive at

$$\begin{split} p(t) &= v_M(w(t))r(t - \tau_M(t), 0) \\ &= \frac{v_M(w(t))}{v_M(w(t - \tau_M(t)))} [v_M(w(t - \tau_M(t)))r(t - \tau_M(t), 0)], \end{split}$$



2 Page 8 of 74 T. Gedeon et al.

where the term $[v_M(w(t - \tau_M(t)))r(t - \tau_M(t), 0)] = F(t - \tau_M(t))$ stands for the onset of transcription of mRNA molecules at time $t - \tau_M(t)$. The differential equation for m thus becomes

$$\frac{dm}{dt}(t) = \frac{v_M(w(t))}{v_M(w(t - \tau_M(t)))} [v_M(w(t - \tau_M(t)))r(t - \tau_M(t), 0)] - \gamma_M m(t)
= \frac{v_M(w(t))}{v_M(w(t - \tau_M(t)))} F(t - \tau_M(t)) - \gamma_M m(t).$$
(2.9)

We now switch to a description of transcription in terms of molecule concentration, rather than numbers of molecules. Since the concentration M is related to the number of molecules m by M = m/V, we have

$$\frac{dm}{dt}(t) = \frac{dM}{dt}(t)V(t) + M(t)\frac{dV}{dt}(t) = V(t)\frac{dM}{dt}(t) + \mu V(t)M(t),$$

under the assumption that the cells are growing exponentially with $\frac{dV}{dt}(t) = \mu V(t)$. Consequently, noting that $V(t) = e^{\mu \tau_M(t)} V(t - \tau_M(t))$, we can rewrite (2.9) as

$$\begin{split} \frac{dM}{dt}(t) &= \frac{1}{V(t)} \frac{dm(t)}{dt} - \mu M(t) \\ &= \frac{v_M(w(t))}{v_M(w(t - \tau_M(t)))} e^{-\mu \tau_M(t)} \frac{F(t - \tau_M(t))}{V(t - \tau_M(t))} - (\gamma_M + \mu) M(t) \end{split}$$

We express the *initiation flux* $\frac{F(...)}{V(...)}$ in concentration units as

$$\frac{F(t - \tau_M(t))}{V(t - \tau_M(t))} =: \beta_M f(w(t - \tau_M(t)))$$

where β_M is the *maximal* initiation flux (units of [concentration·time⁻¹]) and f stands for the fraction of free operator sites on the operon, a function that will vary between a minimal value in (0, 1) and a maximal value of 1.

As derived in Mackey et al. (2016, Chapter 1), the initiation flux is a function of concentration of the effector molecule E, and the velocity v_M also depends on E (Sect. 2.5). Therefore for the transcription process w = E and we obtain

$$\frac{dM}{dt}(t) = \frac{v_M(E(t))}{v_M(E(t - \tau_M(t)))} e^{-\mu \tau_M(t)} \beta_M f(E(t - \tau_M(t))) - (\gamma_M + \mu) M(t),$$
(2.10)

together with Eq. (2.8) for the delay $\tau_M(t)$, which depends on the function E.



2

Intermediate dynamics

We assume that the initiation of the translational production of the mRNA into intermediate protein is a relatively simple process and, unlike the transcription process, not under regulatory control.

For the intermediate molecules, we use i(t, b) to describe their density at time t and location b along the mRNA. We assume that the translation is proceeding at a velocity $v_I(q)$ along the mRNA. This velocity may depend on q, where q is to be determined. Analogous to the transcription process we arrive at

$$\frac{di}{dt}(t) = \frac{v_I(q(t))}{v_I(q(t-\tau_I(t)))} \beta_I m(t-\tau_I(t)) - \gamma_I i(t). \tag{2.11}$$

In Sect. 2.5 we argue that q = M, the concentration of mRNA. Therefore switching to a concentration description using $I(t) = \frac{i(t)}{V(t)}$, following the derivation of (2.10) we can rewrite (2.11) in the form

$$\frac{dI}{dt}(t) = \frac{v_I(M(t))}{v_I(M(t - \tau_I(t)))} e^{-\mu \tau_I(t)} \beta_I M(t - \tau_I(t)) - (\gamma_I + \mu) I(t). \quad (2.12)$$

Effector dynamics

The effector dynamics are the easiest because there is neither transcription nor translation involved. Rather the production of the effector is assumed to be proportional to the intermediate level i at a rate β_E , while the effector is destroyed at a rate γ_E . Thus

$$\frac{de}{dt}(t) = \beta_E i(t) - \gamma_E e(t), \qquad (2.13)$$

and, changing the description from numbers to concentrations, we have simply that

$$\frac{dE}{dt}(t) = \beta_E I(t) - (\gamma_E + \mu)E(t). \tag{2.14}$$

Putting it all together

Denote the transcriptional velocity by $v_M(E(t))$ and the translational velocity by $v_I(M(t))$. Further let $\bar{\gamma}_M = \gamma_M + \mu$, $\bar{\gamma}_I = \gamma_I + \mu$, $\bar{\gamma}_E = \gamma_E + \mu$. Then we can write the state dependent forms of (2.4)–(2.6) as

$$\frac{dM}{dt}(t) = \beta_M e^{-\mu \tau_M(t)} \frac{v_M(E(t))}{v_M(E(t - \tau_M(t)))} f(E(t - \tau_M(t))) - \bar{\gamma}_M M(t), \quad (2.15)$$

$$\frac{dI}{dt}(t) = \beta_I e^{-\mu \tau_I(t)} \frac{v_I(M(t))}{v_I(M(t - \tau_I(t)))} M(t - \tau_I(t)) - \bar{\gamma}_I I(t), \tag{2.16}$$

$$\frac{dE}{dt}(t) = \beta_E I(t) - \bar{\gamma}_E E(t). \tag{2.17}$$



2 Page 10 of 74 T. Gedeon et al.

These equations are supplemented by the two additional equations which define the delays τ_M and τ_I by threshold conditions, namely

$$a_M = \int_{t-\tau_M(t)}^t v_M(E(s)) ds = \int_{-\tau_M(t)}^0 v_M(E(t+s)) ds$$
 (2.18)

$$a_I = \int_{t-\tau_I(t)}^t v_I(M(s)) ds = \int_{-\tau_I(t)}^0 v_I(M(t+s)) ds.$$
 (2.19)

We write $\tau_M(t)$ and $\tau_I(t)$ for the state-dependent delays, but from (2.18) and (2.19) it is clear that the value of each is determined by the values of E(t) or M(t) respectively over the whole integration interval. Using the Banach space notation of the Appendices we ought to write $\tau_M(E_t)$ and $\tau_I(M_t)$ for these delays where E_t and M_t are functions defined by $E_t(\theta) = E(t-\theta)$ and $M_t(\theta) = M(t-\theta)$. But, to hopefully make the presentation accessible to readers who are not comfortable with Banach spaces, we will avoid any Banach space notation in the main body of the text and continue to write $\tau_M(t)$ and $\tau_I(t)$ for the delays at time t.

Velocity ratio terms such as those appearing in (2.15) and (2.16) are ubiquitous in distributed state-dependent DDE problems with either threshold conditions (Craig et al. 2016) or with randomly distributed maturation times (Cassidy et al. 2019). Bernard (2016) explains very clearly why they arise.

2.4 The control of transcription initiation rates

The determination of how effector concentrations modify the fraction of free operator sites, f, has been dealt with by a number of authors. Here we merely summarize the nature of f for inducible and repressible systems, see Mackey et al. (2016, Chapter 1) for details.

For a repressible operon, f is a monotone decreasing function

$$f(E) = \frac{1 + K_1 E^n}{1 + K E^n},\tag{2.20}$$

where $K > K_1$, n > 1, so there is maximal repression for large E. For an inducible system f is a monotone increasing function of the form

$$f(E) = \frac{1 + K_1 E^n}{K + K_1 E^n},\tag{2.21}$$

where K > 1, n > 1. Maximal induction occurs for very large E.

Note that both (2.20) and (2.21) are special cases of

$$f(E) = \frac{1 + K_1 E^n}{A + B E^n} \tag{2.22}$$

The constants $A, B \ge 0$ are defined in Table 1.



2.5 Transcriptional and translational velocities

In this section we discuss cellular processes that affect the transcriptional and translational velocities v_M and v_I . Both transcription and translation are polymerization processes where small parts are associated by an enzymatic reaction catalyzed by a large complex into a long polymer chain.

For the transcription process nucleotides A,C,G,T are incorporated by RNA polymerase (RNAP) into an mRNA chain, and for the translation process peptides are incorporated by ribososomes into a polypeptide that, upon folding, becomes a functional protein. Velocities of both processes depend on a sufficient and timely supply of nucleotides and peptides, respectively. The availability, or paucity, of the parts may result in changes in velocity from position to position along the strand (Zia et al. 2011). The abundance of the parts reflects the overall growth rate of the cell: faster growth leads to greater demand on resources and a slower transcription (v_M) and translation (v_I) velocity. Therefore for an inducible operon, the transcription velocity $v_M(E)$ is a decreasing function of the concentration of the effector E and for a repressible operon $v_M(E)$ is an increasing function of the concentration of the effector E.

The velocity of translation depends on the number of initiations of the translation process, which is directly proportional to the concentration M of mRNA. Since greater demand on peptide availability results in a lower elongation velocity of ribosomes, the translational velocity of ribosomes $v_I(M)$ is a decreasing function of M.

There is a second effect that may affect elongation velocity. This is the effect of elongation interference by multiple RNAP or multiple ribosomes (Klumpp and Hwa 2008; Klumpp 2011). The velocity of elongation decreases with the number of RNAPs and ribosomes that elongate at the same time. Since this number is proportional to the initiation rate, the velocity $v_M = v_M(E)$ is a decreasing function of the concentration of E for an inducible operon and an increasing function of the concentration of E for a repressible operon. The velocity $v_I(M)$ is a decreasing function of M.

Both availability of nucleotides and peptides and elongation interference support the following assumptions on the velocities v_M and v_I :

```
v_M = v_M(E) is a decreasing function of E for an inducible operon v_M = v_M(E) is an increasing function of E for a repressible operon v_I = v_I(M) is always a decreasing function of M.
```

There are no analytic expressions for the dependence of $v_M(E)$ and $v_I(M)$ on E and M respectively, but we have made assumptions for modeling purposes and these are detailed in Table 1. Specifically we have assumed that they can be represented by Hill functions with parameters determining the maximum, minimum and half-maximal values as well as a parameter $(m \text{ or } m_I)$ which controls the slope. We do not offer any detailed stoichiometric justification for these assumptions, but rather assume that they will capture the essential nature of their dependencies.

The parameters v_M^{min} , v_I^{min} describe minimal velocity of transcription and translation, respectively. While the individual polymerases and ribosomes may briefly pause their elongation, in our model where M, I model concentrations in a large population



2 Page 12 of 74 T. Gedeon et al.

Table 1 Summary of the form of the fraction f of free operators as determined by their stoichiometry, and the Hill function forms we have assumed for the transcriptional and translational velocities

Quantity	Repressible (e.g. tryp)	Inducible (e.g. lac)	
Fraction $f(E)$ of free operators	$f(E) = \frac{1 + K_1 E^n}{1 + K E^n}$	$f(E) = \frac{1 + K_1 E^n}{K + K_1 E^n}$	
Qualitative behaviour of f	Monotone ↓	Monotone ↑	
	Max = 1	Min = 1/K < 1	
	$Min = K_1/K < 1$	Max = 1	
Transcription velocity $v_M(E)$	$v_M(E) = \frac{v_M^{min} E_{50}^m + v_M^{max} E^m}{E_{50}^m + E^m}$	$v_M(E) = \frac{v_M^{max} E_{50}^m + v_M^{min} E^m}{E_{50}^m + E^m}$	
	$Min at E = 0 is v_M^{min}$	Max at $E = 0$ is v_M^{max}	
	$v_M(E_{50}) = \frac{1}{2}(v_M^{max} + v_M^{min})$	$v_M(E_{50}) = \frac{1}{2}(v_M^{max} + v_M^{min})$	
	Max as $E \to \infty$ is $v_M^{max} > v_M^{min}$	Min as $E \to \infty$ is $v_M^{min} < v_M^{max}$	
Qualitative τ_M behaviour	Monotone \downarrow with E	Monotone \uparrow with E	
Translation velocity $v_I(M)$	$v_I(M) = \frac{v_I^{max} M_{50}^{mI} + v_I^{min} M^{mI}}{M_{50}^{mI} + M^{mI}}$		
	Max at $M = 0$ is v_I^{max}		
	$v_I(M_{50}) = \frac{1}{2}(v_I^{max} + v_I^{min})$		
	Min as $M \to \infty$ is $v_I^{min} < v_I^{max}$		
Qualitative τ_I behaviour	Monotone \uparrow with M		

of cells,l we assume $v_I^{min} > 0$ and $v_M^{min} > 0$. Violation of this assumption would cause significant problems both with our theory and numerical simulations. The minimal velocity being strictly positive ensures that the maximal delay is bounded since from (2.18) and (2.19)

$$\tau_M(t) \le \frac{a_M}{v_M^{min}}, \qquad \tau_I(t) \le \frac{a_I}{v_I^{min}}.$$

Similarly the maximal velocities define the minimal delays. Interesting dynamics can occur when delays become large and in what follows we will often take v_M^{min} as a bifurcation parameter and study what happens as $v_M^{min} \to 0$ and consequently $\tau_M(t)$ becomes large.

2.6 Equilibria

We next consider the steady states (M^*, I^*, E^*) of (2.15)–(2.19). From (2.18) and (2.19) at steady state the delays satisfy

$$\tau_M = \tau_M^*(E^*) := \frac{a_M}{v_M(E^*)}, \quad \tau_I = \tau_I^*(M^*) := \frac{a_I}{v_I(M^*)}.$$
(2.23)



Then, at the steady state, equations (2.15)–(2.17) simplify to

$$0 = \beta_M e^{-\mu \tau_M^*(E^*)} f(E^*) - \bar{\gamma}_M M^*, \qquad (2.24)$$

$$0 = \beta_I e^{-\mu \tau_I^* (M^*)} M^* - \bar{\gamma}_I I^*, \tag{2.25}$$

$$0 = \beta_E I^* - \bar{\gamma}_E E^*. \tag{2.26}$$

We rearrange (2.24) to obtain

$$M^* = \frac{\beta_M}{\bar{\gamma}_M} e^{-\mu \tau_M^*(E^*)} f(E^*), \tag{2.27}$$

and then substituting this and (2.26) into (2.25) we find that the steady state must satisfy a single equation for E^* :

$$0 = g_E(E^*) := \frac{\beta_M \beta_I \beta_E}{\bar{\gamma}_M \bar{\gamma}_I \bar{\gamma}_E} e^{-\mu(\tau_I^*(M^*) + \tau_M^*(E^*))} f(E^*) - E^*$$
 (2.28)

where the argument of τ_I^* is given by (2.27).

With the functions v_M , v_I and f defined as in Table 1 then $v_M(E) \in [v_M^{min}, v_M^{max}]$ and $v_I(M) \in [v_I^{min}, v_I^{max}]$, so

$$\tau_M \in [a_M/v_M^{max}, a_M/v_M^{min}]$$
 and $\tau_I \in [a_I/v_I^{max}, a_I/v_I^{min}]$

while $f(E) \in (0, 1]$. Thus $g_E(0) > 0$ and

$$g_E(E) \leq \frac{\beta_M \beta_I \beta_E}{\bar{\gamma}_M \bar{\gamma}_I \bar{\gamma}_E} - E.$$

Therefore, $g_E(E) < 0$ for all E sufficiently large, and by the intermediate value theorem there is at least one solution $E^* > 0$ to $g_E(E^*) = 0$. This defines a steady state (M^*, I^*, E^*) . It also follows that any steady-state solution must satisfy

$$E^* \leq \frac{\beta_M \beta_I \beta_E}{\bar{\gamma}_M \bar{\gamma}_I \bar{\gamma}_E}, \qquad I^* \leq \frac{\beta_M \beta_I}{\bar{\gamma}_M \bar{\gamma}_I}.$$

If there is no cell growth, and thus $\mu=0$, and/or if both delays are constant and independent of the state-variables $(v_M^{max}=v_M^{min})$ and $v_I^{max}=v_I^{min}$ then equation (2.28) reduces to the form

$$0 = g_E(E) = C_{\beta\gamma} f(E) - E \tag{2.29}$$

for a suitably defined constant $C_{\beta\gamma} > 0$. The solutions of (2.29) and similar equations are well-studied in the context of monotone-cyclic feedback systems both with and without constant delay (Othmer 1976; Tyson and Othmer 1978; Yildirim et al. 2004). For the repressible case f(E) is monotone decreasing, hence $g_E(E)$ is also monotone



2 Page 14 of 74 T. Gedeon et al.

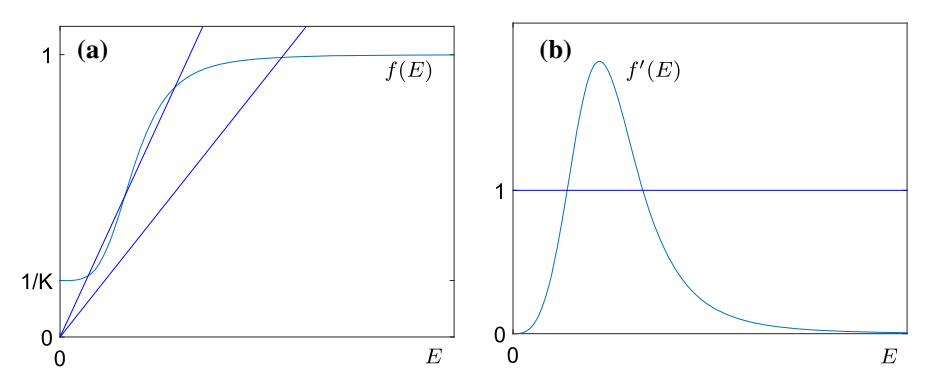


Fig. 2 Inducible constant delays with f as defined in Table 1. **a** Illustration of one or three solutions to (2.29) for different values of $C_{\beta\gamma}$. **b** Because f' is unimodal g'(E) has at most two sign changes so (2.29) cannot have more than three solutions

decreasing and there is a unique steady state. For the inducible case f(E) is non-negative and monotone increasing. Here the number of steady states depends on the exact form of f. With f defined as in Table 1, which has a unique inflection point with f''(E) = 0 and E > 0, there will be at most three steady states as shown in Yildirim et al. (2004) and illustrated in Fig. 2.

In many DDEs the delay(s) only appears in the state variables, and so do not affect the computation of the steady states. This is also the case with our model when $\mu=0$, and the computation of the steady states from (2.24)–(2.26) is independent of the delays in that case.

With state-dependent delays and cell growth, and thus $\mu > 0$, the behaviour of the model (2.15)–(2.19) is quite different. Now, the delays τ_I and τ_M enter explicitly into (2.15)–(2.19) and hence (2.28). While the delay will be constant in time on any steady-state solution, with state-dependent delays the value of the delay will depend on the state variable, which may change the structure of the phase-space of the dynamical system.

As an example consider the repressible case with state-dependent transcription velocity (but constant translation velocity). From Table 1 the transcription velocity $v_M(E)$ is a monotonic increasing function of E, and hence at steady state (from (2.23)) the transcription delay is a monotonic decreasing function of E. Then $g_E(E^*)$ contains the product of a monotonic increasing function $e^{-\mu \tau_M^*(E^*)}$ and monotonic decreasing function $f(E^*)$. The product in $g_E(E)$ need not be monotonic and we can no longer conclude that there is a unique steady state for the repressible case. This is illustrated in panel (a) of Fig. 3 which shows an example where $g_E(E)$ has three zeros corresponding to three different steady states of the model for the repressible case.

For an inducible operon, the situation is reversed. The velocity $v_M(E)$ is a decreasing function and so $e^{-\mu \tau_M^*(E^*)}$ a decreasing function of E^* , while the function $f(E^*)$ is an increasing function of its argument. This can again lead to additional steady states and Fig. 3b shows an example where $g_E(E)$ has five zeros corresponding to five different steady states in the model for the inducible case with state-dependent



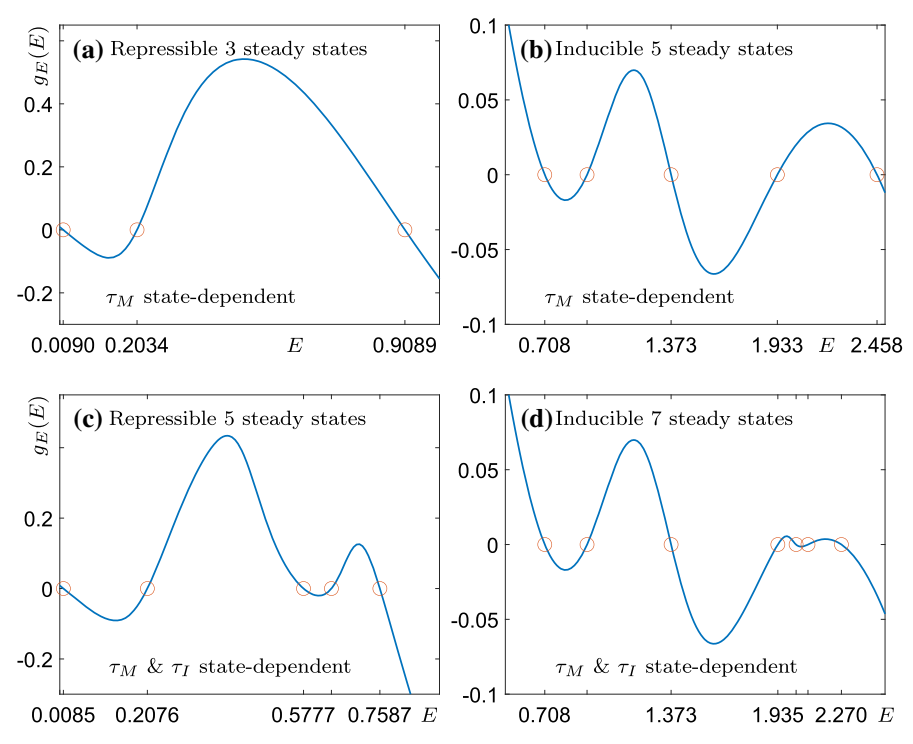


Fig. 3 Examples of the function $g_E(E)$ defined by (2.28) with functions defined in Table 1. **a** and **b** show a repressible and an inducible example with a single state-dependent delay, and parameter values given in Table 2. **c** and **d** show examples with two state-dependent delays with the same parameter values, except for those stated in (2.30) and (2.31) respectively

transcription velocity, but constant translation velocity. The full parameter sets for both of these examples are listed in Table 2.

In the previous examples we set $v_I^{min}=v_I^{max}=v_I$ so the translation velocity $v_I(M)=v_I$ was constant, as was the translation delay $\tau_I=a_I/v_I$. If we allow $v_I^{min}< v_I^{max}$ then the translation delay $\tau_I(M)$ becomes a second state-dependent delay, and in $g_E(E^*)$ the term $e^{-\tau_M^*(E^*)})f(E^*)$ is multiplied by an additional term $e^{-\mu(\tau_I^*(M^*))}$. With the translation velocity defined as in Table 1 we see that $e^{-\mu(\tau_I^*(M^*))}$ is a monotonic increasing function of M^* . However, M^* itself is defined by (2.27) which again contains the product of $e^{-\tau_M^*(E^*)}$ and $f(E^*)$ that we already discussed above. Although a full analysis of this case is beyond the scope of this paper, we note that by changing a few parameters from their values in Table 2 it is possible to obtain additional steady states. For the repressible case with

$$K = 10, \quad n = 10, \quad v_I^{min} = 0.05, \quad v_I^{max} = 0.5.$$
 (2.30)

and with both the delays $\tau_M^*(E^*)$ and $\tau_I^*(M^*)$ state-dependent, we obtain 5 co-existing steady states, as shown in Fig. 3c. For the inducible case with



2 Page 16 of 74 T. Gedeon et al.

Table 2 Parameters used for repressible and inducible examples in **a** and **b** of Fig. 3a, b

Quantity	Repressible	Inducible
μ	0.05	0.034
β_M	1.4	1
β_I	1	2
β_E	1	3
$\bar{\gamma}_M$	1	0.994
$\bar{\gamma}_I$	1	0.994
$ar{\gamma}_E$	1	0.994
K	2	10
K_1	1	1
n	5	4
m	3	10
a_M	1	1
v_M^{min}	0.01	0.05
v_M^{max}	2	1
E_{50}	1	1
m_I	20	80
a_I	1	1
v_I^{min}	1	2
v_I^{max}	1	2
M_{50}	1	0.3374

$$v_I^{min} = 1.1. (2.31)$$

we obtain 7 co-existing steady states, where again both delays are state-dependent. Taken together the examples of Fig. 3 suggest that there can be

$$1 + 2\chi_I + 2n_\tau$$
, $\chi_I = \begin{cases} 0, \text{ repressible case} \\ 1, \text{ inducible case} \end{cases}$ (2.32)

steady states where n_{τ} is the number of delays which are state-dependent. We cannot prove that this is the maximum possible number of steady states, but we can construct examples with this many steady states in a systematic way.

We illustrate this by showing how the example of the inducible operon with two state-dependant delays and 7 steady states in Fig. 3d is constructed from the example with one state-dependent delay and 5 steady states in Fig. 3b. The only difference between the two examples is that in (2.28) the term $e^{-\mu \tau_I^*(M)}$ is constant in the first example, but not in the second. To make τ_I state-dependent we take $v_I^{min} < v_I^{max}$ and $m_I \gg 0$, so that the translation velocity $v_I(M)$ is close to a step function, which results in $e^{-\mu \tau_I^*(M^*)}$ also being essentially a switching function. In Fig. 3 we identify that for $E \approx 2$ we have $0 < g_E(E) \ll 1$ with $g_E'(E) > 0$, and we set the switching function to act at this point by using (2.27) to define M_{50} via



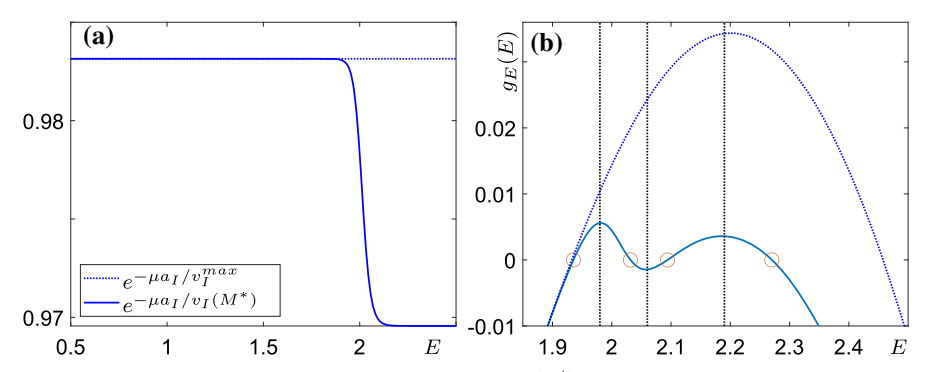


Fig. 4 a For the inducible model, the constant function $e^{-\mu\tau_I(M^*)}$ (broken line) as in Fig. 3b, and the state-dependent function $e^{-\mu\tau_I(M^*)}$ (solid line) as in Fig. 3b. **b** The behaviour of the corresponding functions $g_E(E)$ for $E \approx 2$. The black vertical lines separate the intervals on which $g_E(E)$ is increasing or decreasing

$$M_{50} = \frac{\beta_M}{\bar{\gamma}_M} e^{-\mu \tau_M^*(2)} f(2).$$

Then using (2.27) directly we obtain $e^{-\mu \tau_I^*(M^*)}$ as a function of E^* as shown in Fig. 4a. With this element included in $g_E(E^*)$ the function is modified so that $g_E'(2) < 0$, and the function gains an additional maximum and minimum for $E \approx 2$, as shown in Fig. 4b. From there, parameters can be adjusted as needed to ensure $g_E(E)$ has a zero between each sign change of $g_E'(E)$.

The function g_E can be used to effectively perform a one-parameter continuation of the steady states by varying E and one other parameter, and plotting a single contour of the function corresponding to $g_E=0$. In Fig. 5 we demonstrate four examples of one-parameter continuation in the parameter v_M^{min} starting from the cases illustrated in Fig. 3. Given that we obtained our examples with several co-existing steady states by constructing the function $g_E(E)$ to have multiple nearby zeros, and hence multiple local extrema close to zero, it should be no surprise to see that the steady states from Fig. 3 only co-exist over a small interval of v_M^{min} values and that some of them are destroyed in fold bifurcations. We note also that as v_M^{min} is increased, in the limit as $v_M^{min} \to v_M^{max}$ the delay τ_M becomes constant, and by (2.32) the number of steady states will be reduced. In particular in the cases of Fig. 5a, b when $v_M^{min} = v_M^{max}$ there is no state-dependency in the model and there can only be 1 or 3 steady states in the repressible and inducible cases, respectively.

Figure 5 indicates that the steady states of (2.15)–(2.19) undergo fold bifurcations. Hopf bifurcations are also ubiquitous in DDEs, and already known to occur in the repressible case with constant delays. Hence in the following sections we will study the dynamics and bifurcations of the system (2.15)–(2.19) and will return to the examples of this section.



2 Page 18 of 74 T. Gedeon et al.

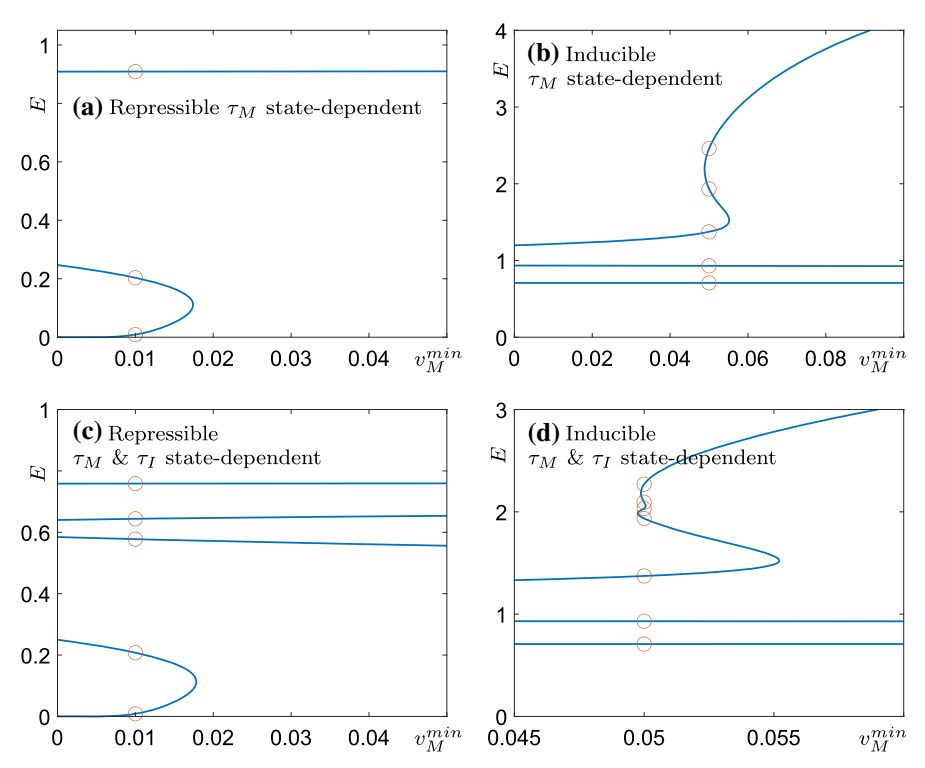


Fig. 5 One parameter continuations of the steady states as the parameter v_M^{min} is varied, obtained by plotting the zero contour of the function g_E . All the other parameters take the same values as in the corresponding panel of Fig. 3. The red circles indicate the co-existing steady states already seen in Fig. 3. In the limit as $v_M^{min} \rightarrow v_M^{max}$ the delay τ_M ceases to be state-dependent (color figure online)

2.7 Linearization by expansion

To determine the stability of the steady states considered Sect. 2.6, we linearize the system (2.15)–(2.17) with (2.18) and (2.19) in a neighborhood of each steady state and examine the nature of the characteristic values.

This can be done rigorously using a functional analytic approach in an appropriate Banach space, and this derivation is presented in "Appendix C". However, that approach will not be accessible to many readers, so here we present an alternative heuristic derivation using elementary techniques which arrives at exactly the same characteristic equation as in "Appendix C".

Assuming linear behaviour of the solution for a small perturbation from the steady state (M^*, I^*, E^*) , we begin by setting

$$M(t) = M^* + \mathcal{E}_M e^{\lambda t}, \tag{2.33}$$

$$I(t) = I^* + \mathcal{E}_I e^{\lambda t}, \tag{2.34}$$

$$E(t) = E^* + \mathcal{E}_E e^{\lambda t}. \tag{2.35}$$



We denote the delays at the steady state by $\tau_M^*(E^*)$ and $\tau_I^*(M^*)$, as defined in (2.23), and again write $\tau_M(t)$ and $\tau_I(t)$ for the time varying delays on a solution close to the steady state (even though as noted after (2.19) these delay terms are properly functions in a Banach space).

From the threshold condition (2.18), Taylor expanding the integrand around the steady state we obtain

$$v_{M}(E^{*})\tau_{M}^{*}(E^{*}) = a_{M} = \int_{t-\tau_{M}(t)}^{t} v_{M}(E(s))ds = \int_{-\tau_{M}(t)}^{0} v_{M}(E(s+t))ds$$

$$= \int_{-\tau_{M}(t)}^{0} v_{M}(E^{*} + \mathcal{E}_{E}e^{\lambda(s+t)})ds$$

$$= \int_{-\tau_{M}(t)}^{0} v_{M}(E^{*}) + v'_{M}(E^{*})\mathcal{E}_{E}e^{\lambda(s+t)} + \mathcal{O}(\mathcal{E}_{E}^{2})ds$$

$$= v_{M}(E^{*})\tau_{M}(t) + \mathcal{E}_{E}v'_{M}(E^{*})e^{\lambda t} \int_{-\tau_{M}(t)}^{0} e^{\lambda s}ds + \mathcal{O}(\mathcal{E}_{E}^{2}). \quad (2.36)$$

Note that for $\lambda \neq 0$,

$$\int_{-a}^{0} e^{\lambda s} \, ds = \frac{1}{\lambda} (1 - e^{-a\lambda}) \tag{2.37}$$

while

$$\lim_{\lambda \to 0} \frac{1}{\lambda} (1 - e^{-a\lambda}) = a = \int_{-a}^{0} e^{0s} \, ds,$$

so $(1 - e^{-a\lambda})/\lambda$ has a removable singularity at $\lambda = 0$. Therefore we can use (2.37) for all $\lambda \in \mathbb{C}$ and (2.36) becomes

$$v_{M}(E^{*})\tau_{M}^{*}(E^{*}) = v_{M}(E^{*})\tau_{M}(t) + \mathcal{E}_{E}e^{\lambda t} \frac{v_{M}^{\prime}(E^{*})}{\lambda} (1 - e^{-\lambda \tau_{M}(t)}) + \mathcal{O}(\mathcal{E}_{E}^{2}).$$
 (2.38)

Notice that $v_M(E^*) > 0$ is required for $\tau_M(E^*)$, defined by (2.23), to be finite; this is ensured by the assumption that $v_M^{min} > 0$. Hence we may rearrange (2.38) as

$$\tau_{M}(t) = \tau_{M}^{*}(E^{*}) - \mathcal{E}_{E}e^{\lambda t} \frac{v_{M}'(E^{*})}{\lambda v_{M}(E^{*})} (1 - e^{-\lambda \tau_{M}(t)}) + \mathcal{O}(\mathcal{E}_{E}^{2}).$$

Noting that this implies that $\tau_M(t) = \tau_M^*(E^*) + \mathcal{O}(\mathcal{E}_E)$, we obtain

$$\tau_M(t) = \tau_M^*(E^*) - \mathcal{E}_E e^{\lambda t} \frac{v_M'(E^*)}{\lambda v_M(E^*)} (1 - e^{-\lambda \tau_M^*(E^*)}) + \mathcal{O}(\mathcal{E}_E^2). \tag{2.39}$$

With (2.39), the factor $e^{-\mu \tau_M(t)}$ in (2.15) behaves as



2 Page 20 of 74 T. Gedeon et al.

$$\begin{split} e^{-\mu\tau_{M}(t)} &= e^{-\mu\tau_{M}^{*}(E^{*})} e^{\mathcal{E}_{E} \frac{\mu\nu_{M}'(E^{*})}{\lambda\nu_{M}(E^{*})}} e^{\lambda t} (1 - e^{-\lambda\tau_{M}^{*}(E^{*})}) e^{-\mu\mathcal{O}(\mathcal{E}_{E}^{2})} \\ &= e^{-\mu\tau_{M}^{*}(E^{*})} \left[1 + \mathcal{E}_{E} \frac{\mu\nu_{M}'(E^{*})}{\lambda\nu_{M}(E^{*})} e^{\lambda t} (1 - e^{-\lambda\tau_{M}^{*}(E^{*})}) + \mathcal{O}(\mathcal{E}_{E}^{2}) \right] \left[1 + \mathcal{O}(\mathcal{E}_{E}^{2}) \right] \\ &= e^{-\mu\tau_{M}^{*}(E^{*})} \left[1 + \mathcal{E}_{E} \frac{\mu\nu_{M}'(E^{*})}{\lambda\nu_{M}(E^{*})} e^{\lambda t} (1 - e^{-\lambda\tau_{M}^{*}(E^{*})}) \right] + \mathcal{O}(\mathcal{E}_{E}^{2}). \end{split} \tag{2.40}$$

For the fraction term $v_M(E)/v_M(E(t-\tau_M(t)))$ in the differential equation, we apply Taylor expansion around the steady state to $v_M(E)$ and $1/v_M(E(t-\tau_M(t)))$ separately and then take the product, which gives:

$$\begin{aligned} v_M(E) &= v_M(E^*) + v_M'(E^*) \mathcal{E}_E e^{\lambda t} + \mathcal{O}(\mathcal{E}_E^2), \\ \frac{1}{v_M(E(t - \tau_M(t)))} &= \frac{1}{v_M(E^*)} + \left(-\frac{v_M'(E^*)}{v_M(E^*)^2} \right) \mathcal{E}_E e^{\lambda (t - \tau_M(t))} + \mathcal{O}(\mathcal{E}_E^2). \end{aligned}$$

Thus

$$\frac{v_M(E)}{v_M(E(t-\tau_M(t)))} = 1 + \mathcal{E}_E \frac{v_M'(E^*)}{v_M(E^*)} e^{\lambda t} (1 - e^{-\lambda \tau_M(t)}) + \mathcal{O}(\mathcal{E}_E^2)
= 1 + \mathcal{E}_E \frac{v_M'(E^*)}{v_M(E^*)} e^{\lambda t} (1 - e^{-\lambda \tau_M^*(E^*)}) + \mathcal{O}(\mathcal{E}_E^2).$$
(2.41)

Following the derivation of (2.40) and (2.41), similarly we have

$$e^{-\mu\tau_{I}(t)} = e^{-\mu\tau_{I}^{*}(M^{*})} \left[1 + \mathcal{E}_{M} \frac{\mu v_{I}'(M^{*})}{\lambda v_{I}(M^{*})} e^{\lambda t} (1 - e^{-\lambda\tau_{I}^{*}(M^{*})}) \right] + \mathcal{O}(\mathcal{E}_{M}^{2}), (2.42)$$

$$\frac{v_{I}(M)}{v_{I}(M(t - \tau_{I}(t)))} = 1 + \mathcal{E}_{M} \frac{v_{I}'(M^{*})}{v_{I}(M^{*})} e^{\lambda t} (1 - e^{-\lambda\tau_{I}^{*}(M^{*})}) + \mathcal{O}(\mathcal{E}_{M}^{2}). (2.43)$$

Now we use these expansions to linearize the system (2.15)–(2.17) equation by equation. Substituting the perturbations (2.33) and (2.35) into (2.15) and using the expansions (2.40) and (2.41) we have

$$\begin{split} \mathcal{E}_{M}\lambda e^{\lambda t} &= \frac{d}{dt}(M^* + \mathcal{E}_{M}e^{\lambda t}) \\ &= \beta_{M} \left[e^{-\mu\tau_{M}^*(E^*)} \left(1 + \mathcal{E}_{E} \frac{\mu v_{M}'(E^*)}{\lambda v_{M}(E^*)} e^{\lambda t} (1 - e^{-\lambda\tau_{M}^*(E^*)}) \right) + \mathcal{O}(\mathcal{E}_{E}^2) \right] \times \\ & \left[1 + \mathcal{E}_{E} \frac{v_{M}'(E^*)}{v_{M}(E^*)} e^{\lambda t} (1 - e^{-\lambda\tau_{M}(E^*)}) + \mathcal{O}(\mathcal{E}_{E}^2) \right] f(E^* + \mathcal{E}_{E}e^{\lambda(t - \tau_{M}(t))}) \\ & - \bar{\gamma}_{M}(M^* + \mathcal{E}_{M}e^{\lambda t}) \\ &= \beta_{M}e^{-\mu\tau_{M}^*(E^*)} \left[1 + \mathcal{E}_{E} \frac{v_{M}'(E^*)}{v_{M}(E^*)} e^{\lambda t} (1 - e^{-\lambda\tau_{M}^*(E^*)}) (1 + \frac{\mu}{\lambda}) \right] \times \\ & \left[f(E^*) + \mathcal{E}_{E} f'(E^*) e^{\lambda(t - \tau_{M}(t))} \right] - \bar{\gamma}_{M}(M^* + \mathcal{E}_{M}e^{\lambda t}) + \mathcal{O}(\mathcal{E}_{E}^2) \end{split}$$



$$= \beta_{M} e^{-\mu \tau_{M}^{*}(E^{*})} \left(f(E^{*}) + \mathcal{E}_{E} f(E^{*}) \frac{v_{M}^{\prime}(E^{*})}{v_{M}(E^{*})} e^{\lambda t} (1 - e^{-\lambda \tau_{M}^{*}(E^{*})}) (1 + \frac{\mu}{\lambda}) \right. \\ \left. + \mathcal{E}_{E} f^{\prime}(E^{*}) e^{\lambda (t - \tau_{M}^{*}(E^{*}))} \right) - \bar{\gamma}_{M} (M^{*} + \mathcal{E}_{M} e^{\lambda t}) + \mathcal{O}(\mathcal{E}_{E}^{2}).$$

Using the equality (2.24) and multiplying by $e^{-\lambda t}$, this simplifies to

$$\mathcal{E}_{M}\lambda = \mathcal{E}_{E}\beta_{M}e^{-\mu\tau_{M}^{*}(E^{*})}\left(f(E^{*})\frac{v_{M}'(E^{*})}{v_{M}(E^{*})}(1 - e^{-\lambda\tau_{M}^{*}(E^{*})})(1 + \frac{\mu}{\lambda}) + f'(E^{*})e^{-\lambda\tau_{M}^{*}(E^{*})}\right) - \mathcal{E}_{M}\bar{\gamma}_{M} + \mathcal{O}(\mathcal{E}_{E}^{2})$$
(2.44)

For the second differential Eq. (2.16), substituting the perturbation (2.33) and (2.34) and the expansion (2.42) and (2.43) we similarly find that

$$\begin{split} \mathcal{E}_{I}\lambda e^{\lambda t} &= \frac{d}{dt}(I^* + \mathcal{E}_{I}e^{\lambda t}) \\ &= \beta_{I}e^{-\mu\tau_{I}^{*}(M^{*})} \bigg(M^* + \mathcal{E}_{M}e^{\lambda(t-\tau_{I}^{*}(M^{*}))} + \mathcal{E}_{M}M^* \frac{v_{I}'(M^{*})}{v_{I}(M^{*})} \times \\ &e^{\lambda t} (1 - e^{-\lambda\tau_{I}^{*}(M^{*})}) (1 + \frac{\mu}{\lambda}) \bigg) - \bar{\gamma}_{I}(I^* + \mathcal{E}_{I}e^{\lambda t}) + \mathcal{O}(\mathcal{E}_{M}^{2}). \end{split}$$

Using the equality (2.25) and multiplying by $e^{-\lambda t}$ we obtain

$$\mathcal{E}_{I}\lambda = \mathcal{E}_{M}\beta_{I}e^{-\mu\tau_{I}^{*}(M^{*})}\left(e^{-\lambda\tau_{I}^{*}(M^{*})} + M^{*}\frac{v_{I}'(M^{*})}{v_{I}(M^{*})}(1 - e^{-\lambda\tau_{I}^{*}(M^{*})})(1 + \frac{\mu}{\lambda})\right) - \bar{\gamma}_{I}\mathcal{E}_{I} + \mathcal{O}(\mathcal{E}_{M}^{2}). \tag{2.45}$$

Lastly, the case of the differential equation (2.17) is simpler, since it is linear with no delays. Substituting the perturbations (2.34) and (2.35) we have

$$\mathcal{E}_E \lambda e^{\lambda t} = \frac{d}{dt} (E^* + \mathcal{E}_E e^{\lambda t}) = \beta_E (I^* + \mathcal{E}_I e^{\lambda t}) - \bar{\gamma}_E (E^* + \mathcal{E}_E e^{\lambda t}).$$

Using the equality (2.26), and multiplying by $e^{-\lambda t}$ this simplifies to

$$\mathcal{E}_E \lambda = \mathcal{E}_I \beta_E - \mathcal{E}_E \bar{\gamma}_E. \tag{2.46}$$

Combining (2.44), (2.45) and (2.46), and dropping the higher order terms gives the linear system

$$A(\lambda) \begin{pmatrix} \mathcal{E}_{M} \\ \mathcal{E}_{I} \\ \mathcal{E}_{E} \end{pmatrix} = \begin{pmatrix} -\bar{\gamma}_{M} - \lambda & 0 & A_{13} \\ A_{21} & -\bar{\gamma}_{I} - \lambda & 0 \\ 0 & \beta_{E} & -\bar{\gamma}_{E} - \lambda \end{pmatrix} \begin{pmatrix} \mathcal{E}_{M} \\ \mathcal{E}_{I} \\ \mathcal{E}_{E} \end{pmatrix} = 0 \qquad (2.47)$$



2 Page 22 of 74 T. Gedeon et al.

where the A_{13} and A_{21} entries of the 3 \times 3-matrix $A(\lambda)$ are defined by

$$\begin{split} A_{13} &= \beta_M e^{-\mu \tau_M^*(E^*)} \bigg(f(E^*) \frac{v_M'(E^*)}{v_M(E^*)} (1 - e^{-\lambda \tau_M^*(E^*)}) (1 + \frac{\mu}{\lambda}) + f'(E^*) e^{-\lambda \tau_M^*(E^*)} \bigg), \\ A_{21} &= \beta_I e^{-\mu \tau_I^*(M^*)} \left(M^* \frac{v_I'(M^*)}{v_I(M^*)} (1 - e^{-\lambda \tau_I^*(M^*)}) (1 + \frac{\mu}{\lambda}) + e^{-\lambda \tau_I^*(M^*)} \right). \end{split}$$

The characteristic equation of (2.15)–(2.17) is

$$\Delta(\lambda) = \det(A(\lambda)) = 0, \tag{2.48}$$

with $\Delta(\lambda)$ given by

$$\Delta(\lambda) = (\bar{\gamma}_M + \lambda)(\bar{\gamma}_I + \lambda)(\bar{\gamma}_E + \lambda) + \beta_M \beta_I \beta_E e^{-\mu(\tau_I^*(M^*) + \tau_M^*(E^*))} k(\lambda), (2.49)$$

where

$$k(\lambda) = \left(\frac{v_M'(E^*)}{v_M(E^*)} f(E^*) (1 - e^{-\lambda \tau_M^*(E^*)}) \left(1 + \frac{\mu}{\lambda}\right) + f'(E^*) e^{-\lambda \tau_M^*(E^*)}\right) \times \left(\frac{v_I'(M^*)}{v_I(M^*)} M^* (1 - e^{-\lambda \tau_I^*(M^*)}) \left(1 + \frac{\mu}{\lambda}\right) + e^{-\lambda \tau_I^*(M^*)}\right)$$
(2.50)

Exactly the same characteristic equation is derived completely rigorously in "Appendices A–C" culminating in equation (C.12).

In contrast to the rigorous variational approach used in the appendices, here we assert without proof that all the quantities of interest can be written as functions of the perturbation parameters \mathcal{E}_M , \mathcal{E}_I and \mathcal{E}_E . For example in Eq. (2.39) we have Taylor expanded the state-dependent delay τ_M as a function of \mathcal{E}_E . To justify that rigorously requires functional analysis, and this is done in Proposition A1 in "Appendix A".

Another drawback of the derivation above is that there is no theory to show that stability of steady states is determined by the characteristic Eq. (2.48). However, since for our model both approaches lead to the same characteristic equation, the theory relating stability to the characteristic equation applies (Hartung et al. 2006). Therefore the stability of equilibria of the system (2.15)–(2.17) is determined by characteristic values arising from (2.48).

3 Numerical methods

In this section, we describe numerical methods to study the distributed state-dependent delay model (2.15)–(2.19). We would like to conduct one-parameter continuation of steady states and periodic orbits and compute local stability and bifurcations in Matlab (Mathworks 2020). The standard package for performing numerical bifurcation analysis of DDEs in Matlab is DDE-BIFTOOL (Sieber et al. 2015). Unfortunately, although it can handle constant or discrete state-dependent delays, DDE-BIFTOOL



cannot be applied directly to problems with distributed state-dependent delays defined by threshold conditions such as (2.18) and (2.19). Likewise, the built-in Matlab function ddesd for solving DDE initial value problems is also only implemented for discrete delays.

In Eqs. (2.18) and (2.19) the delay τ_M or τ_I can be determined by adjusting the lower limit of the integral until the integral has the desired value a_M . Naive numerical implementations would use a bisection or secant iteration to determine the delay, which would necessitate evaluating the integral at each step of the iteration. This would be very slow to compute and would become the main bottleneck slowing down numerical computations. Another problem in evaluating this integral is that the numerical DDE solvers that have been implemented in Matlab are all written for discrete delays and only give access to the value of the solution $u(t - \tau_j)$ at the discrete delays, whereas to evaluate the integral in (2.18) or (2.19) we require the values of the integrand across the whole interval.

We describe below two different implementations of (2.15)–(2.19) in DDE-BIFTOOL, neither of which require an iteration to find the delays, and also show how to apply ddesd to solve the initial value problem.

3.1 Steady state computations: linearization correction

As discussed in Sect. 2.6, we can obtain steady states of (2.15)–(2.19) from the scalar function $g_E(E^*)$ defined in (2.28). Any solution to $g_E(E^*) = 0$ gives the E component of a steady state with corresponding M and I components given by (2.24) and (2.26).

We would like to conduct one-parameter continuation of steady states and compute local stability using DDE-BIFTOOL, but as noted above it cannot be directly applied to solve DDEs when the delay is defined by a threshold condition. Nevertheless, at a steady state the threshold integral conditions (2.18) and (2.19) become integrals of constant functions. Consequently, the delays are defined by (2.23) and can be treated as discrete delays. Therefore we are able to implement the system (2.15)–(2.17) together with (2.23) in DDE-BIFTOOL and use it to continue the steady states. This approach also allows us to locate fold bifurcations of steady states. However, although replacing (2.18) and (2.19) by (2.23) preserves the existence of the steady states, (as detailed in Wang (2020) for a related model) characteristic values and hence stability of the steady state are altered. The reason is that the integration of exponential perturbations along the solution, see Sect. 2.7, are not included.

To recover the correct stability information when using the modified problem (2.15)–(2.17) with discrete delays (2.23) we perform linearization correction using the characteristic equation. The characteristic roots of the steady state of the modified problem are taken as "seed values" which are then corrected by applying the Matlab nonlinear system solver fsolve to the exact characteristic Eq. (2.48) for the original model (2.15)–(2.19). This works well at a majority of points along continuation branch; however, it behaves poorly at some points leading to spurious bifurcations. In addition, sometimes the algorithm does not converge, while sometimes the solver converges to an already found characteristic value. As well as creating duplicates of



characteristic values, this leads to missing some characteristic values, and so does not reliably classify bifurcations.

To deal with these issues, we remove any characteristic values at which the algorithm fails to converge, as well as any duplicate values. To resolve the issue of missing characteristic values, we use the corrected characteristic values from the previous point on the branch as a second set of "seed values" to compute additional characteristic values, where again we remove duplicates. The removal of duplicate characteristic values is somewhat dangerous, because it could result in missing genuine instances of characteristic values with multiplicity larger than one. However, in practice, we did not encounter this problem.

Once the corrected characteristic roots are computed at each steady state, we obtain the correct stability information. Hopf bifurcations occur when two complex conjugate characteristic values cross the imaginary axis, or equivalently when the number of complex characteristic values with positive real part changes by two. Fold bifurcations happen when a real characteristic value changes sign, which we can also detect by the number of complex characteristic values with positive real part changing by one. Because we obtain the stability from a modified problem and we did not alter any of the DDE-BIFTOOL subroutines which use linearization inappropriate for our model, we are not able to use additional DDE-BIFTOOL subroutines such as those that detect criticality of Hopf bifurcations and perform normal form computations.

3.2 Steady state and periodic orbit computation: delay discretization

While the approach of Sect. 3.1 allows us to compute the stability of steady states and hence to detect fold and Hopf bifurcations, it cannot be used to compute periodic orbits, because the delays (2.18)–(2.19) would not be constant on periodic orbits.

The only way to tackle the full distributed state-dependent delay operon model (2.15)–(2.19) is to evaluate the integrals in the threshold conditions (2.18)–(2.19). While this cannot be done exactly in DDE-BIFTOOL, it is enough to evaluate the integral to sufficient accuracy using a numerical quadrature scheme.

As the two delays are of similar form, we will describe the method for approximating τ_M by discretizing the integral in (2.18) using the composite trapezoidal method and seeking the value of τ_M that satisfies (2.18). To do this we introduce extra "dummy" delays as follows.

With a_M fixed and $v_M(E) \in [v_M^{min}, v_M^{max}]$, it follows that $\tau_M \in [a_M/v_M^{max}, a_M/v_M^{min}]$. To obtain the state-dependent delay τ_M that satisfies the threshold condition (2.18), we discretize the interval $[t - a_M/v_M^{max}, t]$ uniformly with a sequence of mesh points

$$t = x_0 > x_1 > \dots > x_N = t - \frac{a_M}{v_M^{max}}$$

and define N constant "dummy" delays

$$\tau_j = t - x_j = t - \frac{j}{N} \frac{a_M}{v_M^{max}}, \quad j = 1, 2, \dots, N.$$



In particular, as $\tau_M \ge a_M/v_M^{max}$, there is no need for detection of the delay τ_M over the interval $[t - a_M/v_M^{max}, t]$.

On the interval $[t - a_M/v_M^{min}, t - a_M/v_M^{max}]$ where the delay τ_M lies, we detect it as follows. Divide the interval $[t - a_M/v_M^{min}, t - a_M/v_M^{max}]$ into N equal width subintervals,

$$t - \frac{a_M}{v_M^{max}} = x_N > x_{N+1} > \dots > x_{2N} = t - \frac{a_M}{v_M^{min}},$$

which implies that

$$x_{N+j} = t - \frac{a_M}{v_M^{max}} - j \frac{a_M}{N} (\frac{1}{v_M^{min}} - \frac{1}{v_M^{max}}), \quad j = 1, 2, \dots, N.$$

We then define another N constant "dummy" delays

$$\tau_{N+j} = t - x_{N+j}, \quad j = 1, 2, \dots, N.$$

To compute τ_M , we take advantage of the functionality of DDE-BIFTOOL which allows state-dependent delays to be defined as functions of the other delays and the solution values at those delays. We let

$$J(j) = \int_{x_j}^{x_0} v_M(E(s)) ds = \int_{t-\tau_j}^t v_M(E(s)) ds, \quad j = 1, 2, \dots, 2N$$

and let $J_h(j)$ be the numerical approximation of J(j) using the composite trapezoidal rule,

$$J_h(j) = \sum_{k=1}^{j-1} \frac{1}{2} \left(v_M(E(x_k)) + v_M(E(x_{k+1})) \right) (x_k - x_{k+1}).$$

We look for the largest j such that $J_h(j) \leq a_M$. Since

$$\begin{split} a_M &> \int_{t-a_M/v_M^{max}}^t v_M(E(s)) ds \\ &\approx \frac{a_M}{N v_M^{max}} \left[\frac{1}{2} v_M(E(t)) + \frac{1}{2} v_M(E(t-\frac{a_M}{v_M^{max}})) + \sum_{j=1}^{N-1} v_M(E(t-\tau_j)) \right] \\ &= J_h(N), \end{split}$$

we successively add subintervals to the integral until we find j such that

$$a_M \ge J_h(j)$$
 and $a_M < J_h(j+1)$. (3.1)



2 Page 26 of 74 T. Gedeon et al.

With such a j, we have $\tau_M \in [\tau_j, \tau_{j+1})$. To locate τ_M more precisely, consider

$$a_M = \int_{t-\tau_M}^t v_M(E(s)) ds = \int_{t-\tau_M}^{t-\tau_j} v_M(E(s)) ds + \int_{t-\tau_j}^t v_M(E(s)) ds,$$

which implies

$$a_M - J_h(j) \approx \int_{t-\tau_M}^{t-\tau_j} v_M(E(s)) ds. \tag{3.2}$$

Applying the trapezoidal rule again, we have

$$\int_{t-\tau_M}^{t-\tau_j} v_M(E(s)) ds \approx \frac{\tau_M - \tau_j}{2} [v_M(E(t-\tau_M)) + v_M(E(t-\tau_j))], \quad (3.3)$$

and using a linearization in the subinterval (which is consistent with the trapezoidal method) we have

$$v_M(E(t - \tau_M)) = v_M(E(t - \tau_j)) + (\tau_M - \tau_j)[v_M(E(t - \tau_{j+1})) - v_M(E(t - \tau_j))].$$
(3.4)

Substituting (3.3) and (3.4) into (3.2) gives

$$a_M - J_h(j) \approx \frac{\tau_M - \tau_j}{2} [(2 + \tau_j - \tau_M) v_M (E(t - \tau_j)) + (\tau_M - \tau_j) v_M (E(t - \tau_{j+1}))].$$

Rearranging this we find that τ_M is given as the solution of $k(\tau_M) = 0$ where

$$k(\tau_M) = \frac{(\tau_M - \tau_j)^2}{2} [v_M(E(t - \tau_j)) - v_M(E(t - \tau_{j+1}))] - (\tau_M - \tau_j)v_M(E(t - \tau_j)) + (a_M - J_h(j))$$
(3.5)

Note that (3.5) is a quadratic function of τ_M and the condition (3.1) guarantees that $k(\tau_M)$ has a zero for $\tau_M \in [\tau_j, \tau_{j+1}]$. Applying the quadratic formula to (3.5), we obtain the solution

$$\tau_{M} = \tau_{j} + \frac{v_{M}(E(x_{j}))}{v_{M}(E(x_{j})) - v_{M}(E(x_{j+1}))} - \frac{\sqrt{v_{M}(E(x_{j})^{2} - 2(a_{M} - J_{h}(j))(v_{M}(E(x_{j})) - v_{M}(E(x_{j+1})))}}{v_{M}(E(x_{j})) - v_{M}(E(x_{j+1}))}$$
(3.6)

where the minus sign in the quadratic formula ensures that the root $\tau_M \in [\tau_j, \tau_{j+1}]$ when $k(\tau_M)$ is either a concave up or concave down parabola.



With this implementation we are able to apply DDE-BIFTOOL directly to an approximation to the system (2.15)–(2.19). Since the stability computations are carried out within DDE-BIFTOOL (as opposed to the linearization correction technique described in Sect. 3.1) we are able to use the full functionality of DDE-BIFTOOL which allows us to determine criticality of bifurcations and also to compute branches of periodic orbits emanating from Hopf bifurcations.

The choice of parameters for the numerical discretization is somewhat delicate. If the discretization is too coarse convergence issues arise in the branch continuation, while finer discretizations allow for a smoother continuation of branches with larger continuation steps, but at the cost of each step being very slow. This arises because the numerical linear algebra problems at the heart of the approximate Newton method in each DDE-BIFTOOL continuation step increase in complexity with both the number of delays and the size of the collocation problem. The total number of delays in the discretized problem is 2N + 2, composed of the 2N dummy delays, the (assumed constant) delay τ_I , and the computed state-dependent delay τ_M given by (3.6).

For the computations in Sect. 4 we use degree 4 or 5 collocation polynomials and 20 to 40 mesh intervals resulting in 80 to 200 collocation points on the periodic orbit. For stability computations of steady states we took N=32 which results in 65 constant delays and one state-dependent delay. For computation of periodic orbits we took N=48 resulting in close to one hundred delays in the discretized problem.

The computation of each step of the continuation is quite slow compared to the implementation of Sect. 3.1. The algorithms give consistent results on problems for which both can be applied (with bifurcation points agreeing to between 3 and 5 significant digits of accuracy), but the algorithm of this section is more widely applicable. For the results shown in Sect. 4, we mainly use the discretization method described in this section, with the linearization correction method of Sect. 3.1 used to validate the results.

3.3 Solving initial value problems (IVPs)

Simulating IVPs allows us to investigate the dynamics in parameter regimes where none of the steady states are stable. In Sect. 4 we find stable periodic orbits which do not arise from Hopf bifurcations by following this procedure.

The Matlab routine ddesd solves DDE initial value problems with discrete state-dependent delays. While we would like to use ddesd to study (2.15)–(2.19), we need to address the issue of implicitly defined delays.

For simplicity, as in the preceding sections, we treat τ_I as a constant delay which is defined by (2.23). We deal with the state-dependent delay τ_M defined by (2.18) by differentiating the integral in (2.18) with respect to t to obtain

$$0 = v_M(E(t)) - \left(1 - \frac{d\tau_M}{dt}(t)\right)v_M(E(t - \tau_M)),$$



2 Page 28 of 74 T. Gedeon et al.

which implies that

$$\frac{d\tau_M}{dt}(t) = 1 - \frac{v_M(E(t))}{v_M(E(t - \tau_M))}. (3.7)$$

We can thus solve the system (2.15)–(2.19) as an initial value problem by considering the system of three equations (2.15)–(2.17) augmented by (3.7) to define the evolution of the state-dependent delay τ_M along with the constant delay $\tau_I = a_I/v_I$ where $v_I = v_I^{min} = v_I^{max}$. The case where τ_I is state-dependent can be handled similarly.

Although this trick avoids the need to evaluate the integral in (2.18) during the simulation, care needs to be taken since information is lost when differentiating and while a solution of (2.18) also solves (3.7), the converse is not necessarily true. To ensure our solution of (3.7) also solves (2.18), we specify history functions so that (2.18) is satisfied at time $t = t_0$. In particular, we require $\tau_M(t_0)$ to satisfy

$$a_M = \int_{t_0 - \tau_M(t_0)}^{t_0} v_M(E(s)) ds.$$
 (3.8)

This will depend on the choice of the history function E(t) defined for $t \le t_0$. In general we need to evaluate this integral only once. Even this can be avoided if $E(t) = E_0$ is constant for $t \le t_0$ since then (3.8) simplifies to $a_M = \tau_M(t_0)v_M(E_0)$ which implies that

$$\tau_M(t_0) = \frac{a_M}{v_M(E_0)}.$$

Although we do not need to solve the integral threshold condition (2.18) during the numerical computation, after a numerical solution is computed, it is very easy to evaluate the integral on the right hand side of (2.18) to check how close it is to a_M . In all the examples presented in Sect. 4, this defect is smaller that 10^{-5} at the final time indicating 5 or more digits of accuracy in the computation of the threshold condition across the interval of computation.

To find the period of a stable periodic solution, a simple technique is to take advantage of the idea of the Poincaré section, and we implement an event function to detect periodicity. While ddesd has a built-in event detection function which can be used to detect periodicity, it slows down the numerical solution drastically. Instead, once the simulation is complete, we fit a spline to the numerical solution and use the spline functions within Matlab to obtain the crossings of the Poincaré section and maxima and minima of solutions and hence period and amplitude information.

Once we find a stable periodic orbit, the solution may be continued as one parameter is varied either by performing additional numerical IVP solves to find a periodic orbit for a perturbed parameter set, or by importing the numerically computed periodic solution into DDE-BIFTOOL and use the discretization of Sect. 3.2 to continue the solution. The DDE-BIFTOOL discretization has the advantage that it can equally well find stable and unstable periodic orbits, and we will use it in Sect. 4 to detect fold bifurcations of periodic orbits where the stability of the periodic orbit changes.



2

ddesd can only be used for the continuation of stable periodic orbits, which is useful for validating the DDE-BIFTOOL results. To perform continuation with ddesd we use the stable periodic solution at each iteration as the history function for the next computation when the continuation parameter is slightly changed. With a small perturbation in the continuation parameter value, we expect to converge to the stable periodic solution as it should still lie in the basin of attraction. Care needs to be taken when doing this, since when making a perturbation of the parameters we need to recompute initial value of the state-dependent delay $\tau_M(t_0)$ so that the integral (3.8) is satisfied at the initial time t_0 with the new parameter set and history function given by the numerical solution with the previous parameter set.

4 Dynamics of repressible and inducible operons with state-dependent delays

In this section, we explore the dynamics of the Goodwin operon model (2.15)–(2.19) incorporating state-dependent delays. We will mainly focus on the case where the transcription delay τ_M is state-dependent and the translation delay τ_I is constant. Then equations (2.15)–(2.19) simplify to

$$\begin{split} \frac{dM}{dt}(t) &= \beta_M e^{-\mu \tau_M(t)} \frac{v_M(E(t))}{v_M(E(t - \tau_M(t)))} f(E(t - \tau_M(t))) - \bar{\gamma}_M M(t), \\ \frac{dI}{dt}(t) &= \beta_I e^{-\mu \tau_I} M(t - \tau_I) - \bar{\gamma}_I I(t), \\ \frac{dE}{dt}(t) &= \beta_E I(t) - \bar{\gamma}_E E(t), \\ a_M &= \int_{t - \tau_M(t)}^t v_M(E(s)) ds = \int_{-\tau_M(t)}^0 v_M(E(t + s)) ds, \end{split} \tag{4.1}$$

with $\tau_I = a_I/v_I$ where $v_I = v_I^{min} = v_I^{max}$. The respective functions for a repressible or inducible system are defined in Table 1. We will treat the minimum transcription velocity, v_M^{min} , as a bifurcation parameter.

4.1 Repressible operon with one state-dependent delay

Recall that when there are no state-dependent delays there are only two possibilities for a repressible system. Namely there is either a globally stable steady state, or a globally stable limit cycle which arises through a supercritical Hopf bifurcation from the steady state. We already showed in Sect. 2.6 (see Figs. 3a and 5a) that it is possible for a repressible system with one state-dependent delay to have multiple steady states, as well as fold bifurcations of steady states. In this section we will explore the dynamics of the repressible system in more depth to reveal the possible dynamics and bifurcations that may arise.

We begin by returning to the example from Sect. 2.6 and consider the state-dependent delay system (4.1) with the repressible parameter set defined in Table 2.



2 Page 30 of 74 T. Gedeon et al.

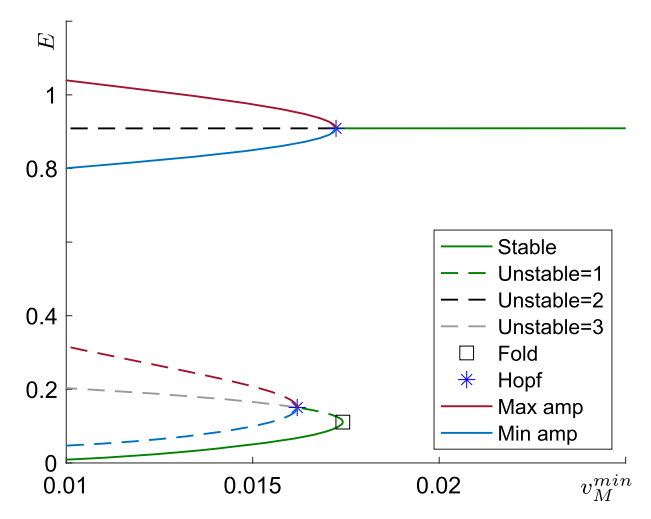


Fig. 6 Bifurcation diagram of the model (4.1) for a repressible system, with parameters defined in Table 2 except v_M^{min} which is taken as the bifurcation parameter. Solid lines represent stable objects including stable steady state (in green) and stable limit cycle (maximum amplitude in red and minimum amplitude in blue). Steady states are represented using the E-component of the solution, and the amplitude of periodic solutions is taken from the maximum and minimum of the E(t) on the periodic solution. Dashed lines represent unstable objects including unstable steady states (depending on the number of eigenvalues with positive real part, green for one, black for two and gray for three and more) and an unstable limit cycle. Bifurcations are listed in Table 3 (color figure online)

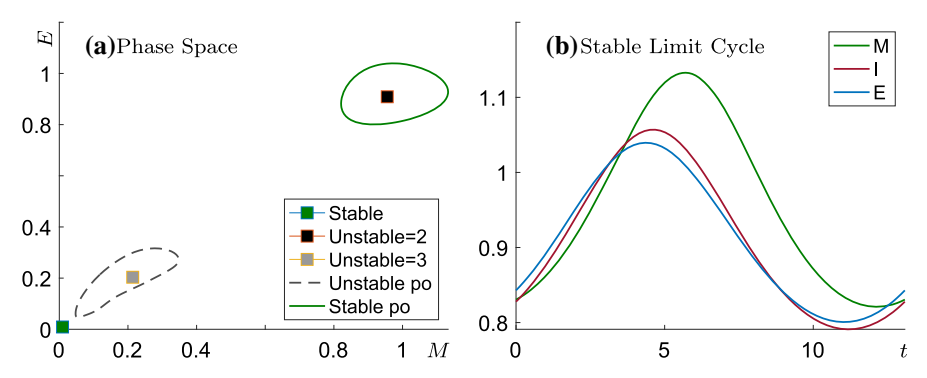


Fig. 7 Repressible system (4.1) with parameters as defined in Table 2 showing the orbits from Fig. 6 at $v_M^{min} = 0.01$. **a** A projection of the phase-space dynamics into the M-E plane in \mathbb{R}^2 with curves formed by the points (M(t), E(t)), $t \in \mathbb{R}$ along periodic solutions (M(t), I(t), E(t)), with squares denoting steady states (colour-coded according to the dimension of their unstable manifold). **b** The three components of the stable periodic solution (color figure online)

The bifurcation diagram in Fig. 6 was computed using DDE-BIFTOOL as detailed in Sect. 3, and extends the diagram previously shown in Fig. 5a to show steady state solutions, periodic orbits along with their stability, as well as Hopf and fold bifurcations. These bifurcations are listed in Table 3.

When $v_M^{min} = v_M^{max}$ both delays τ_M and τ_I are constant, and there can only be one steady state. With the repressible parameter values in Table 2 this steady state is



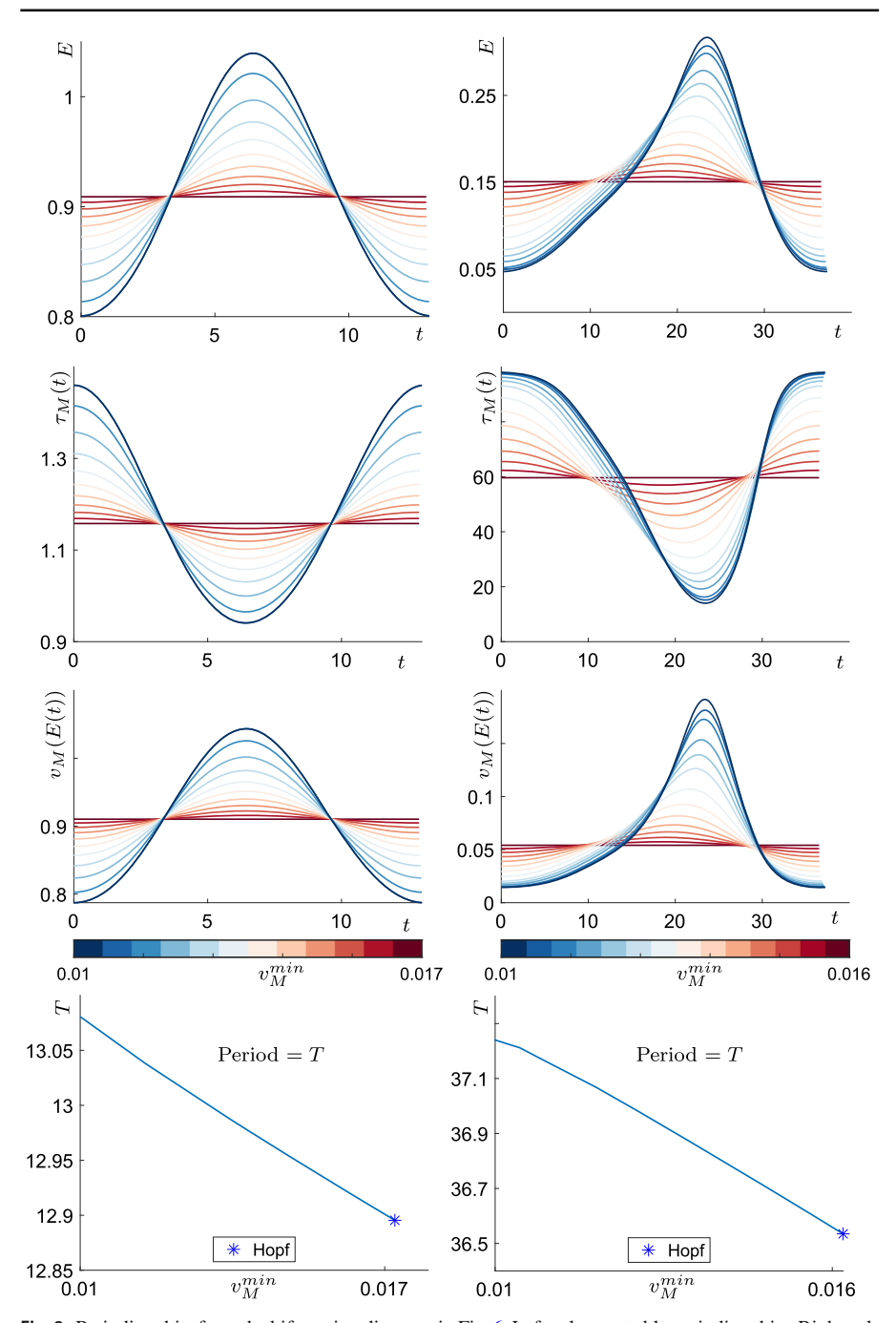


Fig. 8 Periodic orbits from the bifurcation diagrams in Fig. 6. Left column: stable periodic orbits. Right column: unstable periodic orbits. The colormap in each column indicates values of the continuation parameter v_M^{min} (color figure online)



2 Page 32 of 74 T. Gedeon et al.

Bifurcation	Bifurcation parameter value	Unstable eigenvalues	E* value
Fold	$v_M^{min} = 0.017416$	0 to 1	0.1109
Hopf	$v_M^{min} = 0.016193$, period = 36.5348	1 to 3	0.1505
Hopf	$v_M^{min} = 0.017234$, period = 12.8954	0 to 2	0.9090

Table 3 Steady state bifurcations seen on the branches in Fig. 6

stable. As v_M^{min} is decreased there is a fold bifurcation at $v_M^{min} = 0.0174$ giving rise to a pair of additional steady states, one of which is stable. Therefore there is bistability between steady states for the *repressible* model with τ_M state-dependent. However, the bistability region is very narrow as at $v_M^{min} = 0.0172$ there is a Hopf bifurcation from one of the steady states giving rise to a stable periodic orbit. Consequently, for $v_M^{min} < 0.0172$ there is bistability between a steady state and a limit cycle.

There is another Hopf bifurcation at $v_M^{min} = 0.0162$ that gives rise to an unstable limit cycle. Unstable periodic orbits are unlikely to be detected via numerical simulation, but it is possible to compute and follow the unstable periodic orbits in DDE-BIFTOOL for $v_M^{min} < 0.0162$ as shown in Fig. 6. This Hopf bifurcation results in the coexistence of a stable steady state, two unstable steady states, a stable limit cycle and an unstable limit cycle.

Figure 7a shows these coexisting objects at $v_M^{min}=0.01$ in a projection of phase space onto the M-E plane. Since DDEs define infinite dimensional dynamical systems, low dimensional projections of phase space are often used to visualise dynamics, but the projection will, in general, not be one-to-one. Therefore some orbits may appear to intersect in the projection, even though that is impossible in phase space due to uniqueness of solutions. As an illustration of the information that is lost in projection consider the stable limit cycle at v_M^{min} which is shown over one period in Fig. 7b, but is represented by the closed green curve in Fig. 7a and by just two points in Fig. 6.

Figure 8 shows the evolution of the stable and unstable limit cycles generated in the Hopf bifurcations as v_M^{min} decreases. Illustrated are the E component of the limit cycle for different values of v_M^{min} as well as the transcription velocity $v_M(E(t))$ and the delay τ_M as functions of t on the periodic solution. Comparing the two columns of Fig. 8 we see that the stable limit cycles remain fairly sinusoidal over the parameter range, while the unstable limit cycles have larger period than the stable ones and also larger ratios between the maximum and minimum values of the time-dependent components shown.

Homoclinic bifurcation

Now we change two parameter values from the previous example and consider the repressible model (4.1) with parameter values in Table 2 except for n=15 and $v_M^{max}=1$. We again take v_M^{min} as the bifurcation parameter.

When $v_M^{min} = v_M^{max} = 1$ both delays τ_M and τ_I are constant with $\tau_M = \tau_I = 1$. In this case the constant delay repressible model has an unstable steady state and



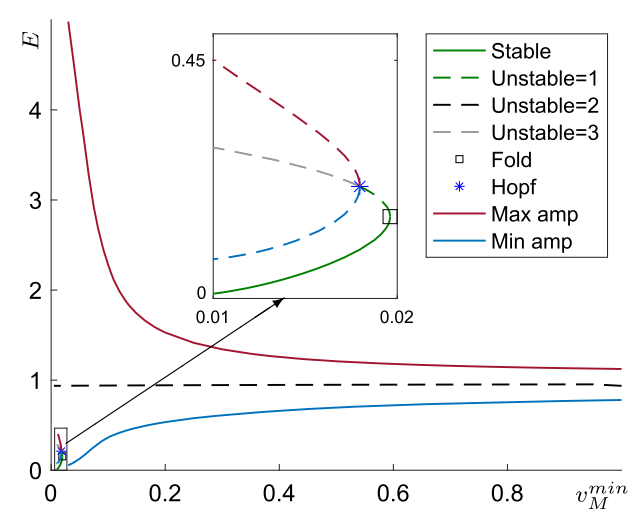


Fig. 9 Bifurcation diagram of the model (4.1) for a repressible system with constant τ_I . Parameter values are as in Table 2 except n=15, $v_M^{max}=1$ and v_M^{min} . Line specifications can be found in Fig. 6

Table 4 Steady state bifurcations seen in Fig. 9

Bifurcation	Bifurcation parameter value	Unstable eigenvalues	E* value
Fold	$v_M^{min} = 0.019610$	0 to 1	0.1546
Hopf	$v_M^{min} = 0.017963$, period = 31.4290	1 to 3	0.2116

a globally stable limit cycle. This limit cycle can be found by simulating the DDE system (as described in Sect. 3.3) using ddesd and then continuing the solution using DDE-BIFTOOL (see Sect. 3.2).

When the parameter value v_M^{min} is decreased the delay τ_M becomes state-dependent and the amplitude of the stable periodic orbit gradually increases as shown in the bifurcation diagram in Fig. 9. Bifurcations are listed in Table 4. Similar to the previous example there is a fold bifurcation when v_M^{min} is very small which leads to two additional steady states, one of which is stable. Thus in this example we obtain two unstable steady states which co-exist with a single stable steady state. There is also an unstable limit cycle generated by a Hopf bifurcation, also similar to the previous example. We are not able to find stable limit-cycles that co-exist with the stable steady state.

This example differs from the previous example in the behaviour of the stable limit cycle. We are able to find the limit cycle only for $v_M^{min} \geq 0.0197$ with the period increasing dramatically as $v_M^{min} \rightarrow 0.0197$ as shown in Fig. 10a, which suggests that a homoclinic bifurcation may occur. For $v_M^{min} = 0.03$ the stable limit cycle is shown in Fig. 10b, and appears to behave like a relaxation oscillator with $(M(t), I(t), E(t)) \approx (0,0,0)$ for much of the time, with one burst of production each period. This periodic solution may have an interesting biological interpretation (see Sect. 5). Namely, the



2 Page 34 of 74 T. Gedeon et al.

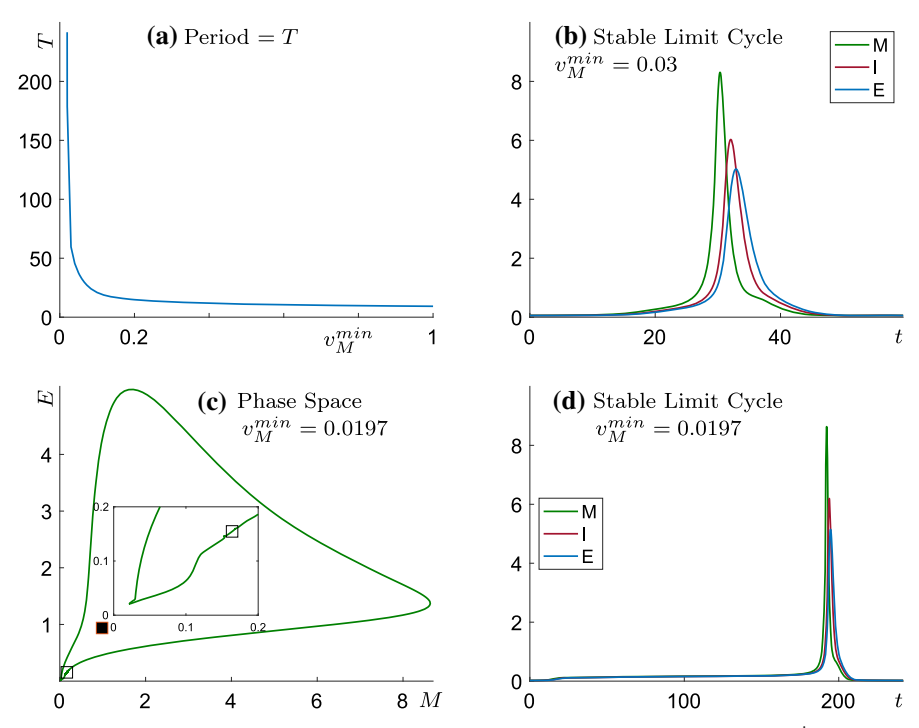


Fig. 10 a The period of the stable periodic orbit (shown in Fig. 9) grows dramatically as v_M^{min} decreases. b Periodic orbit at $v_M^{min}=0.03$. c Projection of the phase space dynamics into the M-E plane at $v_M^{min}=0.0197$. The open square marks the steady state (M^*,E^*) at the fold bifurcation. d Periodic orbit at $v_M^{min}=0.0197$

burst of transcription is followed in short succession by burst of protein production, and this protein represses the initiation of mRNA transcription for a majority of the period. Only when this repression is released, a burst of transcription follows.

The last limit cycle that we are able to compute for $v_M^{min} = 0.0197$ is shown in Fig. 10c, d. If there is a homoclinic orbit then the limit cycle would have to approach a saddle-like steady state. However, in the phase space plot in panel (c), the periodic orbit is always far from the only steady state (denoted by the solid square) that exists for $v_M^{min} = 0.0197$. On the other hand, we do observe that the orbit does pass through the region of phase space containing the 'ghost' of the saddle steady state destroyed in the fold bifurcation at $v_M^{min} = 0.01961$. Panel (d) also shows the solution close to this ghost steady state for $t \in (20, 180)$ which is for most of the period.

In this example it seems that a homoclinic bifurcation occurs very close to the fold bifurcation where the steady state with saddle stability is destroyed. This suggests that our parameter set is close to a higher co-dimension bifurcation where the homoclinic and saddle bifurcations coincide. We investigate this further in the next example.



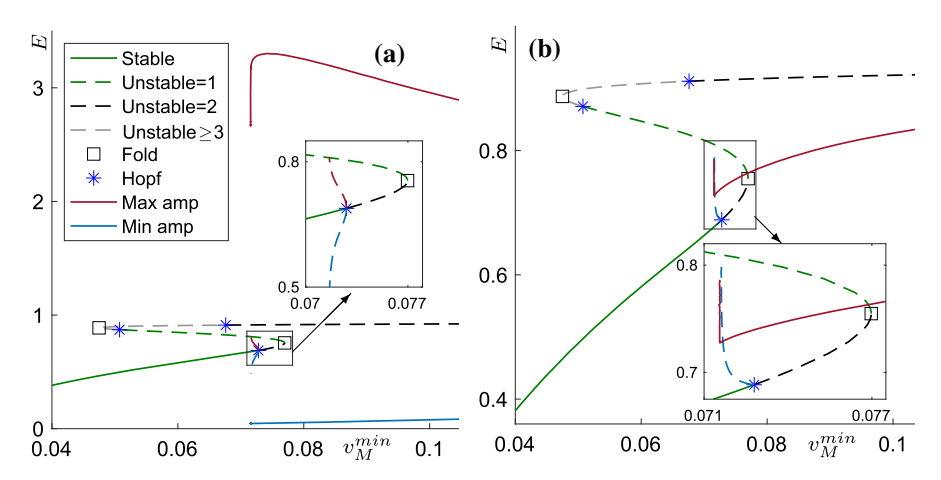


Fig. 11 Bifurcation diagram of the model (4.1) for a repressible system with constant τ_I . Parameter values are as in Table 2 except m=n=15, $v_M^{max}=1$ and v_M^{min} . a Line specifications can be found in Fig. 6. b The same as a except the stable and unstable periodic orbits are represented as a solid red and blue dashed curve respectively using the 1-norm (4.2) of the periodic solution (color figure online)

Table 5	Bifurcation	information	associated	with Fig. 1	1
---------	-------------	-------------	------------	-------------	---

Bifurcation	Bifurcation parameter value	Unstable eigenvalues	E* value
Hopf	$v_M^{min} = 0.072792$, period = 54.7357	0 to 2	0.6885
Fold	$v_M^{min} = 0.076976$	2 to 1	0.7548
Hopf	$v_M^{min} = 0.050745$	1 to 3	0.8711
Fold	$v_M^{min} = 0.047485$	3 to 4	0.8871
Hopf	$v_M^{min} = 0.067602$	4 to 2	0.9116

Zero-Hopf bifurcation and 3DL transition

Next we change a single parameter value from the example shown in Figs. 9 and 10 to consider the model (4.1) in the repressible case with the Hill coefficient in the transcription velocity m=15 (in both the previous examples we took m=3). All the other parameter values remain the same as in the previous example, so n=15, $v_M^{max}=1$ and the rest of the parameters as defined Table 2. The resulting bifurcation diagram is shown in Fig. 11, and the bifurcations are listed in Table 5.

There are several significant differences between the bifurcation diagram in Fig. 11 and the previous case in Fig. 9. Considering first just the steady states, we see that there is an additional fold bifurcation and that all the steady states now lie on a single continuous branch of steady states with two fold bifurcations. As in the previous example there is a single segment of stable steady states, but it loses stability in a subcritical Hopf bifurcation at $v_M^{min} = 0.072792$ whereas in the previous example the stable steady state was destroyed in a fold bifurcation. Comparing the insets in Figs. 9 and 11 we see that the Hopf and the fold bifurcation both occur in each example but,



2 Page 36 of 74 T. Gedeon et al.

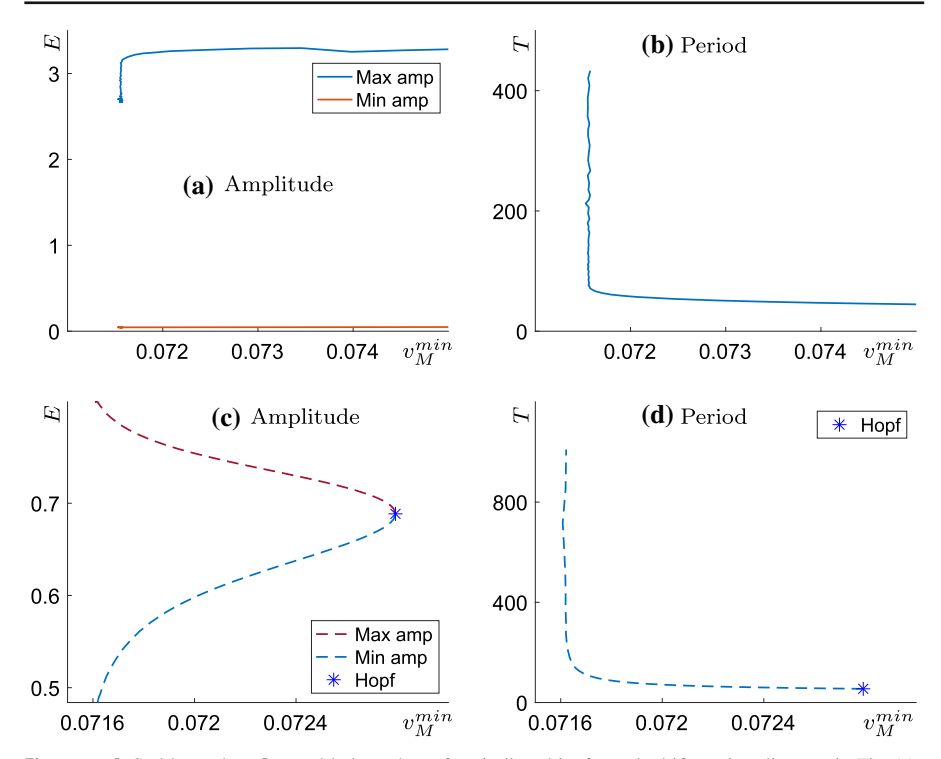


Fig. 12 a, b Stable, and, c, d unstable branches of periodic orbits from the bifurcation diagram in Fig. 11

importantly, their order on the branch is reversed. Therefore there must be an intermediate value of $m \in (3, 15)$ where the two bifurcations will coincide in a so-called zero-Hopf or fold-Hopf bifurcation. The codimension-two zero-Hopf bifurcation is known to generate homoclinic orbits and bifurcations (Kuznetsov 2004), which is further evidence for the existence of homoclinic orbits in the state-dependent delay operon model (4.1).

Consideration of the periodic orbits shown in Fig. 11 provides further evidence supporting existence of homoclinic orbits. While we could imagine that the two branches of periodic orbits shown in Fig. 11a might join up to form one continuous branch that is not what happens. A different representation of the periodic solutions on the bifurcation diagram is appropriate when considering periodic orbits close to homoclinic. In Fig. 11a the periodic orbits are represented by two curves, representing their amplitude. Figure 11b shows exactly the same bifurcation diagram, except that a periodic orbit of period T is now represented by the 1-norm of its E(t) component:

$$\|\cdot\|_1 = \frac{1}{T} \int_0^T E(t)dt \tag{4.2}$$

This representation of periodic orbits is useful because the 1-norm of a periodic orbit approaches the value of E^* as a periodic orbit approaches either a Hopf bifurcation or a homoclinic bifurcation at the steady state (M^*, I^*, E^*) . In Fig. 11b the stable



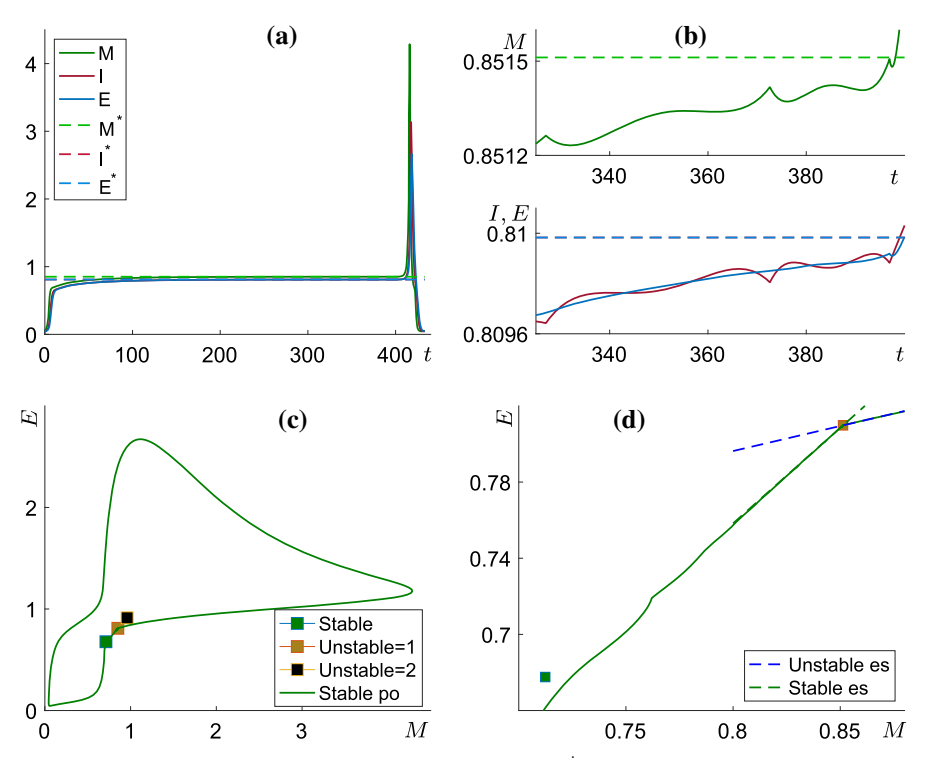


Fig. 13 Stable periodic orbit for repressible system (4.1) with $v_M^{min} = 0.071577$, $v_M^{max} = 1$, m = n = 15, and other parameters as in Table 2. a The unstable periodic solution. b The part of the periodic orbit very close to the middle steady state. c A projection of the phase-space dynamics into the M-E plane showing the unstable periodic solution and steady states (colour coded according to the dimension of their unstable manifold). d Detail of the phase space showing periodic orbit passing very close to middle steady state. Also shown is the projection of the linear unstable manifold (in dashed blue) and the leading linear stable manifold (in dashed green) of this steady state (color figure online)

and unstable periodic orbits are each represented by a single curve using (4.2), and in the inset the periodic solution branches can be seen to both be approaching the intermediate steady state.

Figure 12 shows the evolution of both the amplitude and period of the branch of stable and branch of unstable periodic orbits. The rapidly increasing period at the end of each branch suggests that both terminate in homoclinic bifurcations. This can be seen even more clearly by viewing the periodic orbits in phase space.

Figure 13 shows the last limit cycle that we are able to compute on the branch of stable periodic orbits with $v_M^{min} = 0.071577$. Panel (a) shows all three components of the periodic orbit as well as the unstable steady state from the middle segment of the branch of steady states. This shows that the system spends most of the time close to this steady state with just a short burst of production once per period.

Recall that DDEs define infinite dimensional dynamical systems whose phase space consists of function segments defined over a time interval equal to the largest delay. It follows that for two solutions to be close in phase space, it is necessary that they



2 Page 38 of 74 T. Gedeon et al.

are close in coordinate space for a time interval longer than the largest delay. With the parameters in this example $\tau_I=1$ and at the steady state $E^*=0.81$ and $\tau_M=9.155$. Thus the largest delay is close to 10. Figure 13b shows a zoomed view on the part of the periodic orbit closest to the steady state just before the burst. This shows that all three components of the periodic solution agree with the steady state values to three significant digits over a time interval several times larger than the delay, thus confirming that the periodic orbit passes close to the steady state in phase space.

Figure 13c shows a projection of the phase space dynamics on to the M-E plane showing the stable periodic orbit and the three coexisting steady states at $v_M^{min} = 0.071577$. The periodic orbit appears to pass close to all three steady states, but that is an illusion created partly by the projection from infinite dimensions to \mathbb{R}^2 and partly by the scale which is very compact to show the large amplitude bursting periodic orbit. Also note that one of the steady states is asymptotically stable and so it is impossible for a periodic orbit to lie in its basin of attraction.

Figure 13d shows that the periodic orbit passes close to just the middle steady state, and also shows the behaviour of the solution near to this steady state. The leading characteristic values of the intermediate unstable steady state $(M^*, I^*, E^*) = (0.8515, 0.8100, 0.8100)$ at $v_M^{min} = 0.071577$, where stable periodic orbits cease to exist, are obtained from (2.48) as

$$\lambda_1 = 0.49051,$$
 $\lambda_2 = -0.017729,$
 $\lambda_{3.4} = -0.018217 \pm 0.70175i.$

Following the theory of Sect. 2.7 this leads to linearized solutions close to the steady state (M^*, I^*, E^*) of the form

$$\begin{pmatrix} M(t) \\ I(t) \\ E(t) \end{pmatrix} = \begin{pmatrix} M^* \\ I^* \\ E^* \end{pmatrix} + Ce^{\lambda t} \begin{pmatrix} \mathcal{E}_M \\ \mathcal{E}_I \\ \mathcal{E}_E \end{pmatrix}$$

where the constant eigenvector $(\mathcal{E}_M, \mathcal{E}_I, \mathcal{E}_E)$ lies in the nullspace of the matrix $A(\lambda)$ defined in (2.47). The corresponding eigenvectors for λ_1 and λ_2 are computed as

$$v_1 = \begin{pmatrix} 1 \\ 0.39077 \\ 0.26222 \end{pmatrix}, \quad v_2 = \begin{pmatrix} 1 \\ 0.98572 \\ 1.0035 \end{pmatrix}.$$

Since λ_1 is the only characteristic value with positive real part the linear unstable manifold of the steady state is defined by $e^{\lambda_1 t} v_1$. When projecting phase space into the M-E plane this line has slope $\mathcal{E}_E/\mathcal{E}_M$. The stable manifold of the steady state is infinite-dimensional and so cannot be represented in the M-E plane, but the dominant part of the linear stable manifold (with slowest decay) is given by $e^{\lambda_2 t} v_2$.

The projections of both the dominant part of the linear stable manifold and the linear unstable manifold are shown in Fig. 13d. The stable periodic orbit is seen to approach



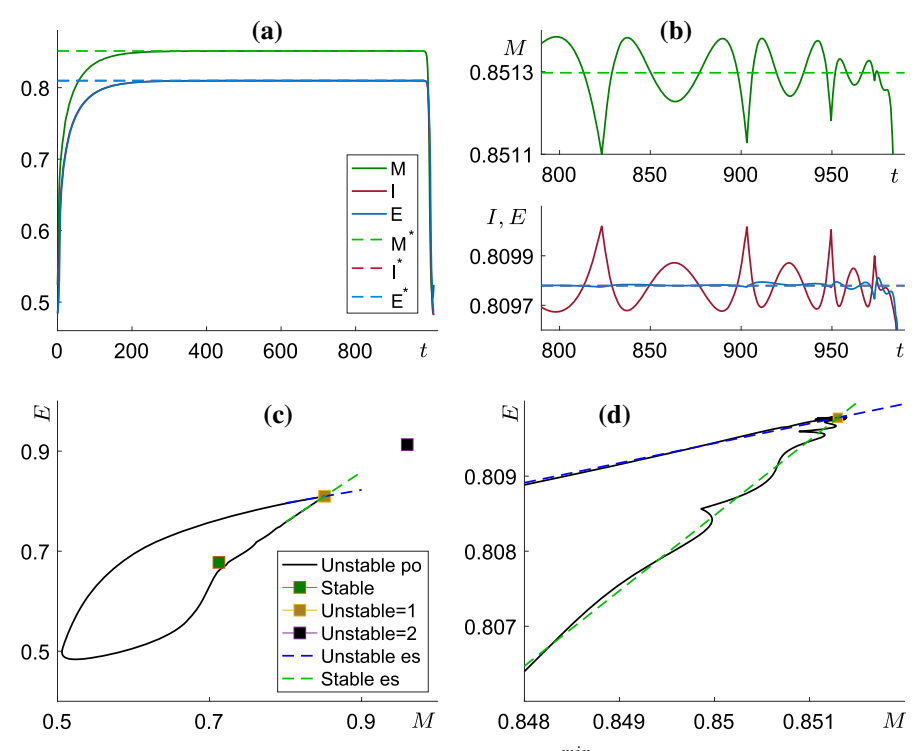


Fig. 14 Unstable periodic orbit for repressible system (4.1) with $v_M^{min}=0.071622$, and the other parameters the same as in Fig. 13. Panels ${\bf a}$ to ${\bf d}$ as described in caption to Fig. 13

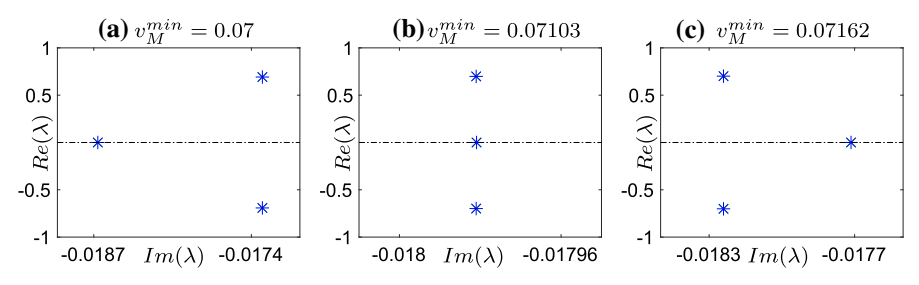


Fig. 15 Configuration of leading negative real and complex-conjugate eigenvalues as v_M^{min} varies. A 3-dimensional transition (Kalia et al. 2019) occurs on the middle branch of unstable steady states as in Fig. 11

the steady state along a direction that is tangential to the dominant stable manifold before leaving along a direction that is tangential to the unstable manifold. Since the orbit passes very close to the steady state, the passage through the neighbourhood of the steady state takes a very long time. This results in the large period of the orbit.

Figure 14 is similar to Fig. 13 but shows the last periodic orbit that we are able to compute on the branch of unstable periodic orbits with $v_M^{min} = 0.071622$. Comparing the two figures we see that the unstable periodic orbit is quite different to the stable orbit. Figure 14a, b show that again the periodic orbit is close to the intermediate



2 Page 40 of 74 T. Gedeon et al.

steady state for most of the period except for a short burst (or antiburst) of *depressed* production.

The characteristic values and corresponding eigenvectors can also be computed for the unstable periodic orbit, but the value of v_M^{min} only differs in the third significant digit between the two examples. The characteristic values and eigenvectors agree with those above to the third significant digit. The phase space plots in Fig. 14c, d again show a periodic orbit close to homoclinic approaching the steady state near the dominant linear stable manifold and leaving tangential to the linear unstable manifold.

There are two significant differences from the stable periodic orbit. Firstly, the unstable periodic orbit leaves the neighbourhood of the steady state in the *opposite* direction to the stable periodic orbit, which results in the production being decreased rather than increased during the burst. Secondly it is apparent in Fig. 14b, d that the periodic orbit is not tangential to the dominant part of the linear stable manifold but rather oscillates about it. This seems to arise because there is only a small difference in the real parts between λ_2 and the next characteristic values which occur as a complex conjugate pair $\lambda_{3,4}$. Furthermore, as shown in Fig. 15, for a very nearby value of v_M^{min} , the leading negative real eigenvalue λ_2 and complex-conjugate eigenvalues $\lambda_{3,4}$ exchange order. Such a transition in a system also having one real positive eigenvalue is called a 3-dimensional or 3DL transition and is associated with rich Shilnikov homoclinic bifurcation structures (Kalia et al. 2019).

4.2 Inducible operon with one state-dependent delay

We now turn to consider the Goodwin model (4.1) with one-state dependent delay in the case of an inducible operon with functions defined in Table 1. Recall that with both delays constant (and also in the absence of delays) an inducible system with n > 1 can have either a single globally stable steady state, or there can be two locally stable steady states and an unstable intermediate steady state. There are no other possibilities when using the functions in Table 1 (Yildirim et al. 2004).

We will show that an inducible operon with state-dependent transcription delay τ_M can support stable and unstable periodic orbits and that these can be generated in supercritical or subcritical Hopf bifurcations, or in fold bifurcations of periodic orbits.

Inducible supercritical hopf bifurcation

We begin by considering the inducible operon model (4.1) with parameters defined in Table 6. With this parameter set and $v_M^{min} = v_M^{max} = 1$, both delays are constant and the model has a single globally stable steady state. For $v_M^{min} < 1$ the transcription delay becomes state-dependent and several bifurcations occur, as shown in Fig. 16 and listed in Table 7.

As v_M^{min} is decreased there is first a fold bifurcation which creates two additional steady states. This results in bistability between two stable steady states for $v_M^{min} \in (0.08, 0.354)$ separated by an intermediate unstable steady state. This configuration is well known for inducible operons with constant delays, but here the bifurcation to three steady states is induced by varying the state-dependency of the delay τ_M .



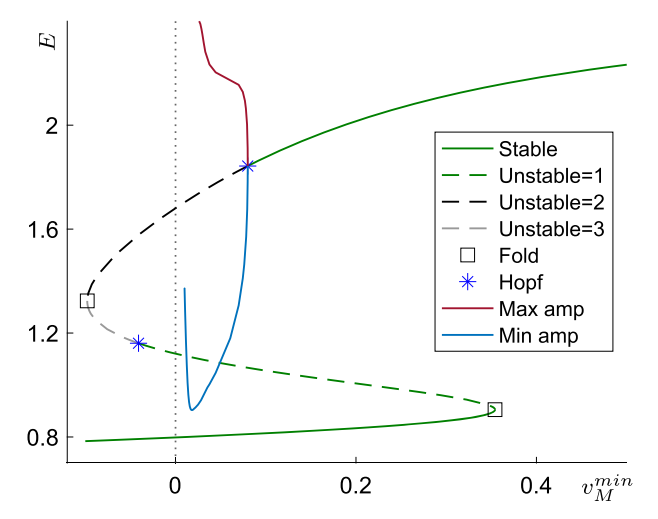


Fig. 16 Bifurcation diagram of the model (4.1) for an inducible system with parameter values as defined in Table 6 and v_M^{min} treated as a continuation/bifurcation parameter. Line specifications can be found in Fig. 6. The amplitudes of E-component of periodic solutions $\mathbb{R} \to \mathbb{R}^3$ are shown. The vertical dotted line at $v_M^{min} = 0$ separates the biologically realistic case $v_M^{min} > 0$ from the biologically unrealistic case $v_M^{min} < 0$ (see text). Bifurcations occurring for $v_M^{min} > 0$ are detailed in Table 7

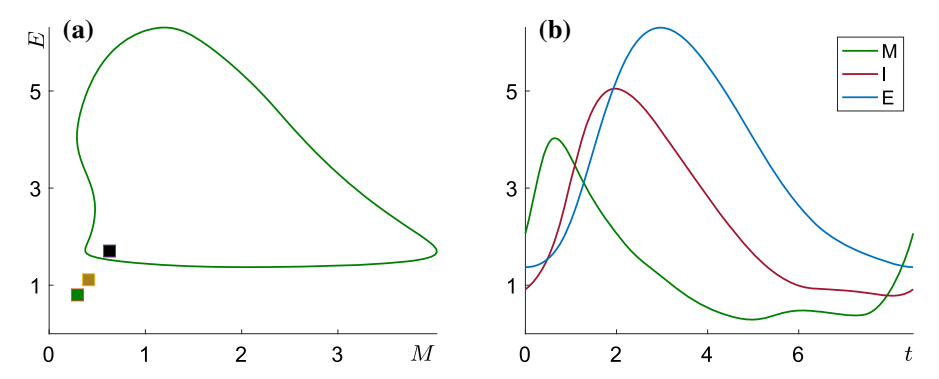


Fig. 17 Inducible system (4.1) with parameters as defined in Table 6 showing the orbits from Fig. 16 at $v_M^{min} = 0.01$. **a** A projection of the phase space dynamics into the M-E plane showing periodic orbits represented by closed curves, and steady states by squares (whose colour indicates the number of unstable eigenvalues as in Fig. 13). **b** The three components of the stable periodic solution

Reducing v_M^{min} further, an unexpected event occurs; the upper steady state loses stability in a supercritical Hopf bifurcation which creates a stable periodic orbit which exists for $v_M^{min} < 0.08$. This stable periodic orbit coexists with one stable and two unstable steady states. Thus we have an interval of bistability between a limit cycle and a steady state for an *inducible* operon.

The stable periodic orbit and a projection of phase space into the M-E plane are shown in Fig. 17 for $v_M^{min}=0.01$. We suspect that the periodic orbit exists for all $v_M^{min}>0$, but the numerical discretization of the threshold integral described in



2 Page 42 of 74 T. Gedeon et al.

Table 6 Parameters for inducible operon example of Fig. 16

Quantity	Value
μ	0.05
eta_M	1
eta_I	1.8
eta_E	1.5
$\bar{\gamma}_M$	1
$ar{\gamma}_I$	0.97
$ar{\gamma}_E$	1
K	4
K_1	1
n	4
m	2
a_M	1
v_M^{max}	0.2
E_{50}	1
$ au_I$	0.5

Table 7 Bifurcation information associated with Fig. 16

Bifurcation	Bifurcation parameter value	Unstable eigenvalues	E* value
Hopf	$v_M^{min} = 0.080031$, period = 6.2271	0 to 2	1.8571
Fold	$v_M^{min} = 0.35409$	1 to 0	0.9052

Those bifurcations occurring for $v_M^{min} < 0$ are not displayed due to lack of physiological meaning

Sect. 3.2 requires v_M^{min} bounded away for zero, and we only compute periodic orbits for $v_M^{min} \ge 0.01$.

The linearization correction method of Sect. 3.1 avoids discretizing the integral and is applicable even when $v_M^{min} < 0$. Though $v_M^{min} < 0$ leads to negative transcription velocities which is not physiological, this can be computationally useful. This is demonstrated in Fig. 16 where continuation through negative values of v_M^{min} reveals that the different branches of steady states are joined at a fold bifurcation with $v_M^{min} < 0$. This allows computation of all the physiological steady states by continuation of a single branch.

Inducible subcritical hopf bifurcation

We now change just one parameter value from the previous example and consider the inducible state-dependent transcription delay operon model (4.1) with parameters as in Table 6, except for the Hill coefficient in the transcription velocity function which we now set to m=4.

Comparing Fig. 18 with the previous example in Fig. 16 we see that changing the value of *m* from 2 to 4 results in two important changes in the bifurcations. Firstly, in



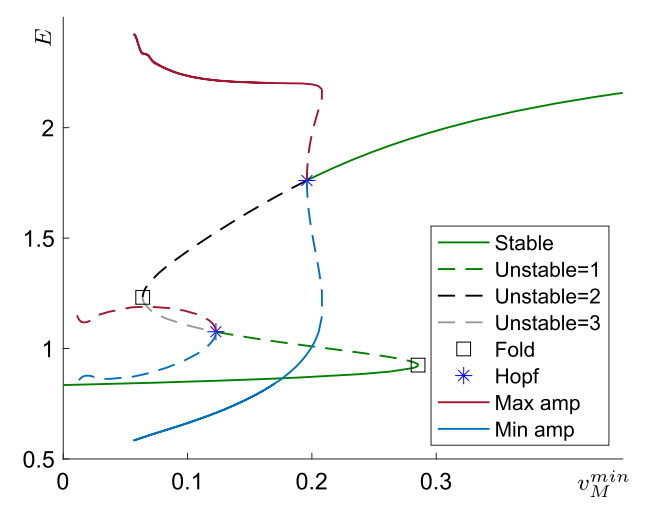


Fig. 18 Bifurcation diagram of the inducible operon model (4.1) with m=4 and all other parameters as defined in Table 6. Bifurcations are listed in Table 8

•		1	C
Bifurcation	Bifurcation parameter value	Unstable eigenvalues	E* value
Hopf	$v_M^{min} = 0.19603$, period = 6.4488	0 to 2	1.7609
Fold	$v_M^{min} = 0.063903$	2 to 3	1.2317
Hopf	$v_M^{min} = 0.12279$, period = 4.7796	3 to 1	1.0759
Fold	$v_M^{min} = 0.28543$	1 to 0	0.9249
Fold of periodic orbits	$v_{in}^{min} = 0.20812$, period = 5.8831	1 to 0	_

Table 8 Steady state and Periodic Orbit Bifurcation information for the Example shown in Fig. 18

Fig. 18 both the fold bifurcations on the branch of steady states now occur for positive values of v_M^{min} . Consequently for $v_M^{min} \in (0.064, 0.285)$ there are three co-existing steady states, while for both larger and smaller values of $v_M^{min} > 0$ there is a unique stable steady state.

The second important difference between the two examples is that the Hopf bifurcation on the upper segment of steady states at $v_M^{min} = 0.196$ in Fig. 18 is subcritical resulting in a branch of unstable periodic orbits. The change in the criticality of this Hopf bifurcation between the two examples implies that for some intermediate value $m \in (2, 4)$ there is a Bautin bifurcation at which the criticality switches. Bautin bifurcations are well studied (Kuznetsov 2004) and in a two-parameter unfolding generate a branch of fold bifurcations of periodic orbits.

The branch of unstable periodic orbits emanating from the subcritical Hopf bifurcation terminates in the fold bifurcation of periodic orbits seen in Fig. 18 at $v_M^{min}=0.20812$, at which the periodic orbit becomes stable. As a consequence of the subcritical Hopf bifurcation and fold of periodic orbits there are stable periodic orbits for $v_M^{min}<0.208$ (to the left of the fold bifurcation of periodic orbits) and



2 Page 44 of 74 T. Gedeon et al.

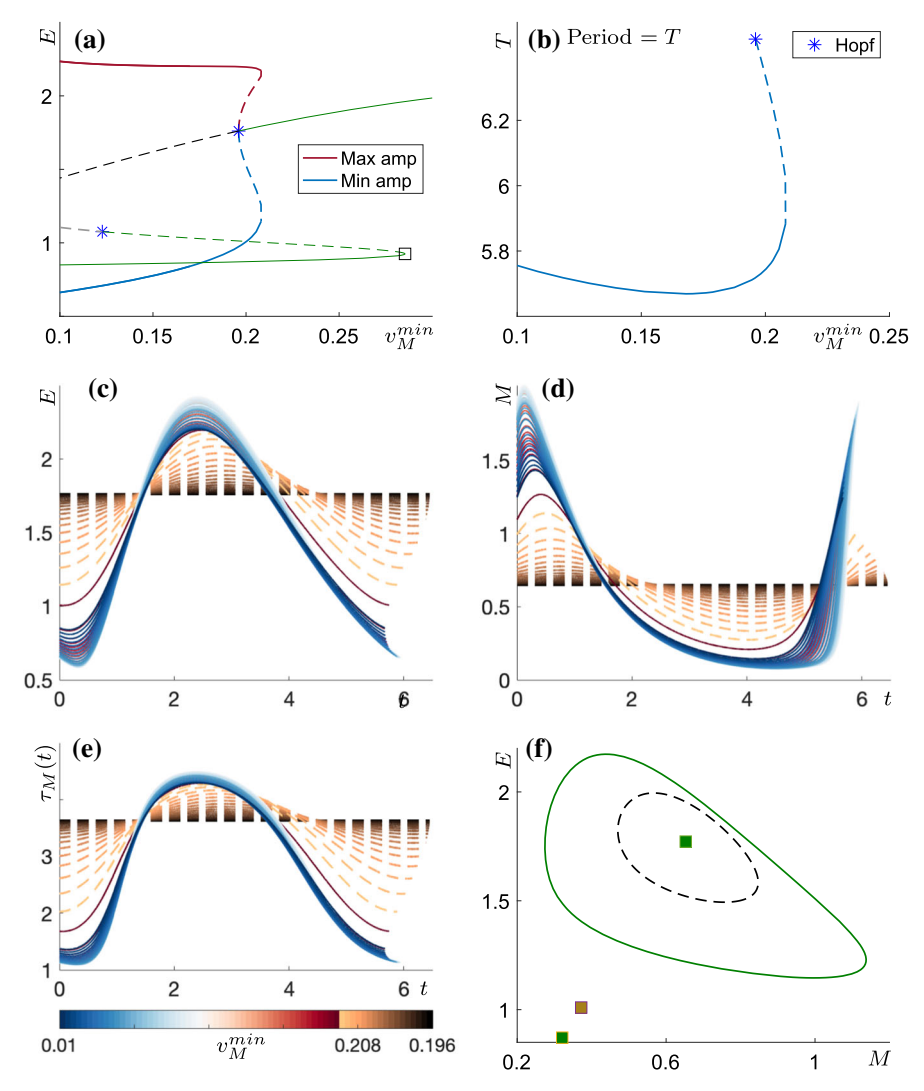


Fig. 19 Stable and unstable periodic orbits on the branch of periodic orbits emanating from the subcritical Hopf bifurcation in Fig. 18. The colormap indicates the value of the continuation parameter v_M^{min} . The periodic orbits are shown in **a** amplitude of E-component, **b** period, **c** profile in E, **d** profile in M, **e** delay τ_M . Panel **f** shows a projection of phase space onto the M-E plane when $v_M^{min} = 0.2$ and tristability occurs. Periodic orbits are represented by closed curves, and steady states by squares (whose colour indicates the number of unstable eigenvalues as in Fig. 13) (color figure online)

co-existing stable steady states for $v_M^{min} \in (0.196, 285)$ (to the right of the Hopf bifurcation). This creates a small parameter interval of tristability for $v_M^{min} \in (0.196, 0.208)$ between the Hopf bifurcation and fold of periodic orbits bifurcation for which a stable periodic orbit coexists with two stable steady states. Figure 19f shows the dynamics when $v_M^{min} = 0.2$ in the tristability region, in a projection of phase space onto the M-E plane. The branch of periodic orbits emanating from the Hopf bifurcation at



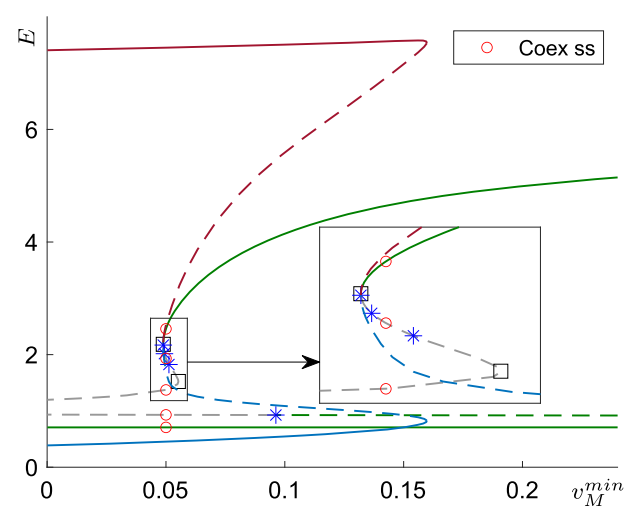


Fig. 20 Bifurcation diagram of the model (4.1) for an inducible system with parameters defined in Table 2 except v_M^{min} which is taken as the bifurcation parameter. Red circles denote the five co-existing steady states at $v_M^{min} = 0.05$. All other lines and symbols are defined as in Figs. 6 and 9 (color figure online)

 $v_M^{min} = 0.19603$ crosses $v_M^{min} = 0.2$ twice and both the stable and unstable periodic orbit are shown in the phase portrait.

The other panels of Fig. 19 show the evolution of the periodic orbit from the Hopf bifurcation on this branch with separate colour maps for the stable and unstable legs of the branch.

For $v_M^{min} \in (0.20812, 0.28543)$ there is bistability between two steady states, and for $v_M^{min} < 0.19603$ there is bistability between a periodic orbit and a steady state. There is also a second Hopf bifurcation at $v_M^{min} = 0.1228$ which generates small amplitude unstable periodic orbits shown on the bifurcation diagram in Fig. 18.

Fold bifurcation of periodic orbits

For our final example of inducible operon dynamics we return to the example from Sect. 2.6 and consider the one state-dependent delay system (4.1) with the inducible parameter set defined in Table 2.

The bifurcation diagram in Fig. 20 extends the diagram previously shown in Fig. 5b to show steady state solutions and periodic orbits along with their stability, as well as Hopf and fold bifurcations. The bifurcations are listed in Table 9.

We already saw in Sect. 2.6 that when $v_M^{min} = v_M^{max}$ and thus both delays are constant, there are three co-existing steady states. Two of these are stable and the intermediate steady state is unstable. When v_M^{min} is reduced the delay τ_M becomes state-dependent and a number of bifurcations may occur. The lower stable steady state remains stable and does not undergo any bifurcations. The intermediate steady state remains unstable for all $v_M^{min} > 0$ but does undergo a Hopf bifurcation. The upper branch of steady states loses stability in a fold bifurcation. There is also another fold



2 Page 46 of 74 T. Gedeon et al.

Bifurcation	Bifurcation parameter value	Unstable eigenvalues	E* value
Hopf	$v_M^{min} = 0.09624$, period = 4.1286	1 to 3	0.9270
Fold	$v_M^{min} = 0.055205$	6 to 7	1.5229
Hopf	$v_M^{min} = 0.051247$, period = 7.1786	7 to 5	1.8245
Hopf	$v_M^{min} = 0.049356$, period = 11.4903	5 to 3	2.0162
Hopf	$v_M^{min} = 0.048868$, period = 23.539	3 to 1	2.1697
Fold	$v_M^{min} = 0.048865$	1 to 0	2.1830
Fold of periodic orbits	$v_M^{min} = 0.1597$, period = 7.6675	1 to 0	_

Table 9 Bifurcation information associated with Fig. 20

bifurcation and several Hopf bifurcations on this branch. Considering all the branches together there may be up to five co-existing steady states, but as the bifurcation diagram shows, there are only ever one or two co-existing stable steady states.

The fold bifurcation at which the steady state loses stability (at $v_M^{min} = 0.048865$) is immediately followed by a Hopf bifurcation (at $v_M^{min} = 0.048868$), indicating that this inducible operon is close to a zero-Hopf bifurcation (in Sect. 4.1 we inferred existence of a zero-Hopf bifurcation for a repressible operon).

The branch of periodic orbits emanating from the Hopf bifurcation is shown in Fig. 21. The bifurcation is a supercritical Hopf bifurcation from an unstable steady state, which gives rise to a branch of unstable periodic orbits bifurcating to the right. The amplitude and period of these orbits are shown in Fig. 21a, b. Interestingly, moving along the branch away from the Hopf bifurcation the period decreases as the amplitude increases until there is a fold bifurcation of periodic orbits at $v_M^{min} = 0.1597$ creating a segment of stable periodic orbits on the branch. The periodic orbit at the fold bifurcation is shown in Fig. 21c, d. For $v_M^{min} > 0.1597$ there is no longer a periodic orbit, but it is still possible to have transient oscillatory dynamics. Figure 21e, f show an example of this for $v_M^{min} > 0.1605$, where an initial function close to the unstable intermediate steady state generates a solution with large oscillations for 200 time units before the solution converges to the stable steady state. When the phase space projection of this solution in Fig. 21f is compared to the periodic orbit at the fold of periodic orbits (in Fig. 21d) it is clear that we are seeing a ghost of the periodic orbit.

For $v_M^{min} \in (0.048865, 0.1597)$ the branch of stable periodic orbits coexists with two stable steady states, creating another example of tristability of solutions. The stable periodic orbit at the left end of the branch with $v_M^{min} = 0.0001$ is shown in Fig. 22.

The transcription velocity is essentially zero for nearly all of the period, with just a short burst of transcription when E is close to its minimum. This sudden release of mRNA gives the M component of the solution the characteristic form of a relaxation oscillator, even though the other components of the solution are smooth.

The variation of the delay as a function of time seen in Fig. 22d shows that the delay is very far from being constant. The delay is increasing linearly on the segment of the orbit for which the transcription velocity is zero, and so no transcripts are being completed. During this time the effector *E* concentration is high and thus the



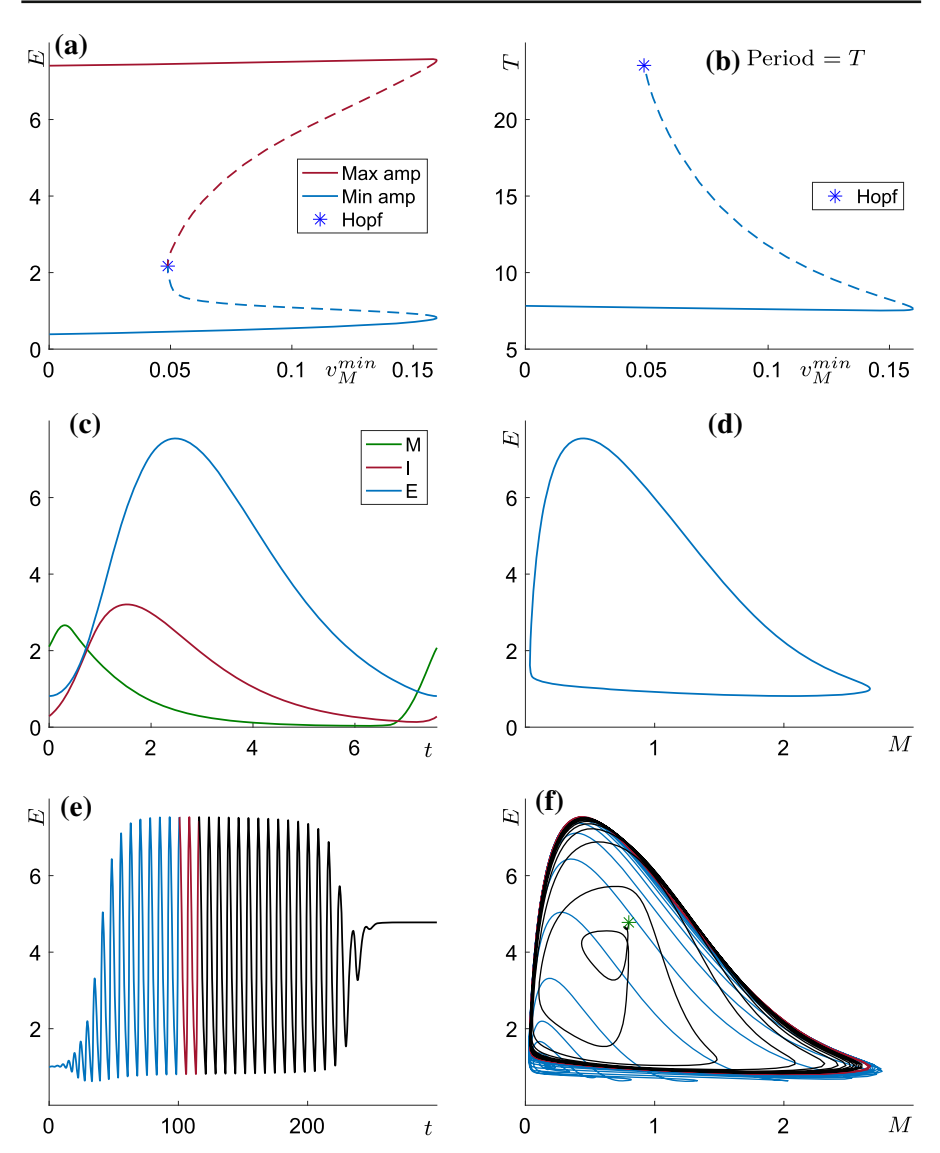


Fig. 21 a Amplitude and **b** Period for the branch of periodic orbits from Fig. 9. **c** The solution components and **d** the projection into phase space of the periodic orbit at the fold bifurcation $v_M^{min} = 0.1597$. **e** E component and **f** phase space projection for a simulation with $v_M^{min} = 0.1605$ and initial function close to the intermediate steady state

transcription initiation rate f(E) is high; at the same time though, the delay $\tau(E)$ is also increasing. Only when the concentration of the effector E drops sufficiently, does transcription proceed during the last quarter of the period.

Finally, we remark that it is highly delicate to numerically compute a branch of periodic orbits emanating from a Hopf bifurcation close to a co-dimension two zero-Hopf bifurcation in the system (4.1) with the threshold integral discretized as in Sect. 3.2.



2 Page 48 of 74 T. Gedeon et al.

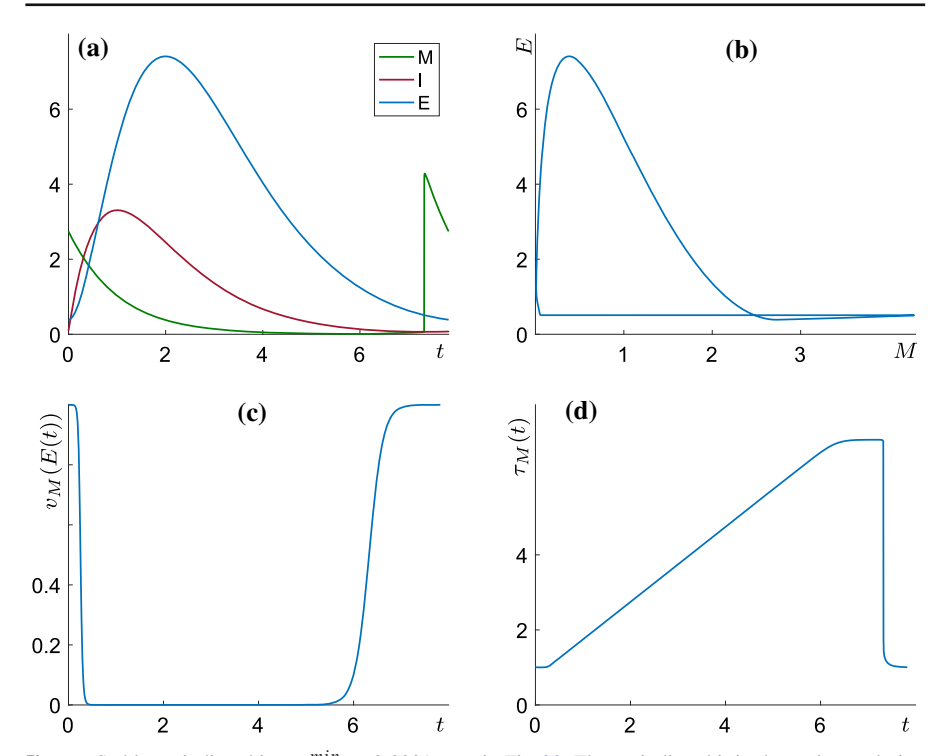


Fig. 22 Stable periodic orbit at $v_M^{min}=0.0001$ seen in Fig. 20. The periodic orbit is shown in ${\bf a}$ solution in all three components over one period, ${\bf b}$ projection of phase space into M-E plane, ${\bf c}$ velocity $v_M(E(t))$ and ${\bf d}$ delay $\tau_M(t)$

 Table 10
 Bifurcation information associated with Fig. 23a

Bifurcation	Bifurcation parameter value	Unstable eigenvalues	E^* value
Fold	$v_M^{min} = 0.017832$	1 to 0	0.1130
Hopf	$v_M^{min} = 0.014483$, period = 34.8874	3 to 1	0.1768

For this reason we were not able to compute this branch starting from the Hopf bifurcation. Instead, noting that for small values of v_M^{min} there are three steady states, but only the lower one is stable, we performed a numerical simulation of dynamics as described in Sect. 3.3 starting close to the upper unstable steady state. This simulation converged to the stable periodic orbit. This periodic orbit was then continued in DDE-BIFTOOL to find the fold bifurcation of periodic orbits and follow the branch of unstable periodic orbits back to the Hopf bifurcation.

4.3 Two state-dependent delays

We briefly return to the model (2.15)–(2.19) with two state-dependent delays. Figure 23 shows the stability of the steady states and also the steady state bifurcations



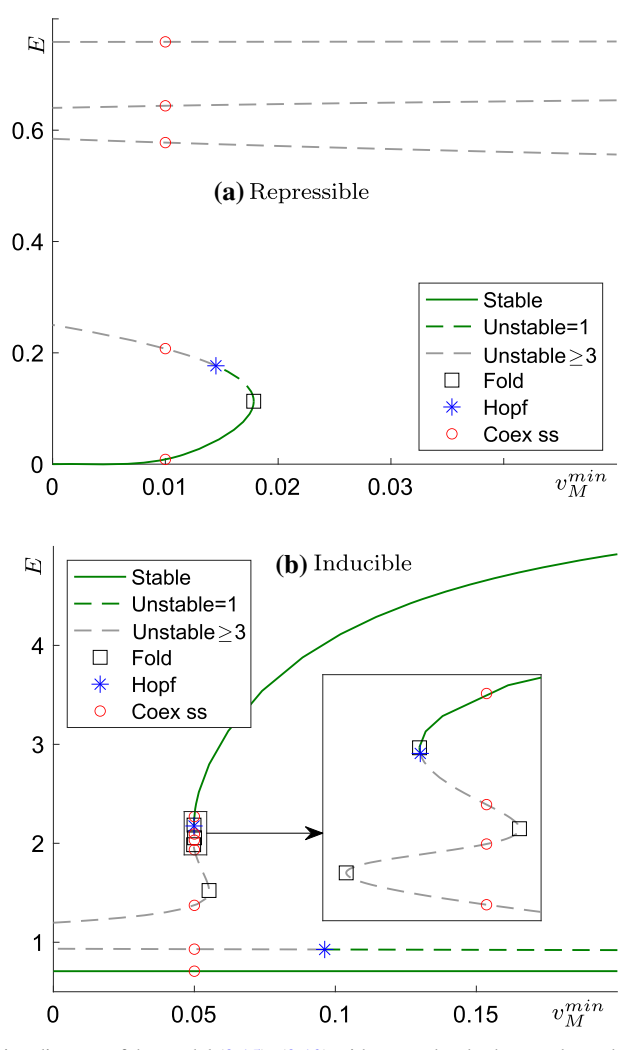


Fig. 23 Bifurcation diagram of the model (2.15)–(2.19) with τ_M and τ_I both state-dependent. a Repressible case with same parameters as in Fig. 5c. b Inducible case with same parameters as in Fig. 5d. Symbols and lines are as defined in Fig. 6, except for the red circles which denote the co-existing steady states shown in Fig. 3c, d (color figure online)

for the two examples first considered in Fig. 5c, d in Sect. 2.6. The principal bifurcations are listed in Tables 10 and 11. For the inducible case our numerical code found many pairs of complex conjugate characteristic values crossing the imaginary axis indicating the possibility of many Hopf bifurcations. In Table 11 we only list with Hopf bifurcations that generate steady states with three or fewer unstable eigenvalues, as Hopf bifurcations with more unstable directions will never change the stability of the stability of the steady state and will only generate periodic orbits with multiple unstable Floquet multipliers.



2 Page 50 of 74 T. Gedeon et al.

Bifurcation	Bifurcation parameter value	Unstable eigenvalues	E* value
Hopf	$v_M^{min} = 0.096224$, period = 4.1287	1 to 3	0.9270
Fold	$v_M^{min} = 0.055205$	6 to 7	1.5230
Fold	$v_M^{min} = 0.049743$	15 to 14	1.9858
Fold	$v_M^{min} = 0.05006$	12 to 13	2.0558
Hopf	$v_M^{min} = 0.049879$, period = 23.5795	3 to 1	2.1751
Fold	$v_M^{min} = 0.049877$	1 to 0	2.1841

Table 11 Bifurcation information associated with Fig. 23b

Compared to the examples from the preceding sections we see that allowing the second delay to also be state-dependent can result in additional co-existing steady states (consistent with (2.32)), however these extra steady states are unstable and there do not seem to be additional stable invariant objects. In Fig. 23a there are four unstable and one stable equilibrium, suggesting existence of one or more stable periodic orbits. In Fig. 23b for low v_{min} there are two unstable and one stable equilibrium, again suggesting existence of a stable periodic orbit.

5 Discussion and summary

This paper studies the Goodwin model of operon dynamics in the presence of state dependent delays in the processes of transcription and translation. The dependence of delays on the state of the system was considered previously (Monk 2003; Verdugo and Rand 2007; Ahmed and Verriest 2017; Wang and Pei 2021) and justified by the existence of transportation delays of mRNA export through the nuclear membrane. We argue that the availability of building blocks for mRNA and protein synthesis, as well as traffic jams of transcribing polymerases and translating ribosomes, affect the velocity of these processes and depend on the state of the cell. In contrast with membrane transportation delays, these effects may influence also prokaryotic operons.

The focus of the paper is on exploring potential operon dynamics in the presence of state dependent delays both in transcription and translation and contrasting its richness with the dynamics of constant delay systems. We consider two different situations of repressible and inducible operon.

In the repressible case with state dependent transcriptional delay τ_M and constant translational delay τ_I we find bistability either between two steady states or a steady state and a stable periodic orbit (Figs. 5, 6, 11). This periodic orbit has the characteristic of a relaxation oscillator, where the velocity of transcription is very low for a majority of the period, only to produce a brief 'spike' of transcription which results in subsequent spikes of the translated protein and the effector protein, Fig. 10.

We also found compelling evidence for the existence of complicated dynamics in the repressible case. In particular, by tracing the trajectory of the stable periodic orbit just before it disappears, we found that it passes very close to a saddle point which



it approaches along the dominant linearized stable direction and leaves along the one-dimensional unstable manifold (Fig. 13). An unstable periodic orbit behaviours very similarly at a near identical paranmeter value, except it leaves along the one-dimensional unstable manifold in the opposite direction (Fig. 14). This suggests that these periodic orbits disappear in a homoclinic bifurcation. Furthermore, linearization at the saddle point at nearby parameters shows that the dominant stable real eigenvalue becomes a dominant complex pair (Fig. 15) whose magnitude satisfies the assumptions guaranteeing existence of Shilnikov type chaotic set (Shilnikov 1965; Kuznetsov 2004). We found two parameter values near each other such that at one the stable periodic orbit loses stability through a Hopf bifurcation and at the other at a fold bifurcation and inferred that at some intermediate parameter value those two bifurcations will coincide in a codimension-two zero-Hopf bifurcation.

When both τ_M and τ_I are variable we show that the system can admit 5 steady states, Figs. 5c and 23a. Further exploration of the range of dynamics in this case is left for future studies.

In the inducible case when the delays are constant we can have either a single steady state or bistability between two steady states. The dynamics are richer in presence of variable delays.

We start with two situations when τ_M and τ_I are constant: either (1) there is a unique steady state or (2) there are 3 steady states, two of which are stable. We then allow τ_M to vary while τ_I remains constant. In case (1) we find coexistence of the steady state with a stable periodic orbit, or another steady state, Fig. 16; and in case (2) we find there are an additional 2 equilibria for a total of 5. This results in tristability between two equilibria and a period orbit (Figs. 18 and 20). The stable periodic orbit in (1) has features of a relaxation oscillator; the velocity of transcription remains close to zero for the majority of the period, only to show a rapid increase in a short burst Figs. 22.

When both τ_M and τ_I are variable the system can have up to 7 steady states, Figs. 5d and 23b. Further exploration of the dynamics in this case is again left for future studies.

The presence of relaxation type oscillations in both inducible and repressible operons provides an intriguing source of pulse generation on a subcellular level. Among several periodic behaviors that have been experimentally observed we focus on transcriptional bursting (Chong et al. 2014; Lenstra et al. 2016; Tunnacliffe and Chubb 2020). The production of mRNA from some genes does not produce a steady stream of mRNAs, but rather proceeds in bursts of production interspersed by periods of quiescence. The most popular model that describes this phenomena is the *telegraph model* (Peccoud and Ycart 1995) where, during the periods when the transcription factor (TF) binds to promoter RNA, polymerases repeatedly initiate transcription, while when transcription factor is off the promoter, the initiation stops. While the data supports temporal coupling between TF binding and initiation of transcriptional bursts, the durations of the binding times and bursts are not equal. For instance, in yeast, an average TF (GAL4) binding time of 34s initiates a mean burst duration of around 2.5 min (Tunnacliffe and Chubb 2020).

We propose that the bursting periodic solutions that we observed in this paper may be one of the mechanisms supporting or enhancing transcriptional bursting. This may be in addition to other proposed mechanisms related to DNA supercoiling (Chong



2 Page 52 of 74 T. Gedeon et al.

et al. 2014), chromatin opening, scaffold presence at initiation site or pulses of nuclear localization (Lenstra et al. 2016).

Acknowledgements MCM would like to thank the Universities of Giessen and Bremen for their hospitality during the time that this work was initiated. ARH is grateful to Stefan Ruschel for introducing him to the 3DL transition literature.

Appendices

A The semiflow of differentiable solution operators generated by the system (2.15)–(2.17) and (2.18)–(2.19)

For delay differential equations a familiar state space is given by continuous functions on a compact interval, see e.g. Hale and Lunel (1993); Diekmann et al. (1995). In case of variable, state-dependent delays, however, there is a specific lack of smoothness which means that in general the initial value problem is not well-posed for only continuous initial data, not to speak of, say, smoothness of solutions with respect to initial data and linearization Walther (2003); Hartung et al. (2006).

In this section we reformulate the system (2.15)–(2.19) as a delay differential equation

$$x'(t) = G(x_t) \tag{A.1}$$

with a vector-valued functional $G: C_3^1 \to \mathbb{R}^3$ on the Banach space $C_3^1 = C^1([-r,0],\mathbb{R}^3)$ of continuously differentiable maps $[-r,0] \to \mathbb{R}^3$, for some r > 0 which is to be determined. The norm on C_3^1 is given by

$$|\phi|_1 = \max_{-r \le t \le 0} |\phi(t)| + \max_{-r \le t \le 0} |\phi'(t)|,$$

with a chosen norm on \mathbb{R}^3 . The argument $x_t \in C_3^1$ in (A.1) is defined for $t \in \mathbb{R}$ with [t-r,t] in the domain of the solution x and given by $x_t(s) = x(t+s)$ for $-r \le s \le 0$. In other words, x_t is the restriction of x to [t-r,t] shifted to the interval [-r,0].

In the sequel shifted segments y_t of maps y from an interval $I \subset \mathbb{R}$ into a set M are defined accordingly: For r > 0 and $t \in \mathbb{R}$ with $[t-r, t] \subset I$ the map $y_t : [-r, 0] \to M$ is given by $y_t(s) = y(t+s), -r \le s \le 0$.

In addition to the space C_3^1 we also need the Banach space $C_3 \supset C_3^1$ of continuous maps $[-r, 0] \to \mathbb{R}^3$, with the norm given by

$$|\phi| = \max_{-r < t < 0} |\phi(t)|,$$

and the Banach spaces C^1 and C of scalar functions $[-r, 0] \to \mathbb{R}$ which are defined analogously to C_3^1 and C_3 .

We shall verify the hypotheses from Walther (2003, 2004); Hartung et al. (2006) which guarantee existence, uniqueness, and differentiability with respect to initial data



of solutions to an initial value problem which is associated with (A.1) in a submanifold of the space C_3^1 .

First we rewrite the system (2.15)–(2.19) in a form which is more convenient for our purpose. Let positive constants

$$c_k$$
 and b_k for $k = 1, 2, 3, a_1$ and a_2, μ

and a continuously differentiable function $g: \mathbb{R} \to \mathbb{R}$ be given, either with

$$g(0) = 1 \quad \text{and g decreasing on } [0, \infty) \text{ with } \quad \lim_{y \to \infty} g(y) > 0,$$

or

$$0 < g(0) < 1$$
 and g increasing on $[0, \infty)$ with $\lim_{y \to \infty} g(y) = 1$.

Let also continuously differentiable functions

$$v_k: \mathbb{R} \to [v_{k min}, \infty)$$

with $0 < v_{k,min}$ be given, for k = 1, 2.

In place of (2.15)–(2.19), we consider the system

$$x_1'(t) = c_1 \frac{v_1(x_3(t))}{v_1(x_3(t - \tau_1(t)))} e^{-\mu \tau_1(t)} g(x_3(t - \tau_1(t))) - b_1 x_1(t), \tag{A.2}$$

$$x_2'(t) = c_2 \frac{v_2(x_1(t))}{v_2(x_1(t - \tau_2(t)))} e^{-\mu \tau_2(t)} x_1(t - \tau_2(t)) - b_2 x_2(t), \tag{A.3}$$

$$x_3'(t) = c_3 x_2(t) - b_3 x_3(t), (A.4)$$

$$a_1 = \int_{t-\tau_1(t)}^t v_1(x_3(s))ds = \int_{-\tau_1(t)}^0 v_1(x_3(t+s))ds, \tag{A.5}$$

$$a_2 = \int_{t-\tau_2(t)}^t v_2(x_1(s))ds = \int_{-\tau_2(t)}^0 v_2(x_1(t+s))ds.$$
 (A.6)

Assume

$$r > \frac{a_k}{v_{k,min}}$$
 for $k = 1, 2$.

Notice that r is an a-priori bound for both delays $\tau_k(t)$, $k \in \{1, 2\}$. Using segment notation the equations (A.5)–(A.6) become

$$a_1 = \int_{-\tau_1(t)}^{0} v_1(x_{3,t}(s))ds$$
 and $a_2 = \int_{-\tau_2(t)}^{0} v_2(x_{1,t}(s))ds$



2 Page 54 of 74 T. Gedeon et al.

with segments $x_{k,t} \in C$, $k \in \{1, 3\}$. More generally, we consider the equations

$$a_k = \int_{-u}^{0} v_k(\phi(s))ds \tag{A.7}$$

for $u \in [0, \infty)$ and $\phi \in C$, $k \in \{1, 2\}$. Using positivity of the functions v_k and the Intermediate Value Theorem we infer that for every $k \in \{1, 2\}$ and for every $\phi \in C$ there is a uniquely determined solution $u = \delta_k(\phi) \in (0, r)$ of Eq. (A.7). This yields maps $\delta_k : C \to (0, r)$, $k \in \{1, 2\}$. The next proposition guarantees that these maps are continuously differentiable and provides formulae for the derivatives.

Proposition A1 Let a>0 and $v_{min}>0$ be given with $\frac{a}{v_{min}}< r$, and let $v:\mathbb{R}\to [v_{min},\infty)$ be continuously differentiable. Then the map $\delta:C\to (0,r)$ given by $\delta(\phi)=u$ with

$$a = \int_{-u}^{0} v(\phi(s))ds \tag{A.8}$$

is continuously differentiable with

$$D\delta(\phi)\chi = -\frac{\int_{-\delta(\phi)}^{0} v'(\phi(s))\chi(s)ds}{v(\phi(-\delta(\phi)))}.$$

In case $\phi(s) = \xi$ for all $s \in [-r, 0]$,

$$\delta(\phi) = \frac{a}{v(\xi)}, \quad and \quad D\delta(\phi)\chi = -\frac{v'(\xi)}{v(\xi)} \int_{-a/v(\xi)}^{0} \chi(s)ds.$$

Before giving the proof recall from Walther (2003, p. 47) or Hartung et al. (2006, p. 466) the elementary facts that the evaluation map

$$ev_C: C \times [-r, 0] \ni (\chi, u) \mapsto \chi(u) \in \mathbb{R}.$$

is continuous (but not locally Lipschitz continuous, let alone differentiable), and that the restricted evaluation map

$$ev:C^1\times (-r,0)\ni (\phi,u)\mapsto \phi(u)\in \mathbb{R}$$

is continuously differentiable with

$$D ev(\phi, u)(\hat{\phi}, \hat{u}) = D_1 ev(\phi, u)\hat{\phi} + D_2 ev(\phi, u)\hat{u} = \hat{\phi}(u) + \phi'(u)\hat{u}$$
 (A.9)

where D_1 and D_2 denote partial derivatives with respect to the argument in C^1 and in (-r,0), respectively. For $v: \mathbb{R} \to \mathbb{R}$ continuously differentiable the substitution operator

$$V: C \ni \phi \mapsto v \circ \phi \in C$$



is continuously differentiable with

$$(DV(\phi)\hat{\phi})(s) = v'(\phi(s))\hat{\phi}(s)$$
 for all $\hat{\phi} \in C$, $s \in [-r, 0]$,

see for example Diekmann et al. (1995, Appendix IV, Lemma 1.5).

Proof of Proposition A1 For every $\phi \in C$ the value $u = \delta(\phi)$ is the unique solution of the equation

$$h(u, \phi) = 0$$

where $h:(0,r)\times C\to\mathbb{R}$ is given by

$$h(u,\phi) = a - \int_{-u}^{0} v(\phi(s))ds = a - ev(I(V(\phi))), -u)$$

with the continuous linear integration operator

$$I: C \to C^1$$
, $(I\psi)(t) = \int_t^0 \psi(s)ds$.

The map h is continuously differentiable with

$$D_1 h(u, \phi) 1 = -v(\phi(-u)) < 0$$

and

$$\begin{split} D_2h(u,\phi)\chi &= -D_1ev(I(V(\phi)), -u)DI(V(\phi))DV(\phi)\chi\\ &= -(DI(V(\phi))DV(\phi)\chi)(-u)\\ &= -(I(DV(\phi)\chi))(-u) = -\int_{-u}^0 v'(\phi(s))\chi(s)ds. \end{split}$$

The Implicit Function Theorem applies at every $(\delta(\phi), \phi) \in (-r, 0) \times C$ and yields that locally, δ is given by a continuously differentiable map. Differentiation of the equation $h(\delta(\phi), \phi) = 0$ gives

$$D\delta(\phi)\chi = -\frac{D_2 h(u,\phi)\chi}{D_1 h(u,\phi)1} \quad \text{(for } u = \delta(\phi))$$
$$= -\frac{\int_{-u}^0 v'(\phi(s))\chi(s)ds}{v(\phi(-u))}.$$

In case ϕ is constant with value $\xi \in \mathbb{R}$ Eq.(A.8) gives $a = \delta(\phi)v(\xi)$, and by the previous formula,



2 Page 56 of 74 T. Gedeon et al.

$$D\delta(\phi)\chi = -\frac{v'(\xi)}{v(\xi)} \int_{-a/v(\xi)}^{0} \chi(s)ds.$$

Using the delay functionals $\delta_k : C \to (0, r), k \in \{1, 2\}$ the system (A.2)–(A.6) is reduced to the system

$$x_1'(t) = c_1 \frac{v_1(x_3(t))}{v_1(x_3(t - \delta_1(x_{3,t})))} e^{-\mu\delta_1(x_{3,t})} g(x_3(t - \delta_1(x_{3,t}))) - b_1 x_1(t), \quad (A.10)$$

$$x_2'(t) = c_2 \frac{v_2(x_1(t))}{v_2(x_1(t - \delta_2(x_{1,t})))} e^{-\mu \delta_2(x_{1,t})} x_1(t - \delta_2(x_{1,t})) - b_2 x_2(t), \tag{A.11}$$

$$x_3'(t) = c_3 x_2(t) - b_3 x_3(t). (A.12)$$

with segments $x_{3,t} \in C$ and $x_{1,t} \in C$. The right hand side of these equations is of the form $G_C(x_t) \in \mathbb{R}^3$ with the map $G_C : C^3 \to \mathbb{R}^3$ given by

$$G_{C,1}(\phi) = c_1 \frac{v_1(\phi_3(0))}{v_1(ev_C(\phi_3, -\delta_1(\phi_3)))} e^{-\mu\delta_1(\phi_3)} g(ev_C(\phi_3, -\delta_1(\phi_3))) - b_1\phi_1(0),$$
(A.13)

$$G_{C,2}(\phi) = c_2 \frac{v_2(\phi_1(0))}{v_2(ev_C(\phi_1, -\delta_2(\phi_1)))} e^{-\mu\delta_2(\phi_1)} ev_C(\phi_1, -\delta_2(\phi_1)) - b_1\phi_2(0),$$
(A.14)

$$G_{C,3}(\phi) = c_3\phi_2(0) - b_3\phi_3(0).$$
 (A.15)

We observe that G_C is continuous. The restriction G of G_C to C_3^1 is continuously differentiable because, for $\phi \in C_3^1 \subset C_3$, we have $ev_C(\phi_3, -\delta_1(\phi_3)) = ev(\phi_3, -\delta_1(\phi_3))$ and $ev_C(\phi_1, -\delta_2(\phi_1)) = ev(\phi_1, -\delta_2(\phi_1))$. Here $ev: C^1 \times (0, r) \to \mathbb{R}$ is continuously differentiable, the maps δ_1 and δ_2 are continuously differentiable, and the projections $C_3^1 \to C^1$ to components as well as the evaluation map $ev_0: C \ni \chi \mapsto \chi(0) \in \mathbb{R}$ are linear and continuous.

In order to simplify calculations below we now introduce the continuous maps

$$E_{C,31}: C_3 \to \mathbb{R}, \quad E_{C,31}(\phi) = ev_C(\phi_3, -\delta_1(\phi_3)),$$

and

$$E_{C,12}: C_3 \to \mathbb{R}, \quad E_{C,12}(\phi) = ev_C(\phi_1, -\delta_2(\phi_1)),$$

and the continuously differentiable maps

$$E_{31}: C_3^1 \to \mathbb{R}, \quad E_{31}(\phi) = ev(\phi_3, -\delta_1(\phi_3)),$$

and

$$E_{12}: C_3^1 \to \mathbb{R}, \quad E_{12}(\phi) = ev(\phi_1, -\delta_2(\phi_1)),$$



with derivatives at $\phi \in C^1$ given by

$$DE_{31}(\phi)\hat{\phi} = D_1 e v(\phi_3, -\delta_1(\phi_3))\hat{\phi}_3 + D_2 e v(\dots)D(-\delta_1)(\phi_3)\hat{\phi}_3$$

$$= \hat{\phi}_3(-\delta_1(\phi_3)) - \phi'_3(-\delta_1(\phi_3))D\delta_1(\phi_3)\hat{\phi}_3,$$

$$DE_{12}(\phi)\hat{\phi} = D_1 e v(\phi_1, -\delta_2(\phi_1))\hat{\phi}_1 + D_2 e v(\dots)D(-\delta_2)(\phi_1)\hat{\phi}_1$$

$$= \hat{\phi}_1(-\delta_2(\phi_1)) - \phi'_1(-\delta_2(\phi_1))D\delta_2(\phi_1)\hat{\phi}_1$$

for all $\hat{\phi} \in C_3^1$. Notice that the right hand sides of these equations make sense also for arguments $\chi \in C_3$ instead of $\hat{\phi} \in C_3^1$. Thus they define linear extensions $D_e E_{31}(\phi)$: $C_3 \to \mathbb{R}$ of $DE_{31}(\phi): C_3^1 \to \mathbb{R}$ and $D_e E_{12}(\phi): C_3 \to \mathbb{R}$ of $DE_{12}(\phi): C_3^1 \to \mathbb{R}$. Using the continuity of the map ev_C , and the fact that differentiation $C^1 \ni \phi \mapsto \phi' \in C$ is linear and continuous we obtain the next result.

Proposition A2 The maps $C_3^1 \times C_3 \ni (\phi, \chi) \mapsto D_e E_{31}(\phi)\chi \in \mathbb{R}$ and $C_3^1 \times C_3 \ni (\phi, \chi) \mapsto D_e E_{12}(\phi)\chi \in \mathbb{R}$ are continuous.

Incidentally, in the case $\phi \in C_3^1$ is constant with value $(\xi_1, \xi_2, \xi_3) \in \mathbb{R}^3$ we have

$$E_{31}(\phi) = \xi_3$$
, $DE_{31}(\phi)\hat{\phi} = \hat{\phi}_3(-a_1/v_1(\xi_3))$

and

$$E_{12}(\phi) = \xi_1, \quad DE_{12}(\phi)\hat{\phi} = \hat{\phi}_1(-a_2/v_2(\xi_1))$$

With the linear continuous evaluation map $ev_0: C \ni \phi \mapsto \phi(0) \in \mathbb{R}$ we obtain for the restriction G of G

$$G_1(\phi) = c_1 \frac{v_1(ev_0\phi_3)}{v_1(E_{31}(\phi))} e^{-\mu\delta_1(\phi_3)} g(E_{31}(\phi)) - b_1 ev_0\phi_1, \tag{A.16}$$

$$G_2(\phi) = c_2 \frac{v_2(ev_0\phi_1)}{v_2(E_{12}(\phi))} e^{-\mu\delta_2(\phi_1)} E_{12}(\phi) - b_2 ev_0\phi_2, \tag{A.17}$$

$$G_3(\phi) = c_3 e v_0 \phi_2 - b_3 e v_0 \phi_3. \tag{A.18}$$

For G_C we have analogous formulas, with $E_{C,31}$ and $E_{C,12}$ instead of E_{31} and E_{12} , respectively. In the sequel we will show that the initial value problem

$$x'(t) = G(x_t)$$
 for $t > 0$, $x_0 = \phi$ (A.19)

is well-posed on the set

$$X_G = \{ \phi \in C_3^1 : \phi'(0) = G(\phi) \}$$

which is a continuously differentiable submanifold of codimension 3 in the space C_3^1 . This result follows from results in Walther (2003, 2004); Hartung et al. (2006)



2 Page 58 of 74 T. Gedeon et al.

provided that the following two assertions are verified:

$$X_G \neq \emptyset$$

and

(e) each derivative $DG(\phi): C_3^1 \to \mathbb{R}^3$, $\phi \in C_3^1$, has a linear extension $D_eG(\phi): C_3 \to \mathbb{R}^3$, and the map

$$C_3^1 \times C_3 \ni (\phi, \hat{\phi}) \mapsto D_e G(\phi) \hat{\phi} \in \mathbb{R}^3$$

is continuous.

Property (e) is a version of being *almost Fréchet differentiable* from Mallet-Paret et al. (1994).

We now proceed to the verification of $X_G \neq \emptyset$. Choose $\phi_3 \in C^1$ to be a constant with value 1. Then $a_1\delta_1(\phi_3) = v_1(1)$. Choose $\xi_1 > 0$ with $0 = c_1e^{-\mu v_1(1)/a_1}g(1) - \xi_1$ and define $\phi_1 \in C^1$ to be constant with value ξ_1 . Define $\xi_2 > 0$ by $0 = c_3\xi_2 - b_3$. There exists $\phi_2 \in C^1$ such that $\phi_2(0) = \xi_2$ and $\phi_2'(0) = c_3\xi_2 - b_3$. Then $\phi \in C_3^1$ with the components ϕ_1, ϕ_2, ϕ_3 satisfies the equation $\phi'(0) = G(\phi)$ defining the set X_G , so $X_G \neq \emptyset$.

To prepare for the proof of extension property (e) we compute the derivatives $DG(\phi)$, $\phi \in C_3^1$. For $\hat{\phi} \in C_3^1$ we have

$$DG(\phi)\hat{\phi} = (DG_1(\phi)\hat{\phi}, DG_2(\phi)\hat{\phi}, DG_3(\phi)\hat{\phi}) \in \mathbb{R}^3.$$

For $\delta_1: C \to \mathbb{R}$ and $\delta_2: C \to \mathbb{R}$ we use the fact that restrictions of differentiable maps $m: C \to \mathbb{R}$ to C^1 remain differentiable, with derivatives $D(m|C^1)(\phi): C^1 \to \mathbb{R}$ being restrictions of the derivatives $Dm(\phi): C \to \mathbb{R}, \phi \in C^1 \subset C$, and obtain

$$\begin{split} DG_{1}(\phi)\hat{\phi} &= -b_{1}\hat{\phi}_{1}(0) + c_{1} \left\{ \frac{1}{[v_{1}(E_{31}(\phi))]^{2}} \right. \\ &\times \left[v_{1}'(\phi_{3}(0))\hat{\phi}_{3}(0) \cdot v_{1}(E_{31}(\phi)) - v_{1}(\phi_{3}(0))v_{1}'(E_{31}(\phi))DE_{31}(\phi)\hat{\phi} \right] \cdot e^{-\mu\delta_{1}(\phi_{3})}g(E_{31}(\phi)) \\ &+ \frac{v_{1}(\phi_{3}(0))}{v_{1}(E_{31}(\phi))} \cdot \left[-\mu e^{-\mu\delta_{1}(\phi_{3})}D\delta_{1}(\phi_{3})\hat{\phi}_{3} \cdot g(E_{31}(\phi)) + e^{-\mu\delta_{1}(\phi_{3})}Dg(E_{31}(\phi))DE_{31}(\phi)\hat{\phi} \right] \right\} \end{split}$$

$$(A.20)$$

and

$$DG_{2}(\phi)\hat{\phi} = -b_{2}\hat{\phi}_{2}(0) + c_{2}\left\{\frac{1}{[v_{2}(E_{12}(\phi))]^{2}}\right\}$$

$$\times \left[v'_{2}(\phi_{1}(0))\hat{\phi}_{1}(0) \cdot v_{2}(E_{12}(\phi)) - v_{2}(\phi_{1}(0))v'_{2}(E_{12}(\phi))DE_{12}(\phi)\hat{\phi}\right] \cdot e^{-\mu\delta_{2}(\phi_{1})}E_{12}(\phi)$$

$$+ \frac{v_{2}(\phi_{1}(0))}{v_{2}(E_{12}(\phi))}\left[-\mu e^{-\mu\delta_{2}(\phi_{1})}D\delta_{2}(\phi_{1})\hat{\phi}_{1} \cdot E_{12}(\phi) + e^{-\mu\delta_{2}(\phi_{1})}DE_{12}(\phi)\hat{\phi}\right]\right\}$$

and

$$DG_3(\phi)\hat{\phi} = -b_3\hat{\phi}_3(0) + c_3\hat{\phi}_2(0).$$



Now we are ready to verify property (e). In the formula for $DG(\phi)\hat{\phi}$, ϕ and $\hat{\phi}$ in C_3^1 , just obtained replace the real numbers $DE_{31}(\phi)\hat{\phi}$, $DE_{12}(\phi)\hat{\phi}$ by $D_e E_{31}(\phi) \chi$, $D_e E_{12}(\phi) \chi$, respectively, with $\chi \in C_3$, and replace the functions $\hat{\phi}_3$, $\hat{\phi}_1$ by χ_3 and χ_1 , respectively. This defines $D_eG(\phi)\chi \in \mathbb{R}^3$ for $\phi \in C_3$ and $\chi \in C_3$ so that the maps $D_eG(\phi): C_3 \to \mathbb{R}^3, \phi \in C_3^1$, are linear. Using the continuous differentiability of $\delta_1: C \to \mathbb{R}$ and $\delta_2: C \to \mathbb{R}$, and Proposition A2, one shows that the map $C_3^1 \times C_3 \ni (\phi, \chi) \mapsto D_e G(\phi) \chi \in \mathbb{R}^3$ is continuous. This finishes the proof of property (e).

Operon dynamics with state dependent transcription and/or...

With $X_G \neq \emptyset$ and property (e) verified, results from Walther (2003, 2004); Hartung et al. (2006) apply and yield the following. The set X_G is a continuously differentiable submanifold of the Banach space C_3^1 , with codimension 3. Each $\phi \in X_G$ uniquely determines a maximal continuously differentiable solution $x:[-r,t_x)\to\mathbb{R}^3, 0<$ $t_x \leq \infty$, of the initial value problem (A.19). That is, x is continuously differentiable and satisfies $x_0 = \phi$ and $x'(t) = G(x_t)$ for all $t \in (0, t_x)$, and any other continuously differentiable function $y:[-r,t_y)\to\mathbb{R}^3, 0< t_y\leq\infty$, which satisfies $y_0=\phi$ and $y'(t) = G(y_t)$ for all $t \in (0, t_y)$ is a restriction of x. All segments $x_t, 0 \le t < \infty$, belong to X_G (because of the differential equation). Write $x^{\phi} = x$ and $t_{\phi} = t_x$. Let

$$\Omega_G = \{(t, \phi) \in [0, \infty) \times X_G : 0 \le t < t_{\phi}\}.$$

The equation

$$S_G(t, \phi) = x_t^{\phi}$$

defines a continuous semiflow $S_G: \Omega_G \to X_G$. For each $t \geq 0$ the set

$$\Omega_{G,t} = \{ \phi \in X_G : t < t_{\phi} \}$$

is an open subset of X_G (possibly empty), $\Omega_{G,0} = X_G$, and each map

$$S_{G,t}: \Omega_{G,t} \ni \phi \mapsto S_G(t,\phi) \in X_G, \quad t > 0,$$

on a non-empty domain is continuously differentiable.

Moreover, the restriction of the semiflow S_G to the open subset $\{(t, \phi) \in \Omega_G : r < 0\}$ t} of the manifold $\mathbb{R} \times X_G$ is continuously differentiable Walther (2004).

We end this section with remarks about linearization at stationary points (equilibria) of the semiflow, for which $t_{\phi} = \infty$ and $S_G(t, \phi) = \phi$ for all $t \ge 0$. Such ϕ are constant since for every t > 0, $x^{\phi}(t) = x_t^{\phi}(0) = S_G(t, \phi)(0) = \phi(0)$, hence

$$\phi(s) = S_G(r, \phi)(s) = x_r^{\phi}(s) = x^{\phi}(r+s) = \phi(0)$$
 for each $s \in [-r, 0]$.

So assume $\phi \in C_3^1$ is constant with value $(\xi_1, \xi_2, \xi_3) \in \mathbb{R}^3$, and $\hat{\phi} \in C_3^1$. We compute $DG(\phi)\hat{\phi}$, using Proposition A1 for the values and for the derivatives of the maps δ_1 , δ_2 in case of constant arguments, and using the calculations right after Proposition A2



2 Page 60 of 74 T. Gedeon et al.

for $DE_{31}(\phi)\hat{\phi}$, $DE_{12}(\phi)\hat{\phi}$ in case of constant arguments. The result is

$$DG_{1}(\phi)\hat{\phi} = -b_{1}\hat{\phi}_{1}(0) + c_{1}\left\{\frac{1}{[v_{1}(\xi_{3})]^{2}}\left[v'_{1}(\xi_{3})\hat{\phi}_{3}(0) \cdot v_{1}(\xi_{3})\right.\right.$$

$$\left. - v_{1}(\xi_{3})v'_{1}(\xi_{3})\hat{\phi}_{3}(-a_{1}/v_{1}(\xi_{3}))\right] \cdot e^{-\mu a_{1}/v_{1}(\xi_{3})}g(\xi_{3})$$

$$\left. + \frac{v_{1}(\xi_{3})}{v_{1}(\xi_{3})}\left[-\mu e^{-\mu a_{1}/v_{1}(\xi_{3})}\left(-\frac{v'_{1}(\xi_{3})}{v_{1}(\xi_{3})}\int_{-a_{1}/v_{1}(\xi_{3})}^{0}\hat{\phi}_{1}(s)ds\right) \cdot g(\xi_{3})\right.$$

$$\left. + e^{-\mu a_{1}/v_{1}(\xi_{3})}g'(\xi_{3})\hat{\phi}_{3}(-a_{1}/v_{1}(\xi_{3}))\right]\right\}$$

$$= -b_{1}\hat{\phi}_{1}(0) + A_{1}\hat{\phi}_{3}(0) + \mu A_{1}\int_{-a_{1}/v_{1}(\xi_{3})}^{0}\hat{\phi}_{3}(s)ds$$

$$\left. + \left(c_{1}e^{-\mu a_{1}/v_{1}(\xi_{3})}g'(\xi_{3}) - A_{1}\right)\hat{\phi}_{3}(-a_{1}/v_{1}(\xi_{3}))\right. \tag{A.21}$$

with

$$A_1 = c_1 \frac{v_1'(\xi_3)}{v_1(\xi_3)} e^{-\mu a_1/v_1(\xi_3)} g(\xi_3)$$
(A.22)

and

$$DG_{2}(\phi)\hat{\phi} = -b_{2}\hat{\phi}_{2}(0) + c_{2}\left\{\frac{1}{[v_{2}(\xi_{1})]^{2}}\left[v_{2}'(\xi_{1})\hat{\phi}_{1}(0) \cdot v_{2}(\xi_{1})\right]\right\}$$

$$-v_{2}(\xi_{1})v_{2}'(\xi_{1})\hat{\phi}_{1}(-a_{2}/v_{2}(\xi_{1}))\right] \cdot e^{-\mu a_{2}/v_{2}(\xi_{1})}\xi_{1}$$

$$+\frac{v_{2}(\xi_{1})}{v_{2}(\xi_{1})}\left[-\mu e^{-\mu a_{2}/v_{2}(\xi_{1})}\left(-\frac{v_{2}'(\xi_{1})}{v_{2}(\xi_{1})}\int_{-a_{2}/v_{2}(\xi_{1})}^{0}\hat{\phi}_{1}(s)ds\right) \cdot \xi_{1}$$

$$+e^{-\mu a_{2}/v_{2}(\xi_{1})}\hat{\phi}_{1}(-a_{2}/v_{2}(\xi_{1}))\right]$$

$$=-b_{2}\hat{\phi}_{2}(0) + A_{2}\hat{\phi}_{1}(0) + \left(c_{2}e^{-\mu a_{2}/v_{2}(\xi_{1})} - A_{2}\right)\hat{\phi}(-a_{2}/v_{2}(\xi_{1}))$$

$$+\mu A_{2}\int_{-a_{2}/v_{2}(\xi_{1})}^{0}\hat{\phi}_{1}(s)ds \qquad (A.23)$$

with

$$A_2 = c_2 \frac{v_2'(\xi_1)}{v_2(\xi_1)} e^{-\mu a_2/v_2(\xi_1)} \xi_1 \tag{A.24}$$

and

$$DG_3(\phi)\hat{\phi} = -b_3\hat{\phi}_3(0) + c_3\hat{\phi}_2(0).$$
 (A.25)



B Positivity, dissipativity, global attractor

Recall that the function g in Eqs. (A.10) and (A.16) has a positive infimum $g_{min} > 0$, and

$$g_{min} \leq g(\xi) \leq 1$$
 for all $\xi \in \mathbb{R}$.

In addition to the hypotheses made in the preceding Sect. A we assume in the present section that the functions v_k , $k \in \{1, 2\}$, are also bounded from above by real numbers $v_{k,max} > 0$. Using Eq. (A.7) we infer

$$\frac{a_k}{v_{k,max}} \le \delta_k(\phi) \le \frac{a_k}{v_{k,min}}$$

for k = 1, 2 and for all $\phi \in C$.

Proposition B1 For every c > 0 there exists c' > 0 so that for all $\phi \in X_G$ with $|\phi(t)| \le c$ on [-r, 0] and for all $t \in [-r, t_{\phi})$ we have $|x^{\phi}(t)| \le c'$.

Proof Let $\phi \in X_G$ with $|\phi(t)| \le c$ on [-r, 0] be given, set $x = x^{\phi}$. The first term on the right hand side of Eq. (A.10) is positive and bounded by the constant

$$d_1^> = c_1 \frac{v_{1,max}}{v_{1,min}}.$$

The variation-of-constants formula yields

$$|x_{1}(t)| = \left| x_{1}(0)e^{-b_{1}t} + \int_{0}^{t} e^{-b_{1}(t-s)} \left[\frac{c_{1}v_{1}(x_{3}(s))}{v_{1}(x_{3}(s-\delta_{1}(x_{3,s})))} e^{-\mu\delta_{1}(x_{3,s})} g(x_{3}(s-\delta_{1}(x_{3,s}))) \right] ds \right|$$

$$\leq c + e^{-b_{1}t} \frac{d_{1}^{>}}{b_{1}} \left(e^{b_{1}t} - 1 \right) \quad \text{for} \quad 0 \leq t < t_{\phi}$$

$$\leq c + \frac{d_{1}^{>}}{b_{1}} \quad \text{for} \quad 0 \leq t < t_{\phi}.$$

Set $d_1 = c + \frac{d_1^>}{b_1}$. With $|x_1(t)| = |\phi_1(t)| \le |\phi| \le c$ on [-r, 0] we get $|x_1(t)| \le d_1$ for all $t \in [-r, t_{\phi})$. Next, the first term on the right hand side of Eq.(A.11) is bounded by

$$d_2^{>} = c_2 \frac{v_{2,max}}{v_{2,min}} d_1.$$

Using the variation-of-constants formula as above, and $|x_2(t)| = |\phi_2(t)| \le |\phi| \le c$ on [-r, 0] we obtain that x_2 is bounded by $d_2 = c + \frac{d_2^{>}}{b_2}$ for all $t \in [-r, t_{\phi})$. We turn



2 Page 62 of 74 T. Gedeon et al.

to Eq. (A.12) where the first term on the right hand side is bounded by

$$d_3^> = c_3 d_2$$
.

Using the variation-of-constants formula once more, and $|x_3(t)| = |\phi_3(t)| \le |\phi| \le c$ on [-r, 0] we obtain that x_3 is bounded by $d_3 = c + \frac{d_3^>}{b_3}$ on $[-r, t_\phi)$.

We continue with an observation. For any (continuously differentiable) solution $x : [-r, t_x) \to \mathbb{R}^3$ of the system (A.10)–(A.12) and for any $t \in [0, t_x)$ the first term on the right hand side of Eq. (A.10) belongs to the interval

$$[d_1^{<}, d_1^{>}] = \left[c_1 \frac{v_{1,min}}{v_{1,max}} e^{-\mu a_1/v_{1,min}} g_{min}, c_1 \frac{v_{1,max}}{v_{1,min}}\right]$$

and in case

$$x_1(t) > \frac{d_1^>}{b_1}$$
 we have $x_1'(t) \le d_1^> - b_1 x_1(t) < 0$

while in case

$$x_1(t) < \frac{d_1^{<}}{b_1}$$
 we have $x_1'(t) \ge d_1^{<} - b_1 x_1(t) > 0$.

Set

$$d_{2}^{<} = c_{2} \frac{v_{2,min}}{v_{2,max}} e^{-\mu a_{2}/v_{2,min}} \frac{d_{1}^{<}}{b_{1}} \quad \text{and} \quad d_{2}^{>} = c_{2} \frac{v_{2,max}}{v_{2,min}} e^{-\mu a_{2}/v_{2,max}} \frac{d_{1}^{>}}{b_{1}},$$

$$d_{3}^{<} = c_{3} \frac{d_{2}^{<}}{b_{2}} \quad \text{and} \quad d_{3}^{>} = c_{3} \frac{d_{2}^{>}}{b_{2}},$$

and

$$Q = \left\lceil \frac{d_1^{<}}{b_1}, \frac{d_1^{>}}{b_1} \right\rceil \times \left\lceil \frac{d_2^{<}}{b_2}, \frac{d_2^{>}}{b_2} \right\rceil \times \left\lceil \frac{d_3^{<}}{b_3}, \frac{d_3^{>}}{b_3} \right\rceil \subset \mathbb{R}^3$$

and

$$R = \{ \phi \in C_3^1 : \phi([-r, 0]) \subset Q \}.$$

Proposition B2 (Global existence, absorption and positive invariance, positivity)

- (i) For all $\phi \in X_G$, $t_{\phi} = \infty$.
- (ii) For every neighbourhood N of Q in \mathbb{R}^3 and for each $\phi \in X_G$ there exists $t(\phi, N) \in [0, \infty)$ with $x^{\phi}(t) \in N$ for all $t \geq t(\phi, N)$.
- (iii) If $\phi \in X_G \cap R$ then $x^{\phi}(t) \in Q$ for all $t \geq 0$.
- (iv) If all 3 components of $\phi \in X_G$ are strictly positive then $x_k^{\phi}(t) > 0$ for all $t \ge -r$, $k \in \{1, 2, 3\}$.



Proof 1. On assertion (i). Let $\phi \in X_G$ be given. Due to Proposition B1 the solution $x = x^{\phi}$ is bounded. Using this and the system (A.10)–(A.12) we infer that x' is bounded. It follows that x is Lipschitz continuous. Assume now $t_{\phi} < \infty$. Then Lipschitz continuity yields that x has a limit $\xi \in \mathbb{R}^3$ at $t = t_{\phi}$. x extends to a continuous map $\hat{x} : [-r, t_{\phi}] \to \mathbb{R}^3$. From uniform continuity on the compact interval $[-r, t_{\phi}]$ it follows that the curve $[0, t_{\phi}] \ni t \mapsto \hat{x}_t \in C_3$ is continuous. Using this and the equation

$$x'(t) = G(x_t) = G_C(\hat{x}_t)$$
 for $0 \le t < t_{\phi}$

with the continuous map $G_C: C^3 \to \mathbb{R}^3$ we also conclude that x' has a limit $\eta \in \mathbb{R}^3$ at $t = t_\phi$. It follows that \hat{x} is continuously differentiable (with $\hat{x}'(t_\phi) = \eta$), and $\hat{x}'(t_\phi) = G_C(\hat{x}_{t_\phi}) = G(\hat{x}_{t_\phi})$. In particular, $\psi = \hat{x}_{t_\phi}$ belongs to X_G , and defines a maximal solution $x^{\psi}: [0, t_{\psi}) \to \mathbb{R}^3$ of Eq.(A.1), with $0 < t_{\psi} \le \infty$. By means of the semiflow properties it follows that in case $t_{\psi} = \infty$ we have $t_{\phi} = \infty$, in contradiction to the assumption above, while in case $t_{\psi} < \infty$ we get $t_{\phi} \ge t_{\phi} + t_{\psi}$, which contradicts $t_{\psi} > 0$.

2. On assertion (ii). Let a neighbourhood N of Q in \mathbb{R}^3 and $\phi \in X_G$ be given. Set $x = x^{\phi}$. There exists $\epsilon > 0$ so that for

$$d_{1,-\epsilon} = \frac{d_1^{<}}{b_1} - \epsilon, \ d_{2,-\epsilon}^* = c_2 \frac{v_{2,min}}{v_{2,max}} e^{-\mu a_2/v_{2,min}} \cdot d_{1,-\epsilon}, \qquad d_{2,-\epsilon} = \frac{d_{2,-\epsilon}^*}{b_2} - \epsilon, \\ d_{1,+\epsilon} = \frac{d_1^{>}}{b_1} + \epsilon, \ d_{2,+\epsilon}^* = c_2 \frac{v_{2,max}}{v_{2,min}} e^{-\mu a_2/v_{2,max}} \cdot d_{1,+\epsilon}, \qquad d_{2,+\epsilon} = \frac{d_{2,-\epsilon}^*}{b_2} + \epsilon$$

we have

$$d_{1,-\epsilon} > 0$$
 and $d_{2,-\epsilon} > 0$ and $\frac{c_3 \cdot d_{2,-\epsilon}}{b_3} - \epsilon > 0$,

and

$$N\supset [d_{1,-\epsilon},d_{1,+\epsilon}]\times [d_{2,-\epsilon},d_{2,+\epsilon}]\times \left\lceil \frac{c_3\cdot d_{2,-\epsilon}}{b_3}-\epsilon,\frac{c_3\cdot d_{2,+\epsilon}}{b_3}+\epsilon\right\rceil.$$

2.1. Proof that in case $x_1(t) \le d_{1,+\epsilon}$ for some $t \ge 0$ we have

$$x_1(s) \le d_{1,+\epsilon}$$
 for all $s \ge t$.

Otherwise $x_1(s) > d_{1,+\epsilon} = \frac{d_1^>}{b_1} + \epsilon$ for some s > t. For the smallest $u \in [t, s]$ with $x_1(u) = x_1(s)$ we have $0 \le x'(u)$ and, on the other hand,

$$x_1'(u) < d_1^> - b_1 x_1(u) = d_1^> - b_1 x_1(s) < -\epsilon b_1 < 0.$$

2.2. Proof that in case $x_1(s) > d_{1,+\epsilon}$ for some $s \ge 0$ there exists t > s with

$$x_1(t) \leq d_{1,+\epsilon}$$
.

2 Page 64 of 74 T. Gedeon et al.

Otherwise $x_1(t) > d_{1,+\epsilon} = \frac{d_1^{>}}{b_1} + \epsilon$ on $[s, \infty)$. Hence

$$x_1'(t) < d_1^> - b_1 x_1(t) < -\epsilon b_1 < 0 \text{ on } [s, \infty),$$

and consequently $x_1(t) \to -\infty$ as $t \to \infty$, in contradiction to the assumption.

2.3. It follows that there exists $t_1^* \ge 0$ with

$$x_1(t) \le d_{1,+\epsilon}$$
 for all $t \ge t_1^*$.

Similarly one finds $t_1 \ge t_1^*$ with

$$x_1(t) \ge d_{1,-\epsilon}$$
 for all $t \ge t_1$.

Hence

$$x_1(t) \in [d_{1-\epsilon}, d_{1+\epsilon}]$$
 for all $t > t_1$.

2.4. We proceed to x_2 . The result of Part 2.3 yields that for $t \ge t_1 + r$ the first term on the right hand side of Eq. (A.11) is contained in the interval

$$\left[c_2 \frac{v_{2,min}}{v_{2,max}} e^{-\mu a_2/v_{2,min}} \cdot d_{1,-\epsilon}, c_2 \frac{v_{2,max}}{v_{2,min}} e^{-\mu a_2/v_{2,max}} \cdot d_{1,+\epsilon}\right] = [d_{2,-\epsilon}^*, d_{2,+\epsilon}^*].$$

Arguing as in Parts 2.1–2.3 we find $t_2 \ge t_1 + r$ so that for all $t \ge t_2$ we have

$$x_2(t) \in [d_{2-\epsilon}, d_{2+\epsilon}].$$

2.5. Consider x_3 . For $t \ge t_2$ the first term on the right hand side of Eq. (A.12) is contained in the interval

$$[c_3 \cdot d_{2,-\epsilon}, c_3 \cdot d_{2,+\epsilon}].$$

Arguing as in Parts 2.1–2.3 we find $t_3 \ge t_2$ so that for all $t \ge t_3$ we have

$$x_3(t) \in \left[\frac{c_3 \cdot d_{2,-\epsilon}}{b_3} - \epsilon, \frac{c_3 \cdot d_{2,+\epsilon}}{b_3} + \epsilon\right].$$

2.6. For all $t \geq t_3$,

$$x(t) \in [d_{1,-\epsilon},d_{1,+\epsilon}] \times [d_{2,-\epsilon},d_{2,+\epsilon}] \times \left[\frac{c_3 \cdot d_{2,-\epsilon}}{b_3} - \epsilon, \frac{c_3 \cdot d_{2,+\epsilon}}{b_3} + \epsilon\right] \subset N.$$

3. The proof of assertion (iii) begins with the assumption that for a given $\phi \in X_G \cap R$ there exists s > 0 with $x^{\phi}(s) > \frac{d_1^{>}}{b_1}$ and is then accomplished by a simplified version of arguments as in Part 2.



4. On assertion (iv). Let $\phi \in X_G$ be given with strictly positive components. Set $x = x^{\phi}$. The assumption $x_1(t) \le 0$ for some t > 0 leads to a smallest t > 0 with $x_1(t) = 0$. Necessarily, $x_1'(t) \le 0$ while Eq. (A.10) yields $x_1'(t) > 0$. It follows that $x_1(t) > 0$ for all $t \ge -r$. Using this and Eq. (A.11) and strict positivity of ϕ_2 one shows in the same way that also x_2 is strictly positive. From this one deduces that x_3 is strictly positive.

The solution manifold X_G is a closed subset of the space C_3^1 , and thereby a complete metric space with respect to the metric given by the norm on C_3^1 . The next result implies that the semiflow S_G on the complete metric space X_G is point dissipative as defined in Hale (1988), which means that there exists a bounded set B such that for every $\epsilon>0$ and for each $\phi\in X_G$ there exists $t_{B,\epsilon,\phi}\geq 0$ with $S_G(t,\phi)$ contained in the ϵ -neighbourhood $U_\epsilon(B)=\cup_{b\in B}U_\epsilon(b)$ of B.

Corollary B3 There is a bounded open subset B_G of the submanifold $X_G \subset C_3^1$, with

$$\phi_k(t) > 0$$
 for all $\phi \in B_G$, $t \in [-r, 0]$, $k \in \{1, 2, 3\}$,

such that for every $\phi \in X_G$ there exists $t(\phi) \geq 0$ with

$$S_G(t, \phi) \in B_G \text{ for all } t \ge t(\phi).$$

Proof Choose c>0 so that $N=(0,c)^3$ is a neighbourhood of Q. Set $\tilde{R}=\{\phi\in C_3^1:\phi([-r,0])\subset N\}$. Le $\phi\in X_G$ be given. Choose $t(\phi,N)$ according to Proposition B1(ii). From Eqs. (A.10)–(A.12)we see that the map G sends the set \tilde{R} (which is not a bounded subset of C_3^1) into a bounded subset of \mathbb{R}^3 , say, into $\{x\in\mathbb{R}^3:|x|< b\}$ for some b>0. It follows that for all $t\geq t(\phi,N)+r$ we have $|(x^\phi)'(t)|< b$. For $t\geq t(\phi,N)+2r$ we obtain $x_t^\phi\in\{\phi\in X_G\cap \tilde{R}:|\phi'|< b\}=B_G$. The set B_G is an open and bounded subset of X_G , with $0<\phi_k(t)$ for all $\phi\in B_G$, $k\in\{1,2,3\}$, $t\in[-r,0]$.

Recall from Hale (1988) the definition of a global attractor of a semiflow, which in case of our semiflow S_G is equivalent to saying that a subset $A_G \subset X_G$ is a global attractor if it is compact, and invariant in the sense that for every $\phi \in A_G$ there exists a complete flowline³ with $\xi(0) = \phi$ and $\xi(\mathbb{R}) \subset A_G$, and if A_G attracts every bounded set $B \subset X_G$ in the sense that given an open neighbourhood $U \supset A_G$ of A_G in X_G there exists $t_{B,U} \geq 0$ such that

$$S_G([t_{B|U},\infty)\times B)\subset U.$$

Hale (1988, Theorem 3.4.8) guarantees the existence of such a global attractor provided the semiflow is point-dissipative and there exists $t_1 \ge 0$ so that the semiflow S_G is completely continuous for $t \ge t_1$. The property of being completely continuous (for $t \ge t_1$) is explained after Hale (1988, Lemma 3.2.1). It means that

³ A complete flowline is a curve $\xi : \mathbb{R} \to X_G$ with $\xi(t+s) = S_G(t,\xi(s))$ for all $t \ge 0$ and $s \in \mathbb{R}$.



2 Page 66 of 74 T. Gedeon et al.

(1) S_G is conditionally completely continuous for $t \ge t_1$ in the sense that for every $t \ge t_1$ and for each bounded set $B \subset X_G$ for which $S_G([0, t] \times B)$ is bounded the set $S_G(t, B)$ is precompact (has compact closure), and that

(2) for each bounded set $B \subset X_G$ and for all $t \geq 0$ the set $S_G([0, t] \times B)$ is bounded.

Theorem B4 The semiflow S_G has a global attractor $A_G \subset X_G$, with $\phi_k(t) > 0$ for all $\phi \in A_G$, $t \in [-r, 0]$, $k \in \{1, 2, 3\}$.

Proof 1. We first show that for every bounded subset $B \subset X_G$ there exists $c_B > 0$ with

$$|x^{\phi}(t)| \le c_B$$
 and $|(x^{\phi})'(t)| \le c_B$ for all $\phi \in B$, $t \ge -r$.

Let $B \subset X_G$ be a bounded subset which is bounded with respect to the norm of the space C_3^1 . Proposition B1 guarantees a constant $c_{B,0}$ with $|x^{\phi}(t)| \leq c_{B,0}$ for all $\phi \in B$, $t \geq -r$. Then the formulae (A.16)–(A.18) show that the set $\{G(x_t^{\phi}) \in \mathbb{R}^3 : \phi \in B, t \geq 0\}$ is bounded, and Eq. (A.1) gives that the set $\{(x^{\phi})'(t) \in \mathbb{R}^3 : \phi \in B, t \geq 0\}$ is bounded. Also the set $\{\phi'(t) \in \mathbb{R}^3 : \phi \in B, -r \leq t \leq 0\}$ is bounded.

2. Claim: For every bounded subset $B \subset X_G$ the set $S_G(r, B) \subset X_G$ has compact closure in C_3^1 .

Proof: (a) Let $B \subset X_G$ be a bounded subset of C_3^1 . Due to Part 1 the sets $\{x^{\phi}(t) \in \mathbb{R}^3 : \phi \in B, -r \leq t \leq r\}$ and $\{(x^{\phi})'(t) \in \mathbb{R}^3 : \phi \in B, -r \leq t \leq r\}$ are bounded. Using the Mean Value Theorem we see that in particular the set $S_G(r, B)$ is equicontinuous. As it also is bounded in C_3 the Ascoli-Arzèla Theorem implies that its closure in C_3 is compact.

(b) We turn to the set $\{S_G(r, \phi)' \in C_3 : \phi \in B\}$ of derivatives, which is bounded in C_3 , and proceed to show that it is also equicontinuous. As in Part (a) one sees that the closure K of the set

$${S_G(t,\phi) \in C_3 : \phi \in B, 0 \le t \le r}$$

in the space C_3 is compact. The map $G: C_3^1 \to \mathbb{R}^3$ is the restriction of the continuous map $G_C: C_3 \to \mathbb{R}^3$ which is uniformly continuous on the compact set $K \subset C_3$. Using the boundedness of the set $\{(x^\phi)'(t) \in \mathbb{R}^3 : \phi \in B, -r \le t \le r\}$ and the Mean Value Theorem one finds that the curves

$$[0, r] \ni t \mapsto S_G(t, \phi) \in C_3, \quad \phi \in B,$$

are uniformly Lipschitz continuous, hence equicontinuous. Now let $t_0 \in [0, r]$ and $\epsilon > 0$ be given. There exists $\delta > 0$ with

$$|G_C(\phi) - G_C(\psi)| \le \epsilon$$
 for all ϕ, ψ in $S_G([0, r] \times B)$ with $|\phi - \psi| \le \delta$,

due to uniform continuity of G_C on K. Due to equicontinuity there exists $\eta > 0$ with

$$|S_G(t,\phi) - S_G(t_0,\phi)| \le \delta$$
 for all $\phi \in B$ and $t \in [0,r]$ with $|t-t_0| < \eta$.



Hence

$$|(x^{\phi})'(t) - (x^{\phi})'(t_0)| = |G(S_G(t, \phi)) - G(S_G(t_0, \phi))|$$

= |G_C(S_G(t, \phi)) - G_C(S_G(t_0, \phi))| < \epsilon

for all $\phi \in B$ and $t \in [0, r]$ with $|t - t_0| < \eta$.

- (c) The Ascoli-Arzèla Theorem implies that the closure of $\{S_G(r,\phi)'\in C_3:\phi\in B\}$ in C_3 is compact. For the closure of $S_G(r,B)$ in C_3^1 to be compact it is sufficient to show that every sequence of points $\phi_j\in S_G(r,B),\ j\in\mathbb{N}$, has a subsequence which converges in C_3^1 . Let a sequence $(\phi_j)_1^\infty$ in $S_G(r,B)$ be given. Part a) yields that there is a subsequence $(\phi_{\alpha(j)})_{j=1}^\infty$ which converges in C_3 to some $\phi\in C_3$. Part b) yields that there is a further subsequence $(\phi_{\alpha(\beta(j))})_{j=1}^\infty$ so that the derivatives $(\phi'_{\alpha(\beta(j))})\in C_3$ converge to some $\psi\in C_3$. It follows that $\phi\in C_3^1$ with $\phi'=\psi$, which in turn yields $\phi_{\alpha(\beta(j))}\to \phi$ in C_3^1 as $j\to\infty$.
- 3. We now show that for every bounded subset $B \subset X_G$ and for every $t \geq r$ the set $S_G(t, B) \subset X_G$ has compact closure in C_3^1 . Let $B \subset X_G$ be bounded and let t > r. Then

$$S_G(t, B) = S_G(t - r, S_G(r, B)).$$

Use that the closure of $S_G(r, B)$ in C_3^1 is compact and belongs to X_G (sinces X_G is a closed subset of C_3^1), and that the map $S_G(t-r,\cdot)$ is continuous, and conclude that the closure of $S_G(t, B)$ in C_3^1 is contained in a compact subset of $X_G \subset C_3^1$.

- 4. According to the remark preceding Corollary B3 the semiflow S_G is point dissipative. The results of Parts 1 and 3 combined yield that S_G is *completely continuous* for t > r as stated before Theorem B4. Using (Hale (1988), Theorem 3.4.8) we infer that S_G has a global attractor.
- 5. We now show that for all $\phi \in A_G$, $t \in [-r, 0]$, $k \in \{1, 2, 3\}$ we have $\phi_k(t) > 0$. Let $\phi \in A_G$ be given. There exists a solution $x : \mathbb{R} \to \mathbb{R}^3$ of the system (A.10)–(A.12) with $x_0 = \phi$ and all segments x_s , $s \in \mathbb{R}$, in A_G . It follows that x is bounded.
 - (a) We now show that $x_1(t) > 0$ for all $t \in \mathbb{R}$. Assume $x_1(t) \le 0$ for some $t \in \mathbb{R}$. In case $x_1(t) = 0$ Eq. (A.10) yields $x_1'(t) > 0 b_1x_1(t) = 0$. It follows that $x_1(u) < 0$ for some $u \in (-\infty, t)$. In case $x_1(t) < 0$ set u = t. For every $s \le u$ the variation-of-constants formula yields

$$x_1(u) \ge x_1(s)e^{-b_1(u-s)} + 0,$$

hence

$$x_1(s) \le x_1(u)e^{b_1(u-s)} \quad (\to -\infty \text{ as } s \to -\infty),$$

and we arrive at a contradiction to the boundedness of x_1 .

(b) Using Part (a) and Eq.(A.11) and arguing as in Part (a) one finds $x_2(t) > 0$ for all $t \in \mathbb{R}$. Using this and Eq.(A.12) and arguing once more as in Part (a)



2 Page 68 of 74 T. Gedeon et al.

we get $x_3(t) > 0$ for all $t \in \mathbb{R}$. In particular, $\phi_k(t) > 0$ for all $t \in [-r, 0]$ and every $k \in \{1, 2, 3\}$.

C Linearization

We turn to linearization. The subsequent description is based on results proved in Hartung et al. (2006, Sections 3.2 and 3.4) and Walther (2003), Walther (2004). At a point $\phi \in X_G$ the tangent space of the manifold X_G is given by

$$T_{\phi}X_G = \{ \chi \in C_3^1 : \chi'(0) = DG(\phi)\chi \}.$$

For $\phi \in \Omega_{G,t}$ the derivative

$$DS_{G,t}(\phi): T_{\phi}X_G \to T_{S_{G,t}(\phi)}X_G$$

is given by

$$DS_{G,t}(\phi)\chi = w_t^{\phi,\chi}$$

where $w^{\phi,\chi}=w$ is the unique continuously differentiable solution $[-r,t_{\phi})\to\mathbb{R}^3$ of the IVP

$$w'(t) = DG(S_G(t, \phi))w_t \quad \text{for} \quad t > 0, \tag{C.1}$$

$$w_0 = \chi \in T_\phi X_G. \tag{C.2}$$

Equation (C.1) is called the linear variational equation along the solution x^{ϕ} or along the flowline

$$S_G(\cdot,\phi):[0,t_\phi)\ni t\mapsto S_G(t,\phi)\in X_G.$$

Suppose now that $\phi \in X_G$ is a stationary point of the semiflow S_G . Then ϕ is constant with value, say, $\xi = (\xi_1, \xi_2, \xi_3) \in \mathbb{R}^3$. The variational equation (C.1) along the constant solution $x^{\phi} : [-r, \infty) \ni t \mapsto \xi \in \mathbb{R}^3$ becomes

$$w_1'(t) = -b_1 w_1(t) + A_1 w_3(t) + \left(c_1 e^{-\mu a_1/v_1(\xi_3)} g'(\xi_3) - A_1\right) w_3(t - a_1/v_1(\xi_3))$$

$$+ \mu A_1 \int_{-a_1/v_1(\xi_3)}^{0} w_3(s) ds$$
(C.3)

$$w_2'(t) = -b_2 w_2(t) + A_2 w_1(t) + \left(c_2 e^{-\mu a_2/v_2(\xi_1)} - A_2\right) w_1(t - a_2/v_2(\xi_1))$$

$$+ \mu A_2 \int_{-a_2/v_2(\xi_1)}^{0} w_1(s) ds$$
(C.4)

$$w_3'(t) = -b_3 w_3(t) + c_3 w_2(t)$$
(C.5)



The derivatives $T_{G,t} = DS_{G,t}(\phi)$, $t \ge 0$, form a strongly continuous semigroup on the closed subspace $T_{\phi}X_G$ of the space C_3^1 . This semigroup is given by $T_{G,t}\chi = T_{G,e,t}\chi$ where $T_{G,e,t}: C_3 \to C_3$ is the solution operator associated with the *classical* initial value problem

$$w'(t) = D_e G(\phi) w_t \quad \text{for} \quad t > 0, \tag{C.6}$$

$$w_0 = \chi \in C_3, \tag{C.7}$$

with a continuous linear vector-valued functional $L: C_3 \to \mathbb{R}^3$, $L = D_e G(\phi)$, as in the monographs, e. g., Hale and Lunel (1993); Diekmann et al. (1995). Recall that by definition the solution $w: [-r, \infty) \to \mathbb{R}^3$ of the initial value problem (C.6)–(C.7) is only continuous, with the restriction $w|_{[0,\infty)}$ continuously differentiable and satisfying (C.6).

The extended derivative $D_eG(\phi): C_3 \to \mathbb{R}^3$ in the case just considered where $\phi \in X_G$ is a stationary point with value ξ is given by (A.21)–(A.25), now for $\hat{\phi} \in C_3$. Therefore the Eq. (C.6) coincides with the system (C.3)–(C.5), considered for continuous maps $[-r, \infty) \to \mathbb{R}^3$ whose restrictions to $[0, \infty)$ are differentiable and satisfy (C.3)–(C.5) for all $t \ge 0$.

The stability of the zero solution of the linear variational Eqs. (C.3)–(C.5) is determined by the spectrum $\sigma \subset \mathbb{C}$ of the generator of the semigroup $(T_{G,t})_{t\geq 0}$ on $T_{\phi}X_G \subset C_3^1$, which coincides with the spectrum $\sigma_e \subset \mathbb{C}$ of the generator of the semigroup on C_3 .

The spectrum σ_e consists of the solutions $\lambda \in \mathbb{C}$ of the *characteristic equation*, which is obtained from the Ansatz $\mathbb{R} \ni t \mapsto e^{\lambda t}z \in \mathbb{C}^3$, $z \in \mathbb{C}^3 \setminus \{0\}$, for a complex-valued solution of the system (C.3)–(C.5) as follows. We write down the system for $w: t \mapsto e^{\lambda t}z$, multiply by $e^{-\lambda t}$, and obtain a linear equation of the form

$$(M(\lambda) - \lambda \cdot I_3)z = 0 \tag{C.8}$$

with a 3 × 3-matrix $M(\lambda)$ (complex coefficients) and with I_3 denoting the 3 × 3-unit matrix. We then set

$$\Delta(\lambda) = \det(M(\lambda) - \lambda \cdot I) = 0. \tag{C.9}$$

Following this recipe we get the linear system

$$\lambda z_{1} = -b_{1}z_{1} + A_{1}z_{3} + \left(c_{1}e^{-\mu a_{1}/v_{1}(\xi_{3})}g'(\xi_{3}) - A_{1}\right)z_{3}e^{-\lambda a_{1}/v_{1}(\xi_{3})}$$

$$+ \mu A_{1} \int_{-a_{1}/v_{1}(\xi_{3})}^{0} e^{\lambda s} ds z_{3}$$

$$\lambda z_{2} = -b_{2}z_{2} + A_{2}z_{1} + \left(c_{2}e^{-\mu a_{2}/v_{2}(\xi_{1})} - A_{2}\right)e^{-\lambda a_{2}/v_{2}(\xi_{1})}z_{1}$$

$$+ \mu A_{2} \int_{-a_{2}/v_{2}(\xi_{1})}^{0} e^{\lambda s} ds z_{1}$$

$$\lambda z_{3} = -b_{3}z_{3} + c_{3}z_{2},$$



2 Page 70 of 74 T. Gedeon et al.

and with the functions $k_1:\mathbb{C}\to\mathbb{C}$ and $k_2:\mathbb{C}\to\mathbb{C}$ given by

$$k_1(\lambda) = A_1 + \left(c_1 e^{-\mu a_1/v_1(\xi_3)} g'(\xi_3) - A_1\right) e^{-\lambda a_1/v_1(\xi_3)} + \mu A_1 \int_{-a_1/v_1(\xi_3)}^{0} e^{\lambda s} ds,$$

$$k_2(\lambda) = A_2 + \left(c_1 e^{-\mu a_2/v_2(\xi_1)} - A_2\right) e^{-\lambda a_2/v_2(\xi_1)} + \mu A_2 \int_{-a_2/v_2(\xi_1)}^{0} e^{\lambda s} ds,$$

respectively, we obtain

$$M(\lambda) = \begin{pmatrix} -b_1 & 0 & k_1(\lambda) \\ k_2(\lambda) & -b_2 & 0 \\ 0 & c_3 & -b_3 \end{pmatrix}$$
 (C.10)

for $\lambda \in \mathbb{C}$, which yields

$$\Delta(\lambda) = \det(M(\lambda) - \lambda I_3) = (b_1 + \lambda)(b_2 + \lambda)(b_3 + \lambda) + k_1(\lambda)k_2(\lambda)c_3.$$

So the characteristic equation associated with the stationary point ϕ with value ξ is

$$\Delta(\lambda) = (b_1 + \lambda)(b_2 + \lambda)(b_3 + \lambda) + k_1(\lambda)k_2(\lambda)c_3 = 0.$$
 (C.11)

Next we rewrite (C.11) in the original notation of (2.15)–(2.19). In terms of the parameters and functions in the system (2.15)–(2.19) the parameters and functions in the system (A.10)–(A.12) are μ and

The equilibria of the systems (2.15)–(2.19) and (A.10)–(A.12) are given by the solutions $(M^*, I^*, E^*) = (\xi_1, \xi_2, \xi_3) \in \mathbb{R}^3$ of the systems

$$\begin{array}{ll} 0 = \beta_M e^{-\mu a_M/v_M(I^*)} f(E^*) - \bar{\gamma}_M M^* & 0 = c_1 e^{-\mu a_1/v_1(\xi_3)} g(\xi_3) - b_1 \xi_1 \\ 0 = \beta_I e^{-\mu a_I/v_I(M^*)} M^* - \bar{\gamma}_I I^* & \Longleftrightarrow & 0 = c_2 e^{-\mu a_2/v_2(\xi_1)} \xi_1 - b_2 \xi_2 \\ 0 = \beta_E I^* - \bar{\gamma}_E E^*. & 0 = c_3 \xi_2 - b_3 \xi_3. \end{array}$$

From (A.22) and (A.24) we can rewrite A_1 and A_2 in the notation of (2.15)–(2.19) as

$$A_1 = \beta_M \frac{v_M'(E^*)}{v_M(E^*)} e^{-\mu a_M/v_M(E^*)} f(E^*), \quad A_2 = \beta_I \frac{v_I'(M^*)}{v_I(M^*)} e^{-\mu a_I/v_I(M^*)} M^*.$$



and hence

$$k_{1}(\lambda) = A_{1} + \left(\beta_{M}e^{-\mu a_{M}/v_{M}(E^{*})}f'(E^{*}) - A_{1}\right)e^{-\lambda a_{M}/v_{M}(E^{*})} + \mu A_{1} \int_{-a_{M}/v_{M}(E^{*})}^{0} e^{\lambda s}ds,$$

$$k_{2}(\lambda) = A_{2} + \left(\beta_{I}e^{-\mu a_{I}/v_{I}(M^{*})} - A_{2}\right)e^{-\lambda a_{I}/v_{I}(M^{*})} + \mu A_{2}\int_{-a_{I}/v_{I}(M^{*})}^{0} e^{\lambda s}ds.$$

For $\lambda \neq 0$ we evaluate the integrals and obtain

$$\begin{split} k_{1}(\lambda) &= A_{1} + \left(\beta_{M}e^{-\mu a_{M}/v_{M}(E^{*})} f'(E^{*}) - A_{1}\right)e^{-\lambda a_{M}/v_{M}(E^{*})} + \frac{\mu A_{1}}{\lambda} \left(1 - e^{-\lambda a_{M}/v_{M}(E^{*})}\right) \\ &= A_{1}(1 - e^{-\lambda a_{M}/v_{M}(E^{*})})\left(1 + \frac{\mu}{\lambda}\right) + \beta_{M}e^{-\mu a_{M}/v_{M}(E^{*})} f'(E^{*})e^{-\lambda a_{M}/v_{M}(E^{*})} \\ &= \beta_{M}e^{-\mu\tau_{M}(E^{*})}\left(\frac{v'_{M}(E^{*})}{v_{M}(E^{*})} f(E^{*})(1 - e^{-\lambda\tau_{M}(E^{*})})\left(1 + \frac{\mu}{\lambda}\right) + f'(E^{*})e^{-\lambda\tau_{M}(E^{*})}\right) \end{split}$$

and

$$\begin{split} k_2(\lambda) &= A_2 + \left(\beta_I e^{-\mu a_I/v_I(M^*)} - A_2\right) e^{-\lambda a_I/v_I(M^*)} + \frac{\mu}{\lambda} A_2 (1 - e^{-\lambda a_I/v_I(M^*)}) \\ &= A_2 (1 - e^{-\lambda a_I/v_I(M^*)}) \left(1 + \frac{\mu}{\lambda}\right) + \beta_I e^{-\mu a_I/v_I(M^*)} e^{-\lambda a_I/v_I(M^*)} \\ &= \beta_I e^{-\mu \tau_I(M^*)} \left(\frac{v_I'(M^*)}{v_I(M^*)} M^* (1 - e^{-\lambda \tau_I(M^*)}) \left(1 + \frac{\mu}{\lambda}\right) + e^{-\lambda \tau_I(M^*)}\right). \end{split}$$

In terms of the parameters and functions of the system (2.15)–(2.19) the characteristic Eq. (C.11) becomes $\Delta(\lambda)=0$ for

$$\Delta(\lambda) = (\bar{\gamma}_M + \lambda)(\bar{\gamma}_I + \lambda)(\bar{\gamma}_E + \lambda) + \beta_E k_1(\lambda)k_2(\lambda), \tag{C.12}$$

which is identical to (2.49), (2.50).

References

Ahmed A, Verriest E (2017) Modeling & analysis of gene expression as a nonlinear feedback problem with state-dependent delay. IFAC PapersOnLine 50(1):12679–12684

an der Heiden U (1979) Delays in physiological systems. J Math Biol 8(4):345-364

an der Heiden U (1983) Periodic, aperiodic, and stochastic behavior of differential-difference equations modeling biological and economical processes. In: Differential-difference equations (Oberwolfach, 1982), Internat. Schriftenreihe Numer. Math., vol 62, Birkhäuser, Basel, pp 91–108

Banks HT (1977) Delay systems in biological models: approximation techniques. In: Nonlinear systems and applications (Proc. Internat. Conf., Univ. Texas, Arlington, Tex., 1976), Academic Press, New York, pp 21–38

Banks H, Mahaffy J (1978a) Global asymptotic stability of certain models for protein synthesis and repression. Q Appl Math 36(3):209–221

Banks H, Mahaffy J (1978b) Stability of cyclic gene models for systems involving repression. J Theor Biol 74(2):323–334



2 Page 72 of 74 T. Gedeon et al.

Bernard S (2016) Moving the boundaries of granulopoiesis modelling. Bull Math Biol 78:2358–2363

- Cassidy T, Craig M, Humphries AR (2019) Equivalences between age structured models and state dependent distributed delay differential equations. Math Biosci Eng 16:5419–5450
- Chong A, Chen C, Ge H, Xie S (2014) Mechanisms of transcriptional bursting in bacteria. Cell 158:314–326
- Craig M, Humphries A, Mackey M (2016) A mathematical model of granulopoiesis incorporating the negative feedback dynamics and kinetics of G-CSF/neutrophil binding and internalisation. Bull Math Biol 78:2304–2357
- Derrida B, Evans M, Hakim V, Pasquier V (1993) Exact solution of a 1D asymmetric exclusion model using a matrix formalism. J Phys A Math Gen 26:1493–1517
- Diekmann O, Van Gils S, Lunel S, Walther HO (1995) Delay equations: functional-, complex-, and nonlinear analysis, vol 110. Springer
- Goodwin BC, et al. (1963) Temporal organization in cells. A dynamic theory of cellular control processes. Temporal organization in cells A dynamic theory of cellular control processes
- Goodwin BC (1965) Oscillatory behaviour in enzymatic control process. Adv Enzyme Regul 3:425-438
- Griffith J (1968a) Mathematics of cellular control processes. I. Negative feedback to one gene. J Theor Biol 20:202–208
- Griffith J (1968b) Mathematics of cellular control processes. II. Positive feedback to one gene. J Theor Biol 20:209–216
- Hale JK (1988) Asymptotic behavior of dissipative systems, mathematical surveys and monographs, vol 25. American Mathematical Society
- Hale JK, Lunel SMV (1993) Introduction to functional differential equations. Springer
- Hartung F, Krisztin T, Walther HO, Wu J (2006) Functional differential equations with state-dependent delays: theory and applications. Handbook of differential equations, ordinary differential equations, vol 3. Elsevier, Amsterdam, pp 435–545
- Jacob F, Monod J (1961) Genetic regulatory mechanisms in the synthesis of proteins. J Mol Biol 3:318–356Jacob F, Perrin D, Sanchez C, Monod J (1960) Operon: a group of genes with the expression coordinated by an operator. C R Hebd Seances Acad Sci 250:1727–1729
- Kalia M, Kuznetsov YA, Meijer HG (2019) Homoclinic saddle to saddle-focus transitions in 4d systems. Nonlinearity 32(6):2024
- Klumpp S (2011) Pausing and backtracking in transcription under dense traffic conditions. J Stat Phys 142:1251–1267
- Klumpp S, Hwa T (2008) Stochasticity and traffic jams in the transcription of ribosomal RNA: intriguing role of termination and anti-termination. PNAS 105(47):18159–164
- Kolomeisky A (1998) Asymmetric simple exclusion model with local inhomogeneity. J Phys A 31:1153–1164
- Kuznetsov YA (2004) Elements of applied bifurcation theory, vol 112, 3rd edn. Springer
- Lenstra T, Rodriguez J, Chen H, Larson D (2016) Transcription dynamics in living cells. Annu Rev Biophys 45(July 5th):25–47
- MacDonald N (1977) Time lag in a model of a biochemical reaction sequence with end product inhibition. J Theor Biol 67(3):549-556
- Mackey M, Santillán M, Tyran-Kamińska M, Zeron E (2016) Simple mathematical models of gene regulatory dynamics. Springer
- Mahaffy J, Pao C (1984) Models of genetic control by repression with time delays and spatial effects. J Math Biol 20(1):39–57
- Mallet-Paret J, Nussbaum RD, Paraskevopoulos P (1994) Periodic solutions for functional differential equations with multiple state-dependent time lags. Topol Methods Nonlinear Anal 3:101–162
- Mathworks (2020) MATLAB 2020b. Mathworks, Natick, Massachusetts, USA
- Monk N (2003) Oscillatory expression of hes1, p53, and nf-κb driven by transcriptional time delays. Curr Biol 13:1409–1413
- Othmer H (1976) The qualitative dynamics of a class of biochemical control circuits. J Math Biol 3:53–78 Peccoud J, Ycart B (1995) Markovian modeling of gene- product synthesis. Theor Popul Biol 48:222–234
- Schrödinger E (1944) What is life? The physical aspect of the living cell. Cambridge University Press Schütz G, Domany E (1993) Phase transitions in an exactly soluble one-dimensional exclusion process. J
- Stat Phys 72:277–296
- Selgrade J (1979) Mathematical analysis of a cellular control process with positive feedback. SIAM J Appl Math 36:219–229



Shaw L, Zia R, Lee K (2003) Totally asymmetric exclusion process with extended objects: a model for protein synthesis. Phys Rev E 68:021910

Shilnikov L (1965) A case of the existence of a denumerable set of periodic motions. Sov Math Dokl 6:163–166

Sieber J, Engelborghs K, Luzyanina T, Samaey G, Roose D (2015) DDE-BIFTOOL Manual-Bifurcation analysis of delay differential equations. arXiv:14067144

Timoféeff-Ressovsky N, Zimmer K, Delbrück M (1935) Über die natur der genmutation und der genstruktur. Nachr Gess Wiss Gottingen 1:189–245

Tunnacliffe E, Chubb J (2020) What is a transcriptional burst? Trends Genet 36(4):288-297

Tyson J, Othmer H (1978) The dynamics of feedback control circuits in biochemical pathways. In: Rosen R (ed) Progress in biophysics, vol 5. Academic Press, New York, pp 1–62

Verdugo A, Rand R (2007) Delay differential equations in the dynamics of gene copying. Proceediings ASME IDETC/CIE 2007, pp 1–6

Walther HO (2003) The solution manifold and C^1 -smoothness of solution operators for differential equations with state dependent delay. J Differ Eqs. 195:46–65

Walther HO (2004) Smoothness properties of semiflows for differential equations with state dependent delay. J Math Sci 124:5193–5207

Wang Z (2020) Dynamics of a state-dependent delay model of repressible and inducible operons. Msc, McGill University, Canada. https://escholarship.mcgill.ca/concern/theses/9019s687q

Wang S, Pei L (2021) Complex dynamics and periodic oscillation mechanism in two novel gene expression models with state-dependent delays. Int J Bifurc Chaos 31(1):2150002

Yildirim N, Mackey MC (2003) Feedback regulation in the lactose operon: a mathematical modeling study and comparison with experimental data. Biophys J 84:2841–2851

Yildirim N, Santillán M, Horike D, Mackey MC (2004) Dynamics and bistability in a reduced model of the lac operon. Chaos 14:279–292

Zia RKP, Dong JJ, Schmittmann B (2011) Modeling translation in protein synthesis with TASEP: a tutorial and recent developments. J Stat Phys 144(2):405–428. https://doi.org/10.1007/s10955-011-0183-1

Publisher's Note Springer Nature remains neutral with regard to jurisdictional claims in published maps and institutional affiliations.

Authors and Affiliations

⊠ Zhao Wang

zhao.wang3@mail.mcgill.ca

Tomáš Gedeon

gedeon@math.montana.edu

Antony R. Humphries tony.humphries@mcgill.ca

Michael C. Mackey michael.mackey@mcgill.ca

Hans-Otto Walther

Hans-Otto.Walther@math.uni-giessen.de

- Department of Mathematics, Montana State University, Bozeman, MT 59717, USA
- Departments of Mathematics and Statistics, and, Physiology, McGill University, Montreal, QC H3A 0B9, Canada



2 Page 74 of 74 T. Gedeon et al.

Departments of Physiology, Physics, and, Mathematics and Statistics, McGill University, 3655 Promenade Sir William Osler, Montreal, QC H3G 1Y6, Canada

- Mathematisches Institut, Universität Giessen, Arndtstrasse 2, 35392 Giessen, Germany
- ⁵ Department of Mathematics and Statistics, McGill University, Montreal, QC H3A 0B9, Canada

